DISSERTATION

ABSORPTION AND SCATTERING PROPERTIES OF MICRO- AND NANO-SIZE PHYTOPLANKTON

2015

SOKA UNIVERSITY

GRADUATE SCHOOL OF ENGINEERING

SHOZO MOTOKAWA

ABSORPTION AND SCATTERING PROPERTIES OF MICRO- AND NANO-SIZE PHYTOPLANKTON

SEPTEMBER 2015

SHOZO MOTOKAWA

SOKA UNIVERSITY

Author: Shozo Motokawa

Title: Absorption and scattering properties of micro- and nano-size phytoplankton

Department: Environmental Engineering for Symbiosis
Faculty: Engineering
Degree: Ph.D.
Convocation: September 2015

We certify that we have read this dissertation and that, in our opinion, it is satisfactory in scope and quality as a dissertation for the degree of Doctor of Philosophy in Engineering.

July 2015

DISSERTATION COMMITTEE

Prof. Dr. Tatsuki Toda

Prof. Dr. Tatsushi Matsuyama

Prof. Dr. Satoru Taguchi

CONTENTS

ACKNOWLEDGMENTS

I am grateful to Professor Satoru Taguchi for his support, numerous suggestions and discussions throughout the course of this study. Without his guidance and persistent help this dissertation would not have been possible.

I would like to gratefully acknowledge Professor Tatsuki Toda and Professor Tatsushi Matsuyama for their thorough discussion, valuable suggestions and review of this dissertation. I express my sincere appreciation to Professor Norio Kurosawa, Dr. Ai Murata, and Dr. Mitsuko Obata for their supports and encouragements.

I would like to thank Professor Tomohiko Kikuchi for providing R/V Tachibana and assisting the sampling in Sagami Bay. I would like to thank Associate Professor Koji Hamasaki, Dr. Hideo Miyaguchi and Dr. Kenji Tsuchiya for assisting me in the sampling at Sagami Bay. I thank the crews of R/V Tachibana, students of Yokohama National University for technical support with sampling.

I would like to thank Professor Hiroshi Sasaki, Professor Hiroshi Hattori, Professor Mitsuo Fukuchi, Associate Professor Gen Hashida, Associate Professor Masato Moteki, Associate Professor Victor S. Kuwahara, Associate Professor Nobue Kasamatsu-Takasawa, and Dr. Takahiro Iida and to support the cruise of TR/V Umitaka-maru in the Southern Ocean. I thank the captain, officers and crews of TR/V Umitaka-maru, students of Tokyo University of Marine Science and Technology and the scientists of Japanese Antarctic Research Expedition (JARE) -52 and -53 for technical support with sampling.

I would like to thank Professor Joji Ishizaka of Nagoya University for lending 9-wavelength absorption-attenuation meter used in Sagami Bay. I would like to thank Associate Professor Toru

Hirawake of the Hokkaido University for lending Profiling Reflectance Radiometer-800 used in the Southern Ocean.

I would like to thank Professor Zoe V. Finkel, Dr. Tetsuichi Fujiki, and Dr. Sandric C. Y. Leong for providing the raw data.

I deeply thank all members of the laboratories of biological oceanography and restoration ecology, especially, Akemi Leong, Nobuyuki Kobashi, Tomoyo Katayama, Kayoko Takimoto, Asami Shinya, and Yasuhiro Masuda for their unlimited support, warmth, and friendship.

I am most grateful to my parents: Katsuyoshi Motokawa and Emiko Motokawa for their encouragement, endless supports throughout my life.

I am greatly indebted to the founder of Soka University: Dr. Daisaku Ikeda and Mrs. Kaneko Ikeda for their guidance and encouragement.

This work was supported in part by the RAMEEC (Responses of Antarctic Marine Ecosystems to global Environmental Changes with Carbonate systems) project of JARE.

ABSTRACT

Size distribution of natural phytoplankton assemblages and the physiological properties are one of the fundamental features in marine carbon cycle. Particularly, large-cell plankton, such as micro- (20 – 200 μm in diameter) and nano-size phytoplankton (2 – 20 μm in diameter) can influence significantly on the production due to the occurrence of opportunistic and sporadic large blooms. One of the bloom-forming species is dinoflagellate. To monitor the size distribution of phytoplankton or the blooms, optical approach would be one of the most effective ways. The optical approach is based on Inherent Optical Properties (IOPs) of phytoplankton, such as absorption and scattering coefficients of phytoplankton ($a_{ph}[\lambda]$ and $b_{ph}[\lambda]$). Both $a_{ph}(\lambda)$ and $b_{ph}(\lambda)$ are influenced by cell volume which is the most critical parameter in the geometrical characteristics of natural assemblages of phytoplankton. Because of the wide difference in the cell volume, the non-linear relationships between phytoplankton biomass, such as chlorophyll *a* (Chl *a*) and IOPs, such as $a_{ph}(\lambda)$ and $b_{ph}(\lambda)$ are observed. Based on the large set of *in situ* data, $a^*_{ph}(\lambda)$ can be used to distinguish cell sizes in natural phytoplankton assemblages, whereas $b^*_{ph}(\lambda)$ have not been used yet to differentiate cell sizes.

In a water column, the IOPs of phytoplankton would be influenced by the physiological properties. The $b^*_{ph}(\lambda)$ is influenced by the intracellular carbon contents, and therefore the $b^*_{ph}(\lambda)$ could be indexed on the ratio of particulate organic carbon to Chl *a* (POC:Chl *a*) as physiological properties of natural assemblages of phytoplankton. In addition, a molar ratio of photoprotective carotenoids (PPC) to total carotenoids (TC, PPC:TC) is one of the index of physiological properties of natural assemblages of phytoplankton. The variations in relative proportions of PPC alter the slope of a^*_{ph} spectra from 488 to 532nm normalized by 676nm ($a^*_{ph}{}^{slope}$). The relationships

between the $b^*_{ph}(\lambda)$ and POC:Chl *a*, and a^*_{ph} spectra and PPC:TC could be utilized to evaluate the physiological properties of natural assemblages of phytoplankton.

The objectives in this study are to investigate the relationship between cell size and IOPs of micro- and nano-size dinoflagellates in culture in relation to published data, and to investigate the cell size effect on IOPs in the natural assemblages of phytoplankton. Furthermore, physiological properties of natural assemblages of phytoplankton are investigated by using IOPs of phytoplankton. A parameterization of IOPs for micro- and nano-size phytoplankton provides a simple tool to monitor the size distribution and the physiological properties by using optical measurements in the ocean. Establishment of relationships between phytoplankton biomass, such as Chl *a* and the IOPs by including dinoflagellate species to each size group will improve our understanding of the optical characteristics of natural assemblages of phytoplankton in relation to cell size.

Equivalent spherical diameters (*d*) of dinoflagellates *Prorocentrum micans* and *P. minimum* under the saturated and supra-saturated light conditions were 25.0 ± 0.22 and 12.6 ± 0.24 μm, respectively. The *d* of *P. micans* was about 2-fold larger than that of *P. minimum*. The a^*_{ph} (676) and b^*_{ph} (676) of *P. micans* were approximately 20% and 35% lower than that of *P. minimum*, respectively. I enumerated the *d*, $a^*_{ph}(676)$, $b^*_{ph}(676)$, and C:Chl *a* of phytoplankton species with various cell sizes in published data to evaluate those of *P. micans* and *P. minimum*. Both $a^*_{ph}(676)$ and $b^*_{ph}(676)$ of various species including *P. micans* and *P. minimum* significantly decreased with increasing *d* ($p<0.05$). The decreasing $a^*_{ph}(676)$ with increasing *d* is due to pigments self-shading in the cell (package effect). The decreasing $b^*_{ph}(676)$ with increasing *d* could be induced by the increasing Chl *a* contents per cell. The $b^*_{ph}(676)$ of various species including *P. micans* and *P. minimum* increased significantly with the C:Chl *a* ($p<0.001$). The significant relationship between the $b^*_{ph}(676)$ and C:Chl *a* suggests that the C:Chl *a* could play a role of the variation in the

$b^*_{ph}(676)$ as a function of cell size.

Natural assemblages of phytoplankton were obtained at the optical depths of 0.0, and 2.3, and 4.6 in the Indian sector of the Southern Ocean (SO) and in Sagami Bay (SB), Japan. The investigations of size distribution of phytoplankton assemblage and the optical properties were divided into four regions according to the differences in the water mass: at the north of Antarctic Convergence (AC) in SO (NAC), at the South of AC in SO (SAC), in SB during winter (from December to February, WSB), and in SB from spring to autumn (from March to November, SSB).

Bulk Chl *a* concentrations ranged from 0.15 to 3.8 mg m^{-3}. The highest and lowest bulk Chl *a* concentrations were observed in SSB and NAC, respectively. The micro- and nano-size fractionated Chl *a* concentrations increased with increasing bulk Chl *a* concentrations. The relative proportion of micro-size fractions to bulk Chl *a* concentrations increased with increasing bulk Chl *a* concentrations, whereas that of nano-size decreased.

Size Indices (SI) of natural assemblages of phytoplankton for absorption (SI_{abs}) and scattering analyses (SI_{scat}) were calculated from relative Chl *a* proportions of micro-, nano-, and pico-size fraction to bulk fraction (%) and weighed values for absorption and scattering of three cell size classes; micro-, nano-, and pico-size. The SI_{abs} and SI_{scat} in all regions were similar because the weighted value of each size class was similar between the absorption and the scattering analyses. The average SI_{abs} and SI_{scat} in NAC, SAC, and WSB fell in the range of the nano-size phytoplankton, whereas the average SI_{abs} and SI_{scat} fell in the range of the micro-size phytoplankton.

The $a^*_{ph}(676)$ and $b^*_{ph}(676)$ decreased significantly with increasing SI_{abs} and SI_{scat}, respectively, when the all regions were considered together. The slopes of the *in situ* relationships between $a^*_{ph}(676)$ and SI_{abs} were not significantly different from the slopes of the cultural relationships between $a^*_{ph}(676)$ and *d*. The similarity suggests that the effect of cell size on

$a^*_{ph}(676)$ of natural assemblage of phytoplankton with various cell sizes could be evaluated by the SI_{abs}. The higher intercept of the *in situ* relationship compared with that of the cultural relationship suggests that the *in situ* relationship could be influenced by the physiological properties of phytoplankton which could covary with the environmental conditions.

The slopes of the *in situ* relationships between $b^*_{ph}(676)$ and SI_{scat} were not significantly different from the slopes of the cultural relationship between $b^*_{ph}(676)$ and d. This similarity confirm that decrease in $b^*_{ph}(676)$ could be determined by not only size distribution of cells, but also cumulative cell volume of phytoplankton assemblage. The intercept of the *in situ* relationship was significantly higher than that of the cultural relationship. The higher intercept of the *in situ* relationship could be due to the high light conditions because the high light conditions could induce the decreasing Chl *a* per cell, and the $b^*_{ph}(676)$ increased consequently. In addition, the difference in $b^*_{ph}(676)$ of natural assemblages of phytoplankton could be induced by the difference in the carbon contents. The significant higher intercept of the *in situ* relationships could be due to the carbon contents other than phytoplankton, such as detritus.

The bulk $a^*_{ph}{}^{slope}$ decreased with decreasing bulk PPC:TC (mol mol^{-1}) of phytoplankton assemblage. The PPC:TC increased with increasing optical depths, so that the PPC:TC could indicate the photoprotective response to light changes in water column. The composition of PPC and TC in phytoplankton cell is different among species, however the PPC:TC as a function of light intensity was similar between micro-size and nano-size fractions. The $a^*_{ph}{}^{slope}$ and PPC:TC was similar between micro-size and nano-size fractions, and therefore the $a^*_{ph}{}^{slope}$ could be utilized to evaluate the photoprotective acclimation of phytoplankton without the size effect on the $a^*_{ph}{}^{slope}$.

The $b_p(676)$ increased with increasing POC ($p<0.001$). The bulk $b^*_{ph}(676)$ increased significantly with the POC:Chl *a* ($p<0.001$) when the regions were considered together. Assuming

that the scattering efficiency of detritus is similar to that of phytoplankton, the similar slopes of the relationships between $b^*_{ph}(676)$ and POC:Chl *a* and/or C:Chl *a* suggest that the relative amount of detrital carbon increase with decrease in C:Chl *a* of phytoplankton cell.

This study presented that both $a^*_{ph}(676)$ and $b^*_{ph}(676)$ decreased with increasing *d* and size index derived from the relative Chl *a* abundance and the weighed values. The relationships could assist the understanding for inverting remotely sensed data to the size distribution of phytoplankton assemblage. In addition, the difference in the intercepts of the relationships between the IOPs and *d* and/or size index suggests that the more accurate evaluation of the effect of cell size on the IOPs would require the knowledge of physiological properties of natural assemblage of phytoplankton. The significant relationships between $a^*_{ph}{}^{slope}$ and PPC:TC, $b^*_{ph}(676)$ and POC:Chl *a* in the present study suggest that the $a^*_{ph}{}^{slope}$ and $b^*_{ph}(676)$ can assist to correct the physiological effect of the cell size. The estimated size distribution and physiological properties of natural assemblage of phytoplankton from remotely sensed data could contribute to the understanding marine carbon cycle.

LIST OF TABLES

LIST OF FIGURES

NOTATION

Symbol	Definition	Units
AC	Antarctic convergence	–
ac-9	9-wavelength absorption attenuation meter	–
$\underline{a}_{CDOM}(\lambda)$	Absorption coefficient of colored dissolved organic matter	m^{-1}
$a_{cell}(\lambda)$	Cell specific absorption coefficient of phytoplankton	m^2 cell^{-1}
$a_{cm}(\lambda)$	Unpackaged chlorophyll *a* specific absorption coefficient	m^2 mg Chl a^{-1}
$a_{d}(\lambda)$	Absorption coefficient of non-pigmented particle	m^{-1}
Allo	Alloxanthin	–
$\underline{a}_{m}(\lambda)$	Absorption coefficient measured by ac-9	m^{-1}
$\underline{a}_{mt}(\lambda)$	Temperature and salinity-corrected absorption coefficient measured by ac-9	m^{-1}
$a_{p}(\lambda)$	Absorption coefficient of particle	m^{-1}
$a_{ph}(\lambda)$	Absorption coefficient of phytoplankton	m^{-1}
$\underline{a}_{ph}(\lambda)$	Absorption coefficient of phytoplankton measured by ac-9	m^{-1}
$\underline{a}_{ref}(\lambda)$	Absorption coefficient of reference seawater measured by ac-9	m^{-1}
$a^*_{ph}(\lambda)$	Chlorophyll *a* specific absorption coefficient of phytoplankton	m^2 mg Chl a^{-1}
$a^*_{ph}{}^{slope}(488\text{-}532)$	Slope of a^*_{ph} spectra from 488 to 532nm	–
$\underline{b}_{p}(\lambda)$	Scattering coefficient of particle measured by ac-9	m^{-1}
$\underline{b}_{ph}(\lambda)$	Scattering coefficient of phytoplankton measured by ac-9	m^{-1}
$\underline{b}^*_{ph}(\lambda)$	Chlorophyll *a* specific scattering coefficient of phytoplankton measured by ac-9	m^2 mg Chl a^{-1}
But-fuco	19'-butanoyloxyfucoxanthin	–
$\underline{c}_{CDOM}(\lambda)$	Attenuation coefficient of colored dissolved organic matter	m^{-1}

NOTATION

Symbol	Definition	Units
C:Chl *a*	Ratio of cellular carbon to cellular chlorophyll *a*	$g\ g^{-1}$
CDOM	Colored dissolved organic matter	–
Chl *a*	Chlorophyll *a*	–
[Chl *a*]	Chlorophyll *a* concentration	$mg\ m^{-3}$
Chl a_i	Intracellular chlorophyll *a* contents	$kg\ Chl\ a\ m^{-3}$
Chl *b*	Chlorophyll *b*	–
Chl c_{1+2}	Chlorophyll c_{1+2}	–
Chl c_3	Chlorophyll c_3	–
C_i	Intracellular carbon contents	$kg\ C\ m^{-3}$
$\underline{c}_m(\lambda)$	Attenuation coefficient measured by ac-9	m^{-1}
$\underline{c}_{mt}(\lambda)$	Temperature and salinity-corrected attenuation coefficient measured by ac-9	m^{-1}
$\underline{c}_p(\lambda)$	Attenuation coefficient of particle measured by ac-9	m^{-1}
$\underline{c}_{ph}(\lambda)$	Attenuation coefficient of phytoplankton measured by ac-9	m^{-1}
$\underline{c}_{ref}(\lambda)$	Attenuation coefficient of reference seawater measured by ac-9	m^{-1}
$\underline{c}^*_{ph}(\lambda)$	Chlorophyll *a* specific attenuation coefficient of phytoplankton measured by ac-9	$m^2\ mg\ Chl\ a^{-1}$
d	Equivalent spherical diameter	μm
$\underline{d}$	Representative equivalent spherical diameter	μm
DD	Diadinoxanthin	–
DP	Diagnostic pigments	–
DP_{micro}	Chemical fraction of micro-size	%

NOTATION

Symbol	Definition	Units
DP_{nano}	Chemical fraction of nano-size	%
DP_{pico}	Chemical fraction of pico-size	%
DT	Diatoxanthin	–
$E_d(z)$	Downward photosynthetically available radiation at z m depth	µmol photons m^{-2} s^{-1}
Fuco	Fucoxanthin	–
h	Height of cell	µm
Hex-fuco	19'-hexanoyloxyfucoxanthin	–
l	Apical axis of cell	µm
n	Number of sample	–
N	Number of cell	cells
[N]	Cell density	cells m^{-3}
NAC	North of Antarctic convergence	–
m	Relative refractive index to water	–
OD_f	Optical density of filtrate particles	–
ODs	Optical density of particles in suspension	–
p	Probability	–
PAR	Photosynthetically available radiation	µmol photons m^{-2} s^{-1}
Peri	Peridinin	–
POC	Particulate organic carbon	–
POC:Chl *a*	Ratio of particulate organic carbon to chlorophyll *a*	g g^{-1}

NOTATION

Symbol	Definition	Units
PPC	Photoprotective carotenoid	–
PPC:TC	Ratio of photoprotective carotenoid to total carotenoid	mol mol^{-1}
$Q_a(\lambda)$	Experimental efficiency factor for absorption	–
$Q_a(\rho')$	Theoretical efficiency factor for absorption	–
$Q^*_a(\lambda)$	Experimental package effect index	–
$Q^*_a(\rho')$	Theoretical package effect index	–
$Q_b(\lambda)$	Experimental efficiency factor for scattering	–
$Q_b(\rho',\rho)$	Theoretical efficiency factor for scattering	–
$Q_c(\rho)$	Theoretical efficiency factor for attenuation	–
QFT	Quantitative filter technique	–
R	Remote sensing reflectance	sr^{-1}
r^2	Determination coefficient	–
s	Cross-sectional area	m^2
S	Salinity of sample	–
SAC	South of Antarctic convergence	–
SB	Sagami Bay	–
S.E.	Standard error	–
Sf	Filtered clearance	m^2
SI_{abs}	Size index for absorption analysis	μm
SI_{scat}	Size index for scattering analysis	μm

NOTATION

Symbol	Definition	Units
SO	Southern Ocean	–
S_r	Salinity of pure water	–
SSB	Sagami Bay from spring to autumn	–
t	Trans-apical of cell	μm
T	Temperature of sample	^{o}C
TC	Total carotenoid	–
T_r	Temperature of pure water	^{o}C
V	Cell volume	μm^3 $cell^{-1}$
Vf	Filtered volume	m^3
Vio	Violaxanthin	–
WSB	Sagami Bay during winter	–
Zea	Zeaxanthin	–
α	Size parameter	–
β-caro	*Beta* -carotene	–
λ	Wavelength	nm
ψ_s	Linear salinity dependence of pure water	–
ψ_t	Linear temperature dependence of pure water	–
ρ	Phase lag	–
ρ'	Optical thickness	–
ζ	Optical depth	–

CHAPTER I

GENERAL INTRODUCTION

1.1. Mico- and nano-size phytoplankton in the marine carbon cycle

Carbon cycle in marine ecosystems is critically dependent on primary production of phytoplankton. Marine phytoplankton is currently responsible for about 50% of global primary production (Falkowski and Raven 2007). The primary production of phytoplankton is linked to not only the biomass but also size distribution of phytoplankton assemblage (Chisholm 1992; Vidussi et al. 2001). This is because primary production rate of phytoplankton often scales with cell size under an optimal growth conditions (Banse 1976; Taguchi 1976; Finkel et al. 2004). The size distribution of phytoplankton can also alter a flow of organic particles in the marine carbon cycle (Armstrong et al. 2002). When large phytoplankton and the herbivorous food web dominated, the export of biogenic carbon occurred, whereas small phytoplankton and the microbial food web lead to the recycling and weaken the exportation of organic material (Michaels and Silver 1988). In the global ocean, the mean export of biogenic carbon is about 15% (Laws et al. 2000). Over the next century, climate change is expected to alter the environmental conditions that can influence on the phytoplankton biomass and the size distribution of phytoplankton assemblage (Sarmiento et al. 2004; Finkel et al. 2010). Therefore the monitoring of the size distribution of phytoplankton is essential to understand the future changes in the marine carbon cycle in response to the environmental conditions.

Size distribution of phytoplankton assemblage is one of the fundamental features in marine carbon cycle. It is well established that the biomass and production of small cell phytoplankton (<2 μm in diameter) tend to remain relatively constant, whereas large cell phytoplankton (>2 μm in diameter) can influence significantly on the change in the marine carbon cycle due to the

occurrence of opportunistic and sporadic large blooms under the adequate conditions of light and nutrient (Chisholm 2000; Cermeño et al. 2005). The large cell phytoplankton is often assigned to the two groups; micro-size (20 – 200 μm in diameter) and nano-size phytoplankton (2 – 20 μm in diameter) (Sieburth et al. 1978). The monitoring of the micro-size and nano-size phytoplankton have particularly an important aspect of the understanding the sporadic changes in the marine carbon cycle.

1.2. Monitoring of the size distribution of phytoplankton by ocean color remote sensing

Ocean color remote sensing by satellite is one of the most effective ways to monitor the phytoplankton biomass, such as chlorophyll *a* (Chl *a*) concentration (O'Reilly et al. 1998) and particulate organic carbon (POC) concentration (Behrenfeld et al. 2005), and size distribution of phytoplankton on spatial and temporal scales in the global ocean (Ciotti and Bricaud 2006; Brewin et al. 2011). Satellite-based estimations of the biomass and the size distribution are permitted to compare the ocean color remote sensing data to sea truth data based upon shipboard measurements (Gordon and Morel 1983; Behrenfeld and Falkowski 1997). Remote optical sensors that are equipped to satellite receive a signal from the ocean. Significant parameter for the monitoring the biomass and the size distribution can be extracted from the signal by using the algorithm for ocean-atmosphere interface and atmospheric attenuation correlation (Hovis et al. 1977; Gordon and Morel 1983). The extracted parameter is the reflectance of sunlight just below the water surface, denoted as the remote sensing reflectance (R). The R is defined as the ratio of the upward radiance (E_u) to the downward irradiance (E_d) just below the water surface as follows:

$$R = E_u / E_d \quad (1.1).$$

The E_u just below the water surface includes the upward radiance through the light propagation in

the seawater (Kirk 2011). In space, downward irradiance can be directly measured by the radiometer that is equipped to the satellite. And then the E_d just below the water surface can be calculated from the downward irradiance in space through the atmospheric correction. Therefore the changes in *R* could be directly linked with the change in the light propagation in the seawater.

Incident sunlight into the seawater is scattered when it interacts with the biogeochemical constituents (Kirk 2011). The incident sunlight finally disappears by the absorption of the biogeochemical constituents in the seawater, as result of interaction with the constituents (Kirk 2011). The light propagation in the seawater is dependent on Inherent Optical Properties (IOPs), such as absorption (*a*) and scattering coefficient (*b*), of the biogeochemical constituents (Preisendorfer 1976; Morel and Bricaud 1986). The *b* at backward angle is denoted as backscattering coefficient (b_b). The proportion of b_b to *b* can be estimated from the size distribution of marine particles (Ulloa et al. 1994; Loisel et al. 2007). The *R* is determined by the given radiance and irradiance (equation 1.1), and the *R* is also estimated from the ratio of b_b to *a* plus b_b in water as follows (Kirk 2011):

$$R = \mathrm{F} \times b_b / (a + b_b) \tag{1.2}$$

where the dimensionless number F particularly depends on the volume scattering function in the seawater (Kirk 2011). The F can be estimated using Monte Carlo simulations based on radiative transfer theory under the representative ocean-atmosphere conditions (Gordon et al. 1975; Morel and Prieur 1977; Kirk 1981). The *a* and *b* of the biogeochemical constituents are constructed by the cumulative *a* and *b* of dissolved materials and the particulates. In previous study, the dissolved materials, such as colored dissolved organic matter (CDOM), are often assumed to covary with Chl *a* concentration (Morel and Prieur 1977; Prieur and Sathyendranath 1981). The characteristics of *a* and *b* of the particulate materials play a significant role on the monitoring the marine particles in

seawater using ocean color remote sensing.

Size distribution of phytoplankton assemblage is often represented as not only the relative biomass proportion of the size class but also the representative size index (Ciotti et al. 2002; Bricaud et al. 2004). A biomass based size index can be calculated from the relative Chl *a* abundance of size class and each weighted values (Bricaud et al. 2004). The size index is based on that the size distribution of phytoplankton may vary significantly for a given bulk Chl *a* content of the assemblage (Bricaud et al. 2004). Although the size index may be a rough indicator of the dominant size class of phytoplankton assemblage, the size index represents the advantage to vary continuously (Bricaud et al. 2004). The size index can be appropriate to monitor the occurrence of opportunistic and sporadic large blooms by the large-cell phytoplankton. However, to apply the size index to the ocean color remote sensing, the understanding of absorption and scattering are warranted in relation to size index. The optical based size index can be constructed by the significant relationship between the optical size index and the IOPs of phytoplankton assemblage.

Most of the large cell phytoplankton is diatom and dinoflagellate (Lalli and Parsons 1997). The some species can form massive bloom, which can cause harmful effect on the marine environment (Cullen 2008). Because of frequent, large contribution of diatom to marine primary production or marine environment, investigations of diatom have been well carried out in the absorption properties (e.g., Geider and Osborne 1987; Finkel 2001) and the scattering properties (e.g., Reynolds et al. 1997; Stramski et al. 2002). On the other hand, the dinoflagellate have been relatively little studied in both absorption properties (e.g., Johnsen et al. 1994; Leong and Taguchi 2006) and scattering properties due to relatively difficult handling in experimentation. The investigation of the absorption and scattering properties of dinoflagellate can help to ensure the significant relationship between the optical size index and the IOPs of phytoplankton assemblage.

1.3. Absorption properties of phytoplankton as a function of cell size

Size distribution of phytoplankton assemblage in seawater can be estimated from Chl *a* normalized absorption coefficient of phytoplankton ($a^*_{ph}[\lambda]$) which can be calculated from the spectral *R* (Ciotti and Bricaud 2006; Hirata et al. 2008; Brewin et al. 2011). Variation in the $a^*_{ph}(\lambda)$ as a function of cell size are mainly caused by the packaging of phytoplankton pigments such as photosynthetic and photoprotective pigments in the phytoplankton cell (Duysens 1956; Morel and Bricaud 1981; Berner et al. 1989; Kirk 2011). The $a^*_{ph}(\lambda)$ is generally decreasing with increasing cell size (Kirk 2011). The retrieval of the size distribution of phytoplankton from the $a^*_{ph}(\lambda)$ is represented as relative abundance of three size classes; pico-, nano-, and micro-size phytoplankton (Hirata et al. 2008) and single size parameter (Ciotti and Bricaud 2006). According to the intercomparison of the relative abundance between the ocean color remote sensing data and the sea truth data measured by high performance liquid chromatography, the validation of the retrievals is reasonably accurate (more than 70%) in detecting size class of phytoplankton, however the detection of nano-size phytoplankton is generally worse than detections of micro-size and pico-size phytoplankton (Brewin et al. 2011). The size parameter is established that the size parameter varies from 0, where it is dominated by micro-size cells (>20 μm in diameter), to 1, where it is dominated by pico-size cells (<2 μm in diameter) (Ciotti et al. 2002). The detecting size parameter, however, may be proposed as a continuum for co-varying pigments packaging, not to identify the dominant size class of phytoplankton (Brewin et al. 2011). Continuous size index as a function of cell size, which can be constructed by the $a^*_{ph}(\lambda)$ of phytoplankton assemblage, can help to bridge the size effect of phytoplankton cell and the packaging effect. Because there are phytoplankton species with various cell sizes within *in situ* phytoplankton assemblage, the absorption based size index of the

assemblage is required to validate by comparing the $a^*_{ph}(\lambda)$ of mono-species phytoplankton cultures.

Physiological properties of phytoplankton have an influence on the absorption properties of phytoplankton. Particularly, the physiological response to the light intensity just below the surface is one of the essential factors for using ocean color remote sensing. Phytoplankton assemblage in a water column can be exposed to increasing levels of light when they are transported to the surface, and therefore most phytoplankton species contain photoprotective carotenoids to protect against high light levels (Bidigare et al. 1987; Claustre et al. 1994; Brunet et al. 2011). The change in the photoprotective carotenoids in the cell can alter the slope and intercept of the relationship between $a^*_{ph}(\lambda)$ and cell size (Fujiki and Taguchi 2002) because the photoprotective carotenoids can alter the shape of a^*_{ph} spectrum (Hoepffner and Sathyendranath 1991; Johnsen et al. 1994). Conversely, the investigation of the $a^*_{ph}(\lambda)$ as a function of cell size can provide a more accurate estimation of the physical properties of natural assemblage of phytoplankton.

1.4. Scattering properties of phytoplankton as a function of cell size

Bulk scattering coefficient of the particle ($b_p[\lambda]$) is constructed by $b_p(\lambda)$ of the various particles which include living particles, such as bacteria and phytoplankton, and non-living particles, such as detritus and minerals (Morel and Bricaud 1986). The size distribution of those particles can be inversely estimated from the bulk $b_p(\lambda)$ (Stramski and Kiefer 1991; Babin et al. 2003). When the particles are assumed as the homogeneous spherical cell, the variation in $b_p(\lambda)$ as a function of particle size can be accounted for by the Mie theory (van de Hulst 1957). In the oligotrophic waters, the size distribution of the marine particles including phytoplankton is generally similar (Jonasz and Fournier 2007). According to the theoretical assumption based on the Mie theory, the contribution

of large-cell phytoplankton is little in oligotrophic waters because the cell concentration of the large-cell phytoplankton is relatively lower than other particles (Stramski and Kiefer 1991). In coastal water, especially rich in phytoplankton, the size distribution of particles is expected to indicate regional differences due to the large contribution of phytoplankton cell to the bulk $b_p(\lambda)$ (Stramski et al. 2001; Reynolds et al. 2008). In *in situ* seawater, however, the relative contributions of the scattering coefficient of phytoplankton ($b_{ph}[\lambda]$) to bulk $b_p(\lambda)$ are experimentally difficult to ascertain because of the great diversity of the particles and size scaling of the particles (Stramski and Kiefer 1991). Since only phytoplankton have Chl *a* within the particle assemblage, Chl *a* normalized $b_p(\lambda)$ ($b^*_p[\lambda]$) may be characterized in the bulk $b_p(\lambda)$. When the size scaling exponent of marine particles as a power law is assumed as similar to the phytoplankton cells, continuous size index as a function of cell size, which can be constructed by Chl *a* normalized scattering coefficient of phytoplankton ($b^*_{ph}[\lambda]$), can help to evaluate the size effect of the marine particles as well as the phytoplankton cells. Because the relative contribution of the $b^*_{ph}(\lambda)$ to bulk $b^*_p(\lambda)$ is uncertain, the scattering based size index of the phytoplankton assemblage is required to validate by comparing the $b^*_{ph}(\lambda)$ of mono-species phytoplankton cultures.

Bulk $b_p(\lambda)$ in seawater has been shown to convey with the POC concentration (DuRand and Olson 1996; Loisel and Morel 1998). In *in situ* seawater, cellular carbon contents of phytoplankton are included in the POC. In previous study, the ratio of cellular carbon to Chl *a* (C:Chl *a*) of phytoplankton in culture can be dependent on the grown conditions, such as light, nutrient, and temperature (Geider et al. 1997; MacIntyre et al. 2002). The C:Chl *a* is one of the index of phytoplankton physiology to be utilized to monitor the phytoplankton growth (Behrenfeld and Boss 2003) and the carbon-based primary production from ocean color remote sensing (Behrenfeld et al. 2005). However the utilizable C:Chl *a* as the physiological index could be consistently estimated

from the surrounding conditions (Geider 1987). If the C:Chl *a* of phytoplankton can be directly estimated from the scattering properties of phytoplankton, the estimates can provide a more accurate estimation of the physical properties of natural assemblage of phytoplankton.

1.5. Aims and scopes of the thesis

I investigated the relationships between cell size and IOPs of dinoflagellates in culture in relation to published data (Chapter II). The cell size was employed to an average equivalent cell diameter of mono-phytoplankton species. The investigation was attempted to understand the size effect on the IOPs of micro-size and nano-size phytoplankton. Secondly, I investigated the relationships between the optical size index and IOPs of natural assemblage of phytoplankton (Chapter III). The optical weighting functions of three cell size classes were determined from the cultural relationship between cell size and IOPs of phytoplankton. The optical size index was calculated from the relative Chl *a* abundances and the optical weighting functions. I validated the size index of natural assemblages of phytoplankton by comparing the cultural and *in situ* experiments. A further motivation for this study was that physiological properties of natural assemblage of phytoplankton, such as photoprotective carotenoids and C:Chl *a*, could be estimated from IOPs of phytoplankton. The photoprotective carotenoids could be utilized to evaluate the relationship between the absorption properties of phytoplankton and the cell size. The C:Chl *a* could be utilized to evaluate the relative contribution of phytoplankton to the bulk marine particles.

1.6. Structure of the thesis

For the sake of simplicity, this thesis including this general introduction and review has been divided into four chapters. In this chapter, the reviews of the ocean color remote sensing for

monitoring the size distribution of phytoplankton have been presented and the aims of the present study have been explained. In the second chapter, studies on the absorption and scattering properties of micro-size and nano-size mono-cultured dinoflagellates have been presented. In the third chapter, the absorption and scattering properties of micro-size and nano-size phytoplankton assemblages in the Indian sector of the Southern Ocean and in Sagami Bay have been presented. Finally, in the fourth chapter, a summary of the absorption and scattering properties of phytoplankton as a function of cell size has been explained and requirements for future research are highlighted.

CHAPTER II

ABSORPTION AND SCATTERING PROPERTIES OF DINOFLAGELLATES

2.1. Introduction

Inherent optical properties (IOPs), such as absorption (*a*) and scattering coefficient (*b*), of marine phytoplankton have been investigated for utilizing ocean color remote sensing, in particular with the monitoring of size distribution of phytoplankton assemblage (e.g., Finkel 2001; Ciotti et al. 2002; Babin et al. 2003; Brewin et al. 2011). The monitoring of the size distribution of phytoplankton by ocean color remote sensing basically relies on the *in vivo* absorption and/or scattering efficiency of living phytoplankton cells as a function of cell size. Chlorophyll *a* (Chl *a*) is primary pigments of phytoplankton and the concentration could be detected by ocean color remote sensing, and therefore Chl *a* specific absorption and scattering of phytoplankton ($a^*_{ph}[\lambda]$ and $b^*_{ph}[\lambda]$) could be utilized to evaluate the *in vivo* absorption and scattering efficiency, respectively. The investigation of the effect of the cell size on the optical efficiencies of phytoplankton could assist to monitor the size distribution of phytoplankton assemblage. For the estimation of the size distribution of phytoplankton assemblage, the bloom-forming phytoplankton with large cell size (>2 μm in diameter) could have significant influence on the variation in size distribution of phytoplankton (Stramski et al. 2001).

Most of the bloom-forming phytoplankton species with large-cell size are diatoms and dinoflagellates (Malone 1980; Lalli and Parsons 1997). Because of the frequent occurrence in marine environment, the optical properties of diatoms have been well investigated (e.g., Geider and Osborne 1987; Reynolds et al. 1997; Stramski et al. 2002), in particular with the $a^*_{ph}(\lambda)$ (Finkel 2001; Fujiki and Taguchi 2002) and the $b^*_{ph}(\lambda)$ as a function of cell size (Morel 1987). However,

the investigation of dinoflagellate has been limited due to relatively difficult handling in experimentation. In addition to the large-cell size, the dinoflagellates have a large intracellular carbon contents compared with other species of a similar cell size, and generally indicate a high ratio of cellular carbon to Chl *a* (C:Chl *a*) (Chan 1980; Tang 1996). The C:Chl *a* is fundamental properties of phytoplankton physiology (Geider 1987; MacIntyre et al. 2002). The relationship between the C:Chl *a* and the optical properties of dinoflagellate could assist to estimate the size distribution of phytoplankton assemblage.

Dinoflagellates *Prorocentrum* species is one of the most common, harmful algae that increase globally in frequency, magnitude, and distribution (Heil et al. 2005; Glibert et al. 2012). The spectral characteristics of the $a^*_{ph}(\lambda)$ are investigated for the optical monitoring of the *Prorocentrum* species (Johnsen et al. 1994). The spectral distribution of the $a^*_{ph}(\lambda)$ is characterized by the absorption peaks by dinoflagellate-specific carotenoid, peridinin (Millie et al. 1997). Although the spectral characteristics of the $a^*_{ph}(\lambda)$ of dinoflagellate are well known, the $a^*_{ph}(\lambda)$ as a function of cell size of dinoflagellate has been uncertain compared with the other species. Since there is the natural assemblage of dinoflagellates with various cell size, the size effect of dinoflagellate on the $a^*_{ph}(\lambda)$ could assist to monitor the dinoflagellates. Among *Prorocentrum* species, the *P. micans* and *P. minimum* are in similar cell shape with different cell size and can form the high-biomass blooms in the surface waters (Glibert et al. 2012). Because the scattering efficiency of phytoplankton could be dependent on the geometrical characteristic of the cell, such as the cell size and shape (Stramski and Kiefer 1991), the investigation of the $b^*_{ph}(\lambda)$ with different cell size and similar cell shape could assist to evaluate the size effect. The investigation of the $a^*_{ph}(\lambda)$ and $b^*_{ph}(\lambda)$ of *P. micans* and *P. minimum* can help to ensure the variation in the IOPs of phytoplankton as a function of cell size.

The effect of cell size on the $a^*_{ph}(\lambda)$ is well recognized as package effect of phytoplankton pigments (e.g., Morel and Bricaud 1981; Kirk 2011). The package effect is caused by pigment self-shading in the cell (Berner et al. 1989). The pigment packaging is enhanced by the cell volume, and therefore phytoplankton with large cell could be strongly influenced (Woźniak and Dera 2007; Kirk 2011). In fact, the spectrally averaged $a^*_{ph}(\lambda)$ decreases significantly with increasing cell size (Finkel 2001). The package effect could be enhanced by not only the cell size but also intracellular pigment concentration (Kirk 2011). Generally the intracellular concentration decreases with increasing cell size (Malone 1980; Finkel et al. 2004). However, the intracellular pigment concentration could covary with not only cell size but also the growth conditions, such as light (MacIntyre et al. 2002). In such case, products of the equivalent spherical diameter (d) and intracellular Chl a concentration (Chl a_i, d×Chl a_i) could be employed to evaluate the $a^*_{ph}(\lambda)$ in relation to the package effect (Woźniak and Dera 2007). Thus, to ensure the effect of cell size on the $a^*_{ph}(\lambda)$, the interrelationships among $a^*_{ph}(\lambda)$, cell size, intracellular pigment concentration, and d×Chl a_i are warranted. In addition, the dimensionless efficiency factor of absorption ($Q_a[\lambda]$) is experimentally calculated from d, Chl a_i, and $a^*_{ph}(\lambda)$. The $Q_a(\lambda)$ is the ratio of the propagation light absorbed from the phytoplankton cell to the light impinging on the geometrical cross section of the cell (Morel and Bricaud 1986). The $Q_a(\lambda)$ can be theoretically estimated from the optical thickness.

The scattering process of phytoplankton in water is influenced by cell size, refractive or reflective contents, such as intracellular carbon (C_i), and absorptive contents, such as Chl a_i (Stramski 1999). The products of $b^*_{ph}(\lambda)$ and Chl a_i ($b^*_{ph}[\lambda]$ × Chl a_i) are mainly dependent on the gepmetrical characteristics of cell, such as cell size and refractive index (Morel and Bricaud 1986). According to theoretical analysis based on the anomalous diffraction approximation (van de Hulst 1957), the association between the real part of the refractive index (m; relative refraction to water)

of phytoplankton and $b^*_{ph}(\lambda) \times$ Chl a_i is sensitive for small cells (d < 10 μm), but insensitive for large cells (d > 15 μm) (Morel 1987). The $b^*_{ph}(\lambda)$ of the small cells has been previously investigated (e.g., Bricaud et al. 1983; Stramski et al. 1993; Reynolds et al. 1997; DuRand et al. 2002). A few studies on the $b^*_{ph}(\lambda)$ based on wide range of cell size including the large cells indicate that the $b^*_{ph}(\lambda)$ of large cells could be low compared with those for small cells (Morel and Bricaud 1986; Ahn et al. 1992). However, the $b^*_{ph}(\lambda)$ could be variable due to the dependence of the cell structure on $b^*_{ph}(\lambda)$.

Large cell diatoms indicate experimentally high $b^*_{ph}(\lambda)$ because of the mineralized cell walls (Morel and Bricaud 1986; Kirk 2011). Large cell diatoms indicate experimentally high $b^*_{ph}(\lambda)$, for example, the $b^*_{ph}(590)$ of large cell diatoms *Chaetoceros lauderi* with 25.5 μm in diameter was about 3-fold higher than that of small naked flagellate *Isochrysis galbana* with 4.2 μm in diameter, maybe due to the mineralized cell wall (Morel and Bricaud 1986; Kirk 2011). The dinoflagellates have a large C_i compared with other species of a similar cell size, and generally indicate a high C:Chl *a* (Chan 1980; Tang 1996). The high C:Chl *a* is expected to induce a high $b^*_{ph}(\lambda)$; however the $b^*_{ph}(\lambda)$ as a function of C:Chl *a* is not evaluated yet. In addition, the efficiency factors for scattering ($Q_b[\lambda]$) is experimentally calculated from d, Chl a_i, and $b^*_{ph}(\lambda)$. The $Q_b(\lambda)$ is the ratio of the propagation light scattered from the phytoplankton cell to the light impinging on the geometrical cross section of the cell (Morel and Bricaud 1986). The $Q_b(\lambda)$ as a function of cell size can be theoretically estimated based on the Mie theory when the cell is assumed as the homogeneous spherical cell (van de Hulst 1957). Since change in the $Q_b(\lambda)$ depends on the intracellular materials (Aas 1996), the $Q_b(\lambda)$ of the dinoflagellates could be high due to the high C:Chl *a*.

To ensure the effect of cell size on the IOPs of phytoplankton, the absorption and scattering

properties of dinoflagellates *P. micans* and *P. minimum* with different cell sizes and C:Chl *a* were investigated. The absorption and scattering properties of *P. micans* and *P. minimum* were investigated under two light conditions which were the saturated and supra-saturated light conditions, respectively. The two light intensities could induce the difference in C:Chl *a* (MacIntyre et al. 2002). The scattering properties as a function of C:Chl *a* could provide a high accuracy for the estimation of the scattering efficiency of phytoplankton. To evaluate the absorption and scattering properties, I adopted a wavelength at 676nm where is the absorption peak by Chl *a* and is least influenced by the pigments other than Chl *a* (Agustí 1991a). The absorption and scattering properties of dinoflagellates with different cell size and C:Chl *a* could assist to ensure the effect of cell size on the absorption and scattering efficiency of phytoplankton.

2.2. Materials and methods

2.2.1. Culture and growth conditions

Dinoflagellates *Prorocentrum micans* Ehrenberg (NIES-218) and *P. minimum* Pavillard (NIES-237) were obtained from the microbial culture collection at National Institute for Environmental Study (NIES), Japan. All cultures were grown in 4L sterilized screw-top polycarbonate bottles at 20°C, 35 PSU salinity in f/2 medium (Guillard and Ryther 1962) without silicate using aged filtered sea water collected from Sagami Bay, Japan. The irradiance of 600 μmol photons m^{-2} s^{-1} (HL) and 300 μmol photons m^{-2} s^{-1} (LL) were provided by cool fluorescent lamps (Panasonic Corporation, Osaka, Japan) on a 12:12 hours light dark cycle. To acclimate phytoplankton to the growth conditions prior to the experiment, the cells were preconditioned in the semi-continuous culture by transferring half of the volume every 2 days. In the middle of the exponential growth phase (usually day 2), subsamples were taken from each experimental bottle at the mid-point of the light phase.

2.2.2. Equivalent spherical diameter

Subsamples were centrifuged for 10 minutes at 4,000 rpm and resuspended in 300μL filtered sea water which were filtered through 0.22μm pore size membrane filter. A shape of *P. micans* and *P. minimum* was assumed to be ellipsoid. The cell volume (V; μm^3) of fifty cells in the suspension was measured under a microscope (LH50A, Olympus, Tokyo, Japan) with an ocular ruler calibrated a micrometer and calculated using the following formulae described by Hillebrand et al. (1999):

$$V = (\pi/6)lth \quad (2.1)$$

where l is the apical axis (length), t is the trans-apical axis (width), h is height, and π refers to the circular constant. The mean d (μm) was calculated from V, assuming that the cells were spherical.

2.2.3. Intracellular chlorophyll *a* and carbon contents

Subsamples for cellular pigment analysis were filtered onto 25mm Whatman glass fiber filters (Whatman type GF/F, GE healthcare UK limited, Buckinghamshire, UK) and stored at –80°C until analysis. The cells which were collected on the filters were homogenized in 2ml of 90% acetone into a 15ml centrifuge tube on ice using an ultrasonic homogenizer (UH-50, SMT Co., Ltd., Tokyo, Japan) and allowed to extract in the dark at –20°C for 24h. The extract was then centrifuged at 1,000 rpm for 5min and the surpernatant were filtered through a 0.20μm filter unit (Millex-LG, Merck Millipore, Billerica, MA, USA). Finally the extracts were run on a high performance liquid chromatography (168 Diode Array Detector, C18 reversed-phase Ultrasphere 3 mm column; Beckman Coulter Instruments, Inc., Fullerton, CA, USA) using a solvent gradient system with solvent A (80% methanol and 20% 0.5M [v/v] ammonium acetate) and solvent B (70% methanol and 30% ethyl acetate) described by Wright et al. (1997). The peaks were quantified using pure Chl

a standard from Danish Hydraulic Institute. Intracellular Chl *a* contents (Chl a_i; kg Chl *a* m^{-3}) were estimated by dividing cellular Chl *a* concentration by cell volume.

Subsamples for cellular carbon analysis were filtered onto 25mm Whatman GF/F filter (Whatman type GF/F; GE healthcare UK limited, Buckinghamshire, UK) pre-combusted at 500°C for 2 hours. Cells on filters were oven-dried at 60°C for 24 hours and stored in a desiccator until analysis. Particulate organic carbon was measured using an elemental analyzer (FlashEA 1112, Thermo Fisher Scientific, MA, USA). Cellular carbon concentrations were determined using acetanilide as the standard (Nagao et al. 2001). Intracellular carbon contents (C_i; kg C m^{-3}) were estimated by dividing the cellular carbon concentration by cell volume. The ratio of cellular carbon to cellular Chl *a* contents (C:Chl *a*) was calculated based on a weight basis.

2.2.4. Absorption properties

The absorption coefficient of phytoplankton was measured by quantitative filter technique (QFT) (Mitchell and Kiefer 1988). Subsamples were filtered onto 25mm Whatman glass fiber filters (Whatman type GF/F; GE healthcare UK limited, Buckinghamshire, UK), and its absorption spectra were directly scanned from 300nm to 800nm by using the dual beam UV-visible spectrophotometer equipped with an integrating sphere (UV-2450, Shimazu corporation, Kyoto, Japan). Filters which were moistened with filtered sea water were used as the reference. Optical density spectra of filtered particles (OD_f) were recorded and corrected for the scattering by subtracting the OD_f between 730nm and 760nm (Babin and Stramski 2002). For conversion of the absorption from OD_f to particles in suspension (OD_s), the following equation of Cleveland and Weidemann (1993) was employed:

$$OD_s(\lambda) = 0.378OD_f(\lambda) + 0.523(OD_f[\lambda])^2 \quad (2.2).$$

The absorption coefficient of particle ($a_p[\lambda]$) was calculated by the following equation:

$$a_p(\lambda) = 2.303\ OD_s(\lambda)\ Sf\ Vf^{-1} \quad (2.3)$$

where the factor 2.303 converts $\log_{10}$ to $\log_e$, Vf is the filtered volume, and Sf is the filtered clearance area. Following measurement of the $OD_f(\lambda)$, filters were immerged in 100% methanol for pigment extraction for 24 h using the method of Kishino et al. (1985) and the de-colorized filters were moistened with filtered seawater. The filter pads were used to measure the absorption spectra of non-pigmented particles ($a_d[\lambda]$). The difference between particulate and non-pigmented particles absorption coefficients was considered to be the absorption coefficient of phytoplankton pigments ($a_{ph}[\lambda]$):

$$a_{ph}(\lambda) = a_p(\lambda) - a_d(\lambda) \quad (2.4).$$

The chlorophyll *a* specific absorption coefficient of phytoplankton ($a_{ph}^*[\lambda]$) was obtained using the equation:

$$a^*_{ph}(\lambda) = a_{ph}(\lambda)\ [\text{Chl } a]^{-1} \quad (2.5)$$

where [Chl *a*] is the concentration of Chl *a* in mg m^{-3}.

The cell specific absorption coefficient of phytoplankton ($a_{cell}[\lambda]$) was obtained using the equation:

$$a_{cell}(\lambda) = a_{ph}(\lambda)\ [N]^{-1} \quad (2.6)$$

where [N] is the cell density in cells m^{-3}. The experimental efficiency factor for absorption ($Q_a[\lambda]$) was defined as follows (Morel and Bricaud 1986):

$$a_{ph}(\lambda) = Q_a(\lambda)\ [N]\ s \quad (2.7)$$

where s is cross sectional area in m^2. The Chl *a* concentration in suspension ([Chl *a*]) was linked to intracellular Chl *a* concentration (Chl a_i) as follows:

$$[\text{Chl } a] = [N]\ \text{Chl } a_i\ V \quad (2.8).$$

By assuming that the phytoplankton cells are spherical with a diameter d, the $Q_a(\lambda)$ was calculated from the equations as follows:

$$Q_a(\lambda) = a_{cell}(\lambda)\ s^{-1} = 4\ a_{cell}(\lambda)\ \pi^{-1}\ d^{-2} \quad (2.9)$$

or

$$Q_a(\lambda) = a_{ph}(\lambda)\ [\text{Chl } a]^{-1}\ \text{Chl } a_i\ V\ s^{-1} = (2/3)\ a^*_{ph}(\lambda)\ d\ \text{Chl } a_i \quad (2.10).$$

Package effect index at 676nm (Q_a*[676]) was calculated as follows:

$$Q_a^*(676) = a^*_{ph}(676)\ a_{cm}(676)^{-1} \quad (2.11)$$

where $a_{cm}(676)$ is unpackaged Chl *a* specific absorption coefficient at 676nm which is assumed as 0.027 m^2 mg Chl *a* (Johnsen et al. 1994).

Compared with the experimental $Q_a(\lambda)$, theoretical efficiency factor for absorption ($Q_a[\rho']$) was calculated as follows:

$$Q_a(\rho') = 1+2\exp(-\rho')(\rho')^{-1} + 2[(\exp(-\rho') -1]\ \rho'^{-2} \quad (2.12)$$

where ρ' is the optical thickness of absorption. The ρ' at 676nm was calculated as follows:

$$\rho'(676) = a_{cm}(676)\ d\ \text{Chl } a_i \quad (2.13).$$

Theoretical package effect index at 676nm (Q_a*[ρ']) was calculated as follows:

$$Q_a^*(\rho') = (3/2)\ Q_a(\rho')\ \rho'^{-1} \quad (2.14).$$

2.2.5. Scattering properties

Scattering coefficient of phytoplankton ($\underline{b}_{ph}[\lambda]$, where underline indicates coefficient measured by absorption and attenuation meter [ac-9]) at nine wavelength (412, 440, 488, 510, 532, 555, 650, 676, and 715nm) was calculated as the difference between $\underline{c}_{ph}(\lambda)$ and $\underline{a}_{ph}(\lambda)$:

$$\underline{b}_{ph}(\lambda) = \underline{c}_{ph}(\lambda) - \underline{a}_{ph}(\lambda) \quad (2.15).$$

The $\underline{c}_{ph}(\lambda)$ and $\underline{a}_{ph}(\lambda)$ at nine wavelength were measured by ac-9 with a 25cm pathlength (WET

Labs, OR, USA). The absorption and attenuation coefficient of the phytoplankton suspension was measured by the reflective and non-reflective flow tubes, respectively. The ac-9 was set up as a bench-top instrument in a fixed tilt position at 45° to avoid trapping air bubbles in the flow tubes (Wet Labs, Inc. 2008). Two reservoirs were attached with tubing to the inlet and outlet of the flow tubes, and the phytoplankton suspension was pumped by peristaltic pump (Tokyo Rikakikai Co. Ltd., Tokyo, Japan). The data measured in the reflective and non-reflective flow tubes were monitored to ensure the absence of air bubbles, and then the data were averaged for at least 3 min. Cell densities of the phytoplankton suspension were ensured to be within the linear range of the relationships between the cell densities, the absorption, and/or the attenuation coefficients. Temperature and salinity correction of absorption and attenuation coefficients measured by ac-9 were applied to account for the difference between the phytoplankton suspension and pure water using the following equations (Pegau et al. 1997):

$$\underline{a}_{mt}(\lambda) = \underline{a}_{m}(\lambda) - (\psi_t[\lambda][T - T_r] + \psi_s[\lambda][S - S_r]) \quad (2.16)$$

and

$$\underline{c}_{mt}(\lambda) = \underline{c}_{m}(\lambda) - (\psi_t[\lambda][T - T_r] + \psi_s[\lambda][S - S_r]) \quad (2.17)$$

where $\underline{a}_{mt}(\lambda)$ is temperature- and salinity-corrected absorption coefficient of the phytoplankton suspension, $\underline{a}_{m}(\lambda)$ is measured absorption coefficient of the phytoplankton suspension, ψ_t is the linear temperature dependence of pure water, ψ_s is the linear salinity dependence of saltwater, T is the temperature of the sample, T_r is the temperature of the pure water for calibration, S is the salinity of the phytoplankton suspension, S_r is the salinity of the pure water ($S_r = 0$), $\underline{c}_{mt}(\lambda)$ is temperature- and salinity-corrected attenuation coefficient of the phytoplankton suspension, and $\underline{c}_{m}(\lambda)$ is measured attenuation coefficient of the phytoplankton suspension (Pegau et al. 1997). The temperature and salinity of the phytoplankton suspension were monitored using a thermometer and

a light refraction salinometer, respectively. To remove the effect of the backscattering by cells in the reflective flow tube, the absorption coefficients were corrected by subtracting $\underline{a}_{mt}(715)$ from all wavelengths (Zaneveld et al. 1994). As the references, the phytoplankton suspension was filtered by 0.22 μm pore size membrane filter (Millex-LG; Merck Millipore, Billerica, MA, USA). The absorption and attenuation coefficient of references ($\underline{a}_{ref}[\lambda]$ and $\underline{c}_{ref}[\lambda]$) were measured by ac-9 and were corrected for the effect of temperature, salinity and backscattering as well as the phytoplankton suspension. Finally, the $\underline{a}_{ph}(\lambda)$ and $\underline{c}_{ph}(\lambda)$ were calculated by subtracting $\underline{a}_{ref}(\lambda)$ and $\underline{c}_{ref}(\lambda)$ from the $\underline{a}_{mt}(\lambda)$ and $\underline{c}_{mt}(\lambda)$, respectively.

The chlorophyll *a* specific scattering coefficient of phytoplankton ($\underline{b}_{ph}^*[\lambda]$) at each wavelength was obtained using the equations:

$$\underline{b}^*_{ph}(\lambda) = \underline{b}_{ph}(\lambda)\,[\text{Chl } a]^{-1} \tag{2.18}$$

The cell specific scattering coefficient of phytoplankton ($\underline{b}_{cell}[\lambda]$) was obtained using the equation:

$$\underline{b}_{cell}(\lambda) = \underline{b}_{ph}(\lambda)\,[\text{N}]^{-1} \tag{2.19}$$

The experimental efficiency factor for scattering ($Q_b[\lambda]$) was calculated as well as $Q_a(\lambda)$ (Morel and Bricaud 1986):

$$Q_b(\lambda) = \underline{b}_{cell}(\lambda)\,s^{-1} = 4\,\underline{b}_{cell}(\lambda)\,\pi^{-1}\,d^{-2} \tag{2.20}$$

or

$$Q_b(\lambda) = \underline{b}_{ph}(\lambda)\,[\text{Chl } a]^{-1}\,\text{Chl } a_i\,V\,s^{-1} = (2/3)\,\underline{b}^*_{ph}(\lambda)\,d\,\text{Chl } a_i \tag{2.21}$$

Compared with the experimental $Q_b(\lambda)$, theoretical efficiency factor for scattering ($Q_b[\rho', \rho]$) was estimated by subtracting the $Q_a(\rho')$ from the theoretical efficiency factor of attenuation ($Q_c[\rho]$) as follows (van de Hulst 1957):

$$Q_b(\rho',\rho) = Q_c(\rho) - Q_a(\rho') \tag{2.22}$$

$$Q_c(\rho) = 2 - 4\exp(-\rho\tan\zeta)(\cos\zeta\,\rho^{-1}\sin[\rho-\zeta] + [\cos\zeta\,\rho^{-1}]^2\cos[\rho-2\zeta])$$

$$+ 4 (\cos\zeta \rho^{-1})^2 \cos 2\zeta \quad (2.23)$$

where ρ is the phase lag suffered by the ray which cross the sphere along its diameter and tan ζ is defined as the ratio of $0.5 \rho'$ to ρ. The ρ is calculated from as follows:

$$\rho = 4\alpha (m-1) \quad (2.24)$$

where α is the size parameter for examining the interaction with an electromagnetic wave, m is the relative refractive index to water. The α is defined as follows:

$$\alpha = \pi d \lambda^{-1} \quad (2.25).$$

2.2.6. Published data

Previously published data of d, Chl a_i, and $a^*_{ph}(676)$ of large phytoplankton species with > 2 μm in diameter (4 class, 13 species) were obtained by Finkel (2001), Fujiki and Taguchi (2002), and Leong and Taguchi (2006) (Table 2-1). The $Q_a(676)$ and $Q^*_a(676)$ of those phytoplankton species were calculated form following equation (2.10) and (2.11), respectively (Table 2-1).

Previously published data of d, Chl a_i, and $b^*_{ph}(676)$ of large phytoplankton species with > 2 μm in diameter (7 class, 22 species) were obtained by Bricaud et al. (1983), Morel and Bricaud (1986), Bricaud et al. (1988), Osborne and Geider (1989), Ahn et al. (1992), Stramski et al. (1993), and Motokawa and Taguchi (2015) (Table 2-2). The d, Chl a_i and $b^*_{ph}(676)$ of chlorophyte *Dunaliella tertiolectra* were obtained under fluctuating high light and constant high light conditions (Stramski et al. 1993) (Table 2-2). The C_i was calculated from the d following Strathmann (1967) (Table 2-2). The $Q_b(676)$ of those phytoplankton species were calculated from following equation (2.21) (Table 2-2).

2.2.7. Statistics

Differences in the optical properties among species and light conditions were tested with a Student's *t*-test.

2.3. Results

2.3.1. Cell size and intracellular Chl *a* and carbon contents

The *d* indicated an approximately 2-fold difference between the large cell *Prorocentrum micans* and the small cell *P. minimum*, whereas the *d* did not differ between HL and LL within the same species (Table 2-3). Mean ± one standard deviations of the *d* of *P. micans* and *P. minimum* were 25.0 ± 0.22 μm and 12.6 ± 0.24 μm, respectively.

The Chl a_i of both *P. micans* and *P. minimum* exhibited a 1.5-fold difference between the two light conditions, whereas the C_i did not differ between the light conditions (Table 2-3). The Chl a_i of large cell *P. micans* at HL and LL were 30% and 37% lower than those of *P. minimum*, respectively (Table 2-3). The small cell *P. minimum* indicated a 1.7-fold higher C_i compared with large cell *P. micans* (Table 2-3).

The product *d*×Chl a_i of *P. micans* and *P. minimum* at HL were 30% and 40% lower than those at LL, respectively (Table 2-3). The product *d*×Chl a_i of *P. micans* at HL and LL were 42% and 23% higher than those of *P. minimum*, respectively (Table 2-3). The Chl a_i indicated a reverse trend to the *d*, whereas *d*×Chl a_i indicated a similar trend to the *d* (Table 2-3).

The C:Chl *a* (g g^{-1}) of the small cell *P. minimum* exhibited a stronger influence of irradiance on the reduction in cellular Chl *a* and consequently a 1.7-fold higher C:Chl *a* under HL compared with LL (Table 2-3). The large cell *P. micans* indicated a 1.5-fold higher C:Chl *a* under HL compared with LL (Table 2-3).

2.3.2. Absorption properties

Spectra of a^*_{ph} of *P. micans* and *P. minimum* exhibited the peaks at around 440 and 676nm (Figure 2-1). The $a^*_{ph}(\lambda)$ of *P. micans* and *P. minimum* at HL were higher than that at LL in blue-green regions (approximately from 440 nm to 510nm) and red region (surrounding 676nm), whereas the $a^*_{ph}(\lambda)$ in the other regions was similar between *P. micans* and *P. minimum* (Figure 2-1). The higher $a^*_{ph}(\lambda)$ at HL than that at LL, and the higher $a^*_{ph}(\lambda)$ of *P. minimum* than that of *P. micans* clearly exhibited at 676nm (Figure 2-1).

The $a^*_{ph}(676)$ of *P. micans* and *P. minimum* at HL were 1.3- and 1.1-folds higher than that at LL, respectively (Table 2-4). The $a^*_{ph}(676)$ of *P. micans* at HL and LL were 22% and 11% lower than that of *P. minimum*, respectively (Table 2-4). The $a_{cell}(676)$ did not differ between HL and LL within the same species, whereas *P. micans* indicated 3.2-fold higher $a_{cell}(676)$ than *P. minimum* (Table 2-4). The $Q_a(676)$ did not differ among species and light conditions (Table 2-4). The relationships between species and light conditions were same as the $a^*_{ph}(676)$ (Table 2-4).

2.3.3. Scattering properties

As measured by ac-9, spectra of $\underline{c}^*_{ph}(\lambda)$ of both *P. micans* and *P. minimum* indicated a power law relationship with the visible wavelength (Figure 2-2). Spectra of $\underline{a}^*_{ph}(\lambda)$ of both *P. micans* and *P. minimum* indicated the maximum at 676nm and increased with shorter wavelength (Figure 2-2). As a result of difference between the $\underline{c}^*_{ph}(\lambda)$ and the $\underline{a}^*_{ph}(\lambda)$, spectra of $\underline{b}^*_{ph}(\lambda)$ of both *P. micans* and *P. minimum* represented the presence of a minimum at 676nm and increased with shorter wavelength (Figure 2-2). The $\underline{b}^*_{ph}(\lambda)$ of *P. micans* and *P. minimum* at HL were higher than those at LL, and the $a^*_{ph}(\lambda)$ of *P. minimum* were higher than those of *P. micans* at both light conditions. The differences in $\underline{b}^*_{ph}(\lambda)$ among species and light conditions clearly exhibited at 676nm (Figure 2-2).

The $\underline{b}^*_{ph}(676)$ did not differ between HL and LL within the same species, whereas the $\underline{b}^*_{ph}(676)$ of small cell *P*. *minimum* indicated a 1.6-fold higher than that of large cell *P*. *micans* (Table 2-5). Both species indicated a 1.4-fold higher $\underline{b}_{cell}(676)$ under LL compared with HL (Table 2-5). The large cell *P*. *micans* indicated a 3.4-fold higher $\underline{b}_{cell}(676)$ than *P*. *minimum* (Table 2-5). The $Q_b(676)$ did not differ between large cell *P. micans* and small cell *P. minimum* under the same light conditions, whereas both species indicated about 1.2-fold higher $Q_b(676)$ under LL compared with HL (Table 2-5).

2.4. Discussion

The higher Chl a_i and C_i of the small cell *P*. *minimum* than those of *P*. *micans* confirm previous findings that the cell size of phytoplankton is inversely correlated with Chl a_i (Malone 1980; Finkel et al. 2004) and C_i (Vaillancourt et al. 2004). At a given irradiance, decreasing Chl a_i as a function of *d* of *P*. *micans* and *P*. *micans* is similar to those observed for other species including diatoms (Finkel et al. 2004). According to the relationship between *d* and C_i in previous studies, the C_i of both species is higher than diatoms because the carbon contents of dinoflagellates are significantly denser than those of diatoms (Strathmann 1967; Menden-Deuer and Lessard 2000). The dependence of C:Chl *a* on irradiance has been suggested to reflect photoacclimation due to the change in cellular Chl *a* content (Geider 1987; MacIntyre et al. 2002). The C:Chl *a* of dinoflagellates is considerably higher compared with other species of a similar cell size (Tang 1996) because of the high carbon contents, including proteins (Chan 1980; Hitchcock 1982). The difference in C:Chl *a* in phytoplankton species could be determined by intracellular materials other than protein, such as carbohydrates and pigments, and cell structures, such as the cell wall and vacuoles. The difference in those constituents of phytoplankton cells could influence the real part of the *m* of phytoplankton

cells (Aas 1996). The significant relationship between C_i and the real part of the *m* is held for a variety of some phytoplankton species (Reynolds et al. 1997; Stramski 1999; DuRand et al. 2002), whereas the C:Chl *a* and the real part of the *m* has not been evaluated. Changes in C:Chl *a* might influence the real part of the *m*. Because the C:Chl *a* could represent the physiological state of phytoplankton, such as photoacclimation (MacIntyre et al. 2002), the real part of the *m* could raise the possibility of an estimation of the physiological state from the scattering properties. Further investigation of the relationship between C:Chl *a* and the *m* is warranted.

Lower $a^*_{ph}(676)$ of *P. micans* than *P. minimum* is simply due to 2-fold difference in *d* because of the lower Chl a_i of *P. micans* than *P. minimum* at both light conditions. The low $a^*_{ph}(676)$ of *P. micans* is represented by the low $Q_a^*(676)$. As a result of the large *d*, the higher $d \times$Chl a_i of *P. micans* than those of *P. minimum* suggests that larger cells increase the self-shading of pigments in comparison to smaller cells regardless of the decreasing Chl a_i with increasing cell size (Morel and Bricaud 1981; Agustí 1991b). In the previous study, the $a^*_{ph}(676)$ of micro-size phytoplankton ranges from 0.0059 m^2 mg Chl a^{-1} to 0.025 m^2 mg Chl a^{-1}, and the $a^*_{ph}(676)$ of nano-size phytoplankton ranges from 0.0075 m^2 mg Chl a^{-1} to 0.028 m^2 mg Chl a^{-1} (Table 2-1). Although the similar cell sizes exhibit a half order of the variation in $a^*_{ph}(676)$, the $a^*_{ph}(676)$ of various species significantly decrease with increasing *d* (Table 2-6, Figure 2-3A). The negative relationship between *d* and $a^*_{ph}(676)$ suggests that the package effect on the $a^*_{ph}(676)$ increases with the cell size regardless of the differences in the Chl a_i and species of phytoplankton (Figure 2-3A). On the other hand, the $a^*_{ph}(676)$ of various species did not indicate significant relationship with Chl a_i (Table 2-6, Figure 2-3B). When $a^*_{ph}(676)$ are plotted against $d \times$Chl a_i, it indicates significant correlation (Table 2-6, Figure 2-4). The establishment of the relationship between $d \times$Chl a_i and $a^*_{ph}(676)$ suggests that the $d \times$Chl a_i could be employed to evaluate the variation in the

$a^*_{ph}(676)$ under various light conditions.

Experimentally calculated $Q_a(676)$ from d, Chl a_i, and $a^*_{ph}(676)$ increase exponentially with increasing d×Chl a_i as well as the theoretical $Q_a(\rho')$ (Figure 2-5A). And the experimental $Q_a^*(676)$ decrease exponentially with increasing d×Chl a_i as well as the theoretical $Q_a^*(\rho')$ (Figure 2-5B). The theoretical $Q_a^*(\rho')$ are estimated based on the assumption that the particles are not only externally homogeneous, but also internally homogeneous particle which the intracellular materials, such as pigments, are distributed evenly. Thus the lower experimental $Q_a^*(676)$ than theoretical $Q_a^*(\rho')$ confirm that increasing package effect might be caused by not only cell size and intracellular pigment concentration, but also the intracellular structure, such as thylakoid membranes.

The trend in the $\underline{b}_{cell}(676)$ of the large cell *P. micans* and the small cell *P. minimum* confirms dependence of the $\underline{b}_{cell}(676)$ on the cell volume, as suggested by Stramski et al. (2001). The reverse trend of $\underline{b}^*_{ph}(676)$ and $\underline{b}_{cell}(676)$ with cell volume could reflect the reverse relationship between cell size and Chl a_i (Agustí 1991b). In the previous studies, the $\underline{b}^*_{ph}(676)$ of phytoplankton with d < 10 μm ranged from 0.042 m^2 mg Chl a^{-1} for chlorophytes to 0.51 m^2 mg Chl a^{-1} for haptophytes, and the $\underline{b}^*_{ph}(676)$ of phytoplankton with d >10 μm ranged from 0.032 m^2 mg Chl a^{-1} for chlorophytes to 0.17 m^2 mg Chl a^{-1} for diatoms (Table 2-2). The high $\underline{b}^*_{ph}(676)$ of haptophytes and diatoms could reflect the mineralized cell wall (Kirk 2011). The constituents of the mineralized cell wall of haptophytes such as coccoliths indicated a higher carbon-specific scattering coefficient than that of the cells themselves (Balch et al. 1996). Although *P. micans* and *P. minimum* do not have mineralized cell walls, the $\underline{b}^*_{ph}(676)$ was similar to those of diatoms and haptophytes of similar or smaller size. The high $\underline{b}^*_{ph}(676)$ could be caused by the thecal plate. However, the $\underline{b}^*_{ph}(676)$ of various species decreased significantly with increasing d (p<0.05, Table 2-7, Figure 2-6). Because

of the reverse relationship between the d and Chl a_i, the decreasing $\underline{b}^*_{ph}(676)$ with cell size d suggests that the larger cell could enhance the efficiency for scattering relative to smaller cells.

Higher $Q_b(676)$ under LL could be a result of the high Chl a_i under LL, because there was little difference in the d and C_i between the two light conditions. The previous studies indicated that the $Q_b(676)$ of phytoplankton with d < 10 μm ranged from 0.19 for cyanophytes to 3.19 for haptophytes, whereas the $Q_b(676)$ of phytoplankton with d >10 μm was generally < 2 (Figure 2-7). The $Q_b(676)$ of both species were relatively higher than diatoms and haptophytes with smaller cell size. The high $Q_b(676)$ could be caused by high $b^*_{ph}(676)$ as a function cell size. Besides the $Q_b(676)$ of *P. micans* was higher than that of the same species of the literature (Ahn et al. 1992) due to about 4-fold high $b^*_{ph}(676)$. The high $b^*_{ph}(676)$ of this study could be due to low Chl a_i, and accordingly the difference in the $Q_b(676)$ could be due to the C:Chl *a* as discussed below.

The theoretical $Q_b(676)$ based on the anomalous diffraction approximation indicates the oscillations with cell size and the convergence to 1 when the dimensionless efficiency factor for absorption at 676 nm converges to 1 (Morel and Bricaud 1986). The experimentally obtained $Q_b(676)$ in previous studies (Bricaud et al. 1983; Bricaud et al. 1988; Ahn et al. 1992; Stramski et al. 1993; DuRand et al. 2002) was similar to or lower than the theoretical values of the real part of m = 1.06, which was the mean index of pure phytoplankton cultures (Aas 1996). However, the $Q_b(676)$ of *P. micans* and *P. minimum* indicated 2-fold higher than theoretical values for similar cell sizes, regardless of the variation in the m (Figure 2-7). Therefore, the high $Q_b(676)$ might be mainly induced by the high $b^*_{ph}(676)$. A significant linear relation between $b^*_{ph}(676)$ of various species including *P. micans* and *P. minimum* and C:Chl *a* (Table 2-7, Figure 2-8) suggests that the C:Chl *a* could play a role of the variation in the $b^*_{ph}(676)$ as a function of cell size (Motokawa and Taguchi 2015).

This study presents that the reliable relationships between the *d* and the $a^*_{ph}(676)$, and the *d* and the $\underline{b}^*_{ph}(676)$ could be established. The relationships suggest that the cell size of phytoplankton species could be estimated from both $a^*_{ph}(676)$ and $\underline{b}^*_{ph}(676)$. Furthermore the relationship between C:Chl *a* and $\underline{b}^*_{ph}(676)$ suggests that the C:Chl *a* may provide a better estimate of the scattering efficiency of phytoplankton. The cumulative scattering coefficient of phytoplankton is constructed by the scattering efficiency and the biomass, so that the scattering efficiency as a function of C:Chl *a* should provide to a better understanding the light availability in the phytoplankton assemblages.

Table 2-1. Literature values of biogeochemical and absorption factors.

Class	Species	d (μm)	Chl a_i (kg Chl a m^{-3})	$a^*_{ph}(676)$ (m^2 mg Chl a^{-1})	$Q_a(676)$	$Q_a^*(676)$	Refrences
Diatom	*Chaetoceros calcitrans*	2.6	11.8	0.028	0.57	1.03	Finkel (2001)
Diatom	*Cyclotella nana*	4.9	5.3	0.025	0.43	0.92	Finkel (2001)
Diatom	*Chaetoceros* sp.	6.5	2.9	0.027	0.33	0.99	Finkel (2001)
Diatom	*Thalassiosira weissflogii*	15.8	3.4	0.017	0.62	0.64	Finkel (2001)
Diatom	*Hyalodiscus* sp.	25.8	0.7	0.025	0.28	0.92	Finkel (2001)
Diatom	*Coscinodiscus* 312	89.2	0.3	0.015	0.28	0.55	Finkel (2001)
Diatom	*Coscinodiscus* 1583	77.8	1.1	0.015	0.85	0.57	Finkel (2001)
Haptophyte	*Isochrysis galbana*	4.4	21.6	0.012	0.74	0.43	Fujiki and Taguchi (2002)
Haptophyte	*Isochrysis galbana*	4.3	20.3	0.012	0.72	0.46	Fujiki and Taguchi (2002)
Haptophyte	*Isochrysis galbana*	4.1	13.9	0.013	0.51	0.50	Fujiki and Taguchi (2002)
Haptophyte	*Isochrysis galbana*	3.9	11.8	0.015	0.46	0.55	Fujiki and Taguchi (2002)
Haptophyte	*Isochrysis galbana*	4.0	8.9	0.016	0.37	0.58	Fujiki and Taguchi (2002)
Haptophyte	*Isochrysis galbana*	4.2	7.9	0.018	0.39	0.66	Fujiki and Taguchi (2002)
Haptophyte	*Pleurochrysis carterae*	4.7	24.6	0.009	0.71	0.34	Fujiki and Taguchi (2002)
Haptophyte	*Pleurochrysis carterae*	4.6	17.3	0.010	0.51	0.36	Fujiki and Taguchi (2002)
Haptophyte	*Pleurochrysis carterae*	4.4	12.7	0.011	0.41	0.41	Fujiki and Taguchi (2002)
Haptophyte	*Pleurochrysis carterae*	4.2	9.7	0.013	0.34	0.47	Fujiki and Taguchi (2002)

Table 2-1. Continue.

Class	Species	d (μm)	Chl a_i (kg Chl a m^{-3})	$a^*_{ph}(676)$ (m^2 mg Chl a^{-1})	$Q_a(676)$	$Q_a^*(676)$	Refrences
Haptophyte	*Pleurochrysis carterae*	4.3	9.7	0.013	0.37	0.50	Fujiki and Taguchi (2002)
Haptophyte	*Pleurochrysis carterae*	4.4	6.6	0.016	0.31	0.58	Fujiki and Taguchi (2002)
Diatom	*Chaetoceros gracilis*	5.3	16.2	0.010	0.59	0.39	Fujiki and Taguchi (2002)
Diatom	*Chaetoceros gracilis*	5.2	15.2	0.011	0.55	0.39	Fujiki and Taguchi (2002)
Diatom	*Chaetoceros gracilis*	5.0	14.9	0.011	0.53	0.40	Fujiki and Taguchi (2002)
Diatom	*Chaetoceros gracilis*	4.8	11.4	0.012	0.43	0.43	Fujiki and Taguchi (2002)
Diatom	*Chaetoceros gracilis*	4.9	10.3	0.013	0.45	0.49	Fujiki and Taguchi (2002)
Diatom	*Chaetoceros gracilis*	5.1	5.2	0.017	0.29	0.62	Fujiki and Taguchi (2002)
Chlorophyte	*Dunaliella tertiolecta*	9.0	11.3	0.010	0.70	0.38	Fujiki and Taguchi (2002)
Chlorophyte	*Dunaliella tertiolecta*	8.8	12.2	0.011	0.78	0.40	Fujiki and Taguchi (2002)
Chlorophyte	*Dunaliella tertiolecta*	8.7	7.4	0.011	0.48	0.42	Fujiki and Taguchi (2002)
Chlorophyte	*Dunaliella tertiolecta*	7.9	7.2	0.013	0.50	0.49	Fujiki and Taguchi (2002)
Chlorophyte	*Dunaliella tertiolecta*	8.1	6.1	0.015	0.48	0.54	Fujiki and Taguchi (2002)
Chlorophyte	*Dunaliella tertiolecta*	8.5	4.0	0.016	0.35	0.58	Fujiki and Taguchi (2002)
Diatom	*Thalassiosira weisflogii*	11.5	11.5	0.008	0.66	0.28	Fujiki and Taguchi (2002)
Diatom	*Thalassiosira weisflogii*	11.2	10.3	0.010	0.77	0.37	Fujiki and Taguchi (2002)
Diatom	*Thalassiosira weisflogii*	10.8	6.2	0.012	0.54	0.44	Fujiki and Taguchi (2002)

Table 2-1. Continue.

Class	Species	d (μm)	Chl a_i (kg Chl a m^{-3})	$a^*_{ph}(676)$ (m^2 mg Chl a^{-1})	$Q_a(676)$	$Q_a^*(676)$	Refrences
Diatom	*Thalassiosira weisflogii*	11.0	5.2	0.013	0.49	0.47	Fujiki and Taguchi (2002)
Diatom	*Thalassiosira weisflogii*	11.1	4.6	0.014	0.47	0.51	Fujiki and Taguchi (2002)
Diatom	*Thalassiosira weisflogii*	11.3	3.7	0.015	0.43	0.57	Fujiki and Taguchi (2002)
Diatom	*Coscinodiscus* sp.	70.7	2.0	0.006	0.55	0.22	Fujiki and Taguchi (2002)
Diatom	*Coscinodiscus* sp.	70.6	1.8	0.007	0.58	0.25	Fujiki and Taguchi (2002)
Diatom	*Coscinodiscus* sp.	70.4	1.6	0.007	0.53	0.27	Fujiki and Taguchi (2002)
Diatom	*Coscinodiscus* sp.	70.1	1.3	0.009	0.55	0.33	Fujiki and Taguchi (2002)
Diatom	*Coscinodiscus* sp.	69.7	1.4	0.011	0.69	0.40	Fujiki and Taguchi (2002)
Diatom	*Coscinodiscus* sp.	69.3	0.8	0.013	0.47	0.48	Fujiki and Taguchi (2002)
Dinoflagellate	*Alexandrium tamarense*	29.2	5.3	0.013	1.36	0.48	Leong and Taguchi (2006)
Dinoflagellate	*Alexandrium tamarense*	28.8	5.2	0.010	1.05	0.39	Leong and Taguchi (2006)
Dinoflagellate	*Alexandrium tamarense*	28.8	5.8	0.013	1.48	0.49	Leong and Taguchi (2006)
Dinoflagellate	*Prorocentrum micans*	25.1	1.2	0.019	0.39	0.69	Present study
Dinoflagellate	*Prorocentrum micans*	24.8	1.8	0.015	0.43	0.54	Present study
Dinoflagellate	*Prorocentrum minimum*	12.4	1.8	0.023	0.33	0.85	Present study
Dinoflagellate	*Prorocentrum minimum*	12.8	2.8	0.020	0.49	0.76	Present study

Table 2-2. Literature values of biogeochemical and scattering factors.

Class	Species	d (μm)	Chl a_i (kg Chl a m^{-3})	C_i (kg C m^{-3})	C:Chl a (g g^{-1})	$b^*_{ph}(676)$ (m^2 mg Chl a^{-1})	$Q_b(676)$	References
Haptophyte	*Hymenomonas elongata*	13.6	2.9	132	45	0.073	1.94	Bricaud et al. (1983)
Prasinophyte	*Platymonas* sp.	6.8	1.9	175	94	0.180	1.53	Bricaud et al. (1983)
Prasinophyte	*Tetraselmis maculata*	8.5	1.6	160	99	0.169	1.55	Bricaud et al. (1983)
Haptophyte	*Coccolithus huxleyi*	3.4	1.1	231	203	0.510	1.32	Bricaud et al. (1983)
Diatom	*Skeletonema costatum*	5.5	0.9	128	141	0.443	1.48	Morel and Bricaud (1986)
Prasinophyte	*Platymonas suecica*	3.4	6.4	232	36	0.159	2.27	Morel and Bricaud (1986)
Diatom	*Chaetoceros curvisetum*	7.5	1.4	102	76	0.216	1.46	Bricaud et al. (1988)
Diatom	*Chaetoceros lauderi*	25.5	0.3	42	132	0.168	0.91	Bricaud et al. (1988)
Haptophyte	*Pavlova pinguis*	3.6	4.3	226	52	0.136	1.42	Bricaud et al. (1988)
Haptophyte	*Pavlova luheri*	4.5	2.6	207	79	0.314	2.47	Bricaud et al. (1988)
Haptophyte	*Prymnesium parvum*	5.7	2.6	188	73	0.202	1.97	Bricaud et al. (1988)
Chlorophyte	*Dunaliella salina*	10.2	6.2	149	24	0.032	1.33	Bricaud et al. (1988)
Red algae	*Porphyridium cruentum*	4.9	4.3	200	47	0.159	2.21	Bricaud et al. (1988)
Diatom	*Thalassiosira* sp.	5.2	5.6	135	24	0.119	2.28	Osborne and Geider (1989)

Table 2-2. Continue.

Class	Species	d (μm)	Chl a_i (kg Chl a m^{-3})	C_i (kg C m^{-3})	C:Chl a (g g^{-1})	$b^*_{ph}(676)$ (m^2 mg Chl a^{-1})	$Q_b(676)$	References
Chlorophyte	*Nannochloris atomus*	3.7	3.6	225	62	0.251	2.20	Osborne and Geider (1989)
Chlorophyte	*Dunaliella bioculata*	6.7	14.1	176	13	0.042	2.64	Ahn et al. (1992)
Haptophyte	*Emiliania huxleyi*	4.9	3.7	199	53	0.260	3.19	Ahn et al. (1992)
Haptophyte	*Isochrysis galbana*	4.5	6.9	207	30	0.113	2.30	Ahn et al. (1992)
Dinoflagellate	*Prorocentrum micans*	27.6	2.3	100	44	0.036	1.49	Ahn et al. (1992)
Cryptomonad	*Chroomonas fragarioide*	5.6	3.6	190	53	0.169	2.24	Ahn et al. (1992)
Chlorophyte	*Dunaliella tertiolectra*	8.3	3.2	162	51	0.075	1.33	Stramski et al. (1993)
Chlorophyte	*Dunaliella tertiolectra*	7.9	3.9	165	43	0.086	1.75	Stramski et al. (1993)
Dinoflagellate	*Prorocentrum micans*	25.1	1.2	183	148	0.142	2.95	Motokawa and Taguchi (2015)
Dinoflagellate	*Prorocentrum micans*	24.8	1.8	178	99	0.140	4.16	Motokawa and Taguchi (2015)
Dinoflagellate	*Prorocentrum minimum*	12.4	1.8	323	183	0.250	3.61	Motokawa and Taguchi (2015)
Dinoflagellate	*Prorocentrum minimum*	12.8	2.8	307	108	0.192	4.65	Motokawa and Taguchi (2015)

Table 2-3. Mean ± one standard deviation of d, Chl a_i, C_i, d×Chl a_i, and C:Chl a of *Prorocentrum micans* and *P. minimum* at HL (irradiance of 600 µmol photons m^{-2} s^{-1}) and LL (irradiance of 300 µmol photons m^{-2} s^{-1}).

Species	Irradiance	d (µm)	Chl a_i (kg Chl a m^{-3})	C_i (kg C m^{-3})	d× Chl a_i (mg Chl a m^{-2})	C : Chl a (g g^{-1})
P. micans	HL	25.1 ± 0.28	1.2 ± 0.04	183 ± 10	31 ± 0.7	148 ± 7.2
	LL	24.8 ± 0.10	1.8 ± 0.05	178 ± 9	45 ± 1.5	99 ± 6.8
P. minimum	HL	12.4 ± 0.11	1.8 ± 0.23	323 ± 19	22 ± 2.8	184 ± 14.0
	LL	12.8 ± 0.18	2.8 ± 0.40	307 ± 32	36 ± 4.7	108 ± 4.4

Table 2-4. Mean ± one standard deviation of $a^*_{ph}(676)$, $a_{cell}(676)$, $Q_a(676)$, and $Q_a^*(676)$ of *Prorocentrum micans* and *P. minimum* at HL (irradiance of 600 µmol photons m^{-2} s^{-1}) and LL (irradiance of 300 µmol photons m^{-2} s^{-1}).

Species	Irradiance	$a^*_{ph}(676)$ (m^2 mg Chl a^{-1})	$a_{cell}(676)$ (10^{-10} m^2 $cell^{-1}$)	$Q_a(676)$	$Q_a^*(676)$
P. micans	HL	0.019 ± 0.0012	1.90 ± 0.151	0.39 ± 0.033	0.69 ± 0.046
	LL	0.015 ± 0.0010	2.09 ± 0.111	0.43 ± 0.024	0.54 ± 0.036
P. minimum	HL	0.023 ± 0.0010	0.40 ± 0.049	0.33 ± 0.040	0.85 ± 0.037
	LL	0.020 ± 0.0012	0.63 ± 0.061	0.49 ± 0.050	0.76 ± 0.046

Table 2-5. Mean ± one standard deviation of $\underline{b}^*_{ph}(676)$, $\underline{b}_{cell}(676)$, and $Q_b(676)$ of *Prorocentrum micans* and *P. minimum* at HL (irradiance of 600 µmol photons m^{-2} s^{-1}) and LL (irradiance of 300 µmol photons m^{-2} s^{-1}).

Species	Irradiance	$\underline{b}^*_{ph}(676)$ (m^2 mg Chl a^{-1})	$\underline{b}_{cell}(676)$ (10^{-9} m^2 $cell^{-1}$)	$Q_b(676)$
P. micans	HL	0.14 ± 0.018	1.45 ± 0.179	2.9 ± 0.41
	LL	0.14 ± 0.005	2.02 ± 0.062	4.2 ± 0.11
P. minimum	HL	0.25 ± 0.033	0.42 ± 0.021	3.6 ± 0.25
	LL	0.19 ± 0.003	0.60 ± 0.064	4.7 ± 0.61

Table 2-6. Regression analyses between log $a^*_{ph}(676)$ and log d, log Chl a_i, and log d×Chl a_i. N.S. indicates not significant. n, S.E., r^2, and p indicate the number of sample, standard error, determination coefficient, and probability, respectively.

Regression equation	n	Y_{int} ± S.E.	Slope ± S.E.	r^2	p
$\text{Log } a^*_{ph}(676) = Y_{int} + \text{Slope} \times \text{Log } d$	50	−1.8 ± 0.05	−0.094 ± 0.045	0.08	<0.05
$\text{Log } a^*_{ph}(676) = Y_{int} + \text{Slope} \times \text{Log Chl } a_i$	50	−1.8 ± 0.04	−0.064 ± 0.047	0.04	N. S.
$\text{Log } a^*_{ph}(676) = Y_{int} + \text{Slope} \times \text{Log } d \times \text{Chl } a_i$	50	−1.0 ± 0.08	−0.474 ± 0.046	0.69	<0.001

Table 2-7. Regression analyses between log $\underline{b}^*_{ph}(676)$ and log *d*, log $\underline{b}^*_{ph}(676)$ and log C:Chl *a*. n, S.E., r^2, and *p* indicate the number of sample, standard error, determination coefficient, and probability, respectively.

Regression equation	n	Y_{int} ± S.E.	Slope ± S.E.	r^2	*p*
Log $\underline{b}^*_{ph}(676) = Y_{int}$ + Slope × Log *d*	26	–0.46 ± 0.18	–0.42 ± 0.20	0.16	<0.05
Log $\underline{b}^*_{ph}(676) = Y_{int}$ + Slope × Log C:Chl *a*	26	–2.16 ± 0.03	0.74 ± 0.15	0.52	<0.001

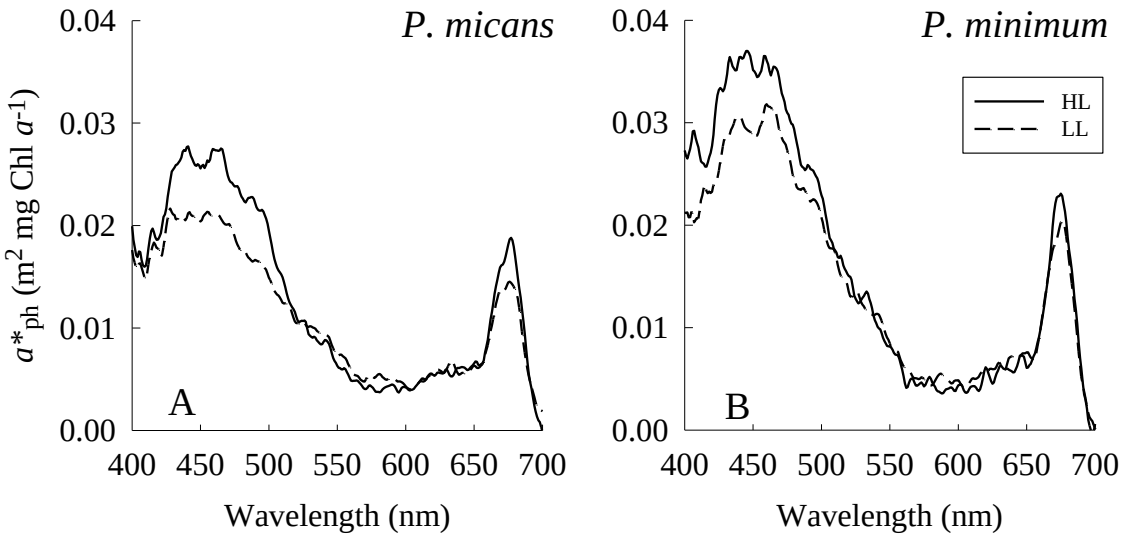

Figure 2-1. The a^*_{ph} spectra of *P. micans* (A) and *P. minimum* (B) at HL and LL. Solid and dashed lines indicate HL and LL, respectively.

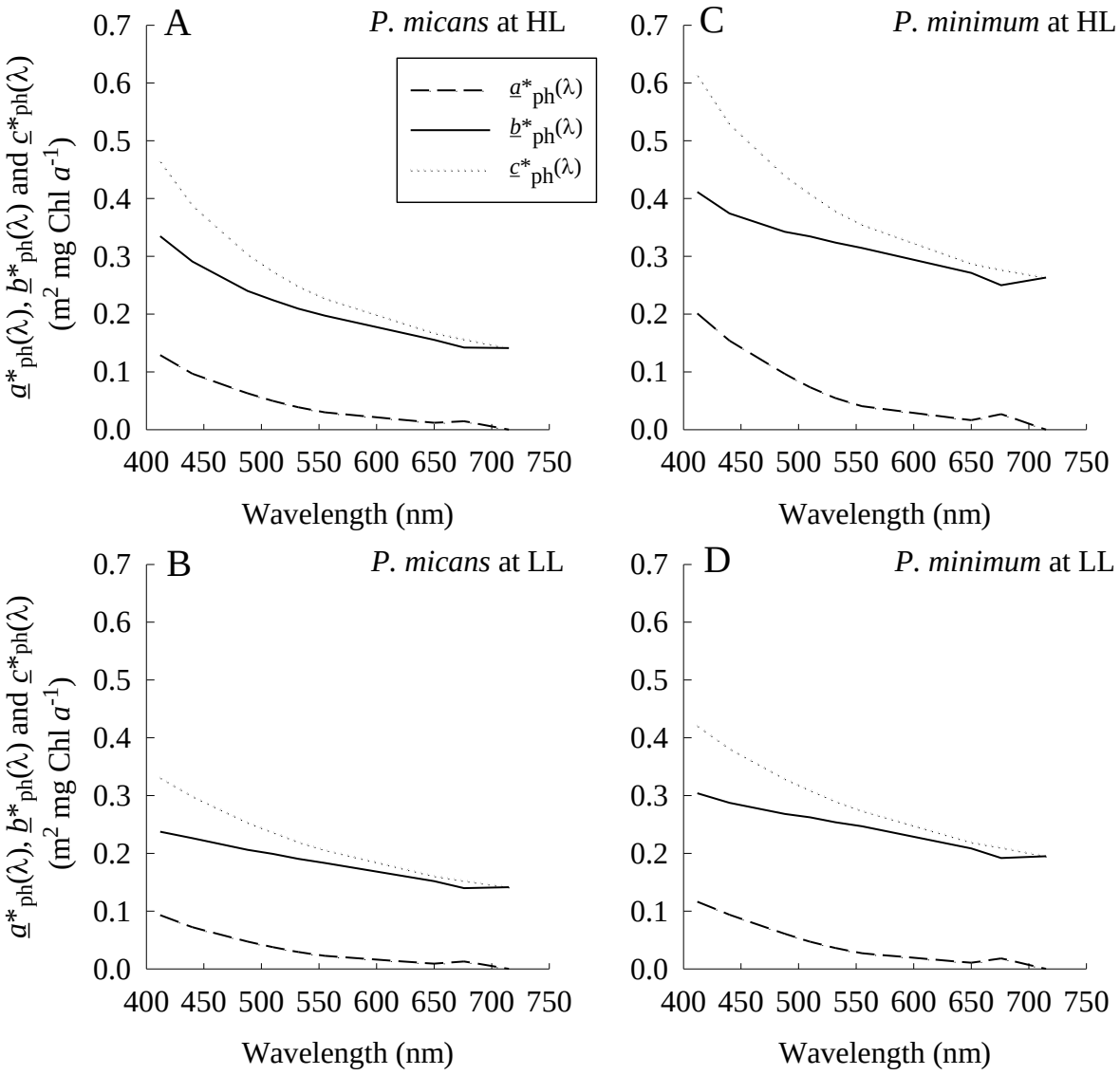

Figure 2-2. The $\underline{a}^*_{ph}$, $\underline{b}^*_{ph}$, and $\underline{c}^*_{ph}$ spectra of *P. micans* at HL (A) and LL (B) and *P. minimum* at HL (C) and LL (D) measured by ac-9. Dashed, solid, and dotted lines indicate $\underline{a}^*_{ph}(\lambda)$, $\underline{b}^*_{ph}(\lambda)$, and $\underline{c}^*_{ph}(\lambda)$, respectively.

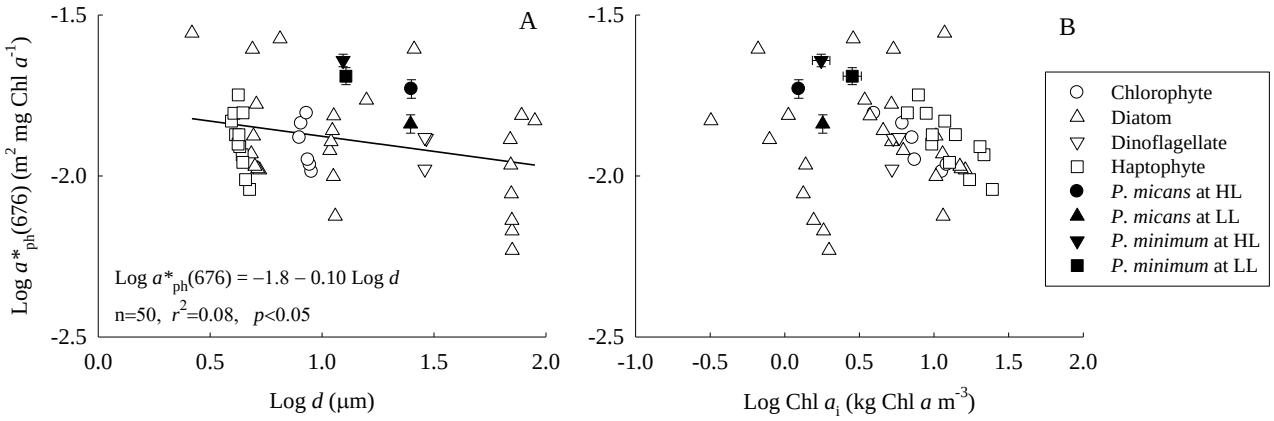

Figure 2-3. Relationships between log d and log $a^*_{ph}(676)$ (A), log Chl a_i and log $a^*_{ph}(676)$ (B). Open and closed symbols indicate literature and this study, respectively. Solid line indicates regression line (p<0.05). Error bars indicate one standard deviations.

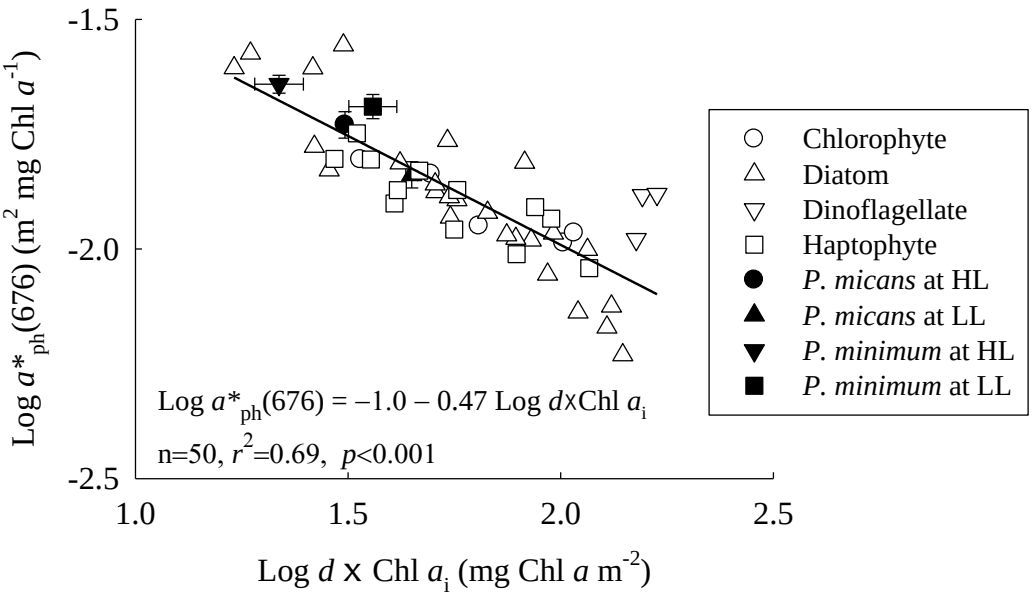

Figure 2-4. Relationships between log d×Chl a_i and log a^*_{ph}(676) of literature values (open symbols) and this study (closed symbols). Solid line indicates regression line (p<0.001). Error bars indicate one standard deviations.

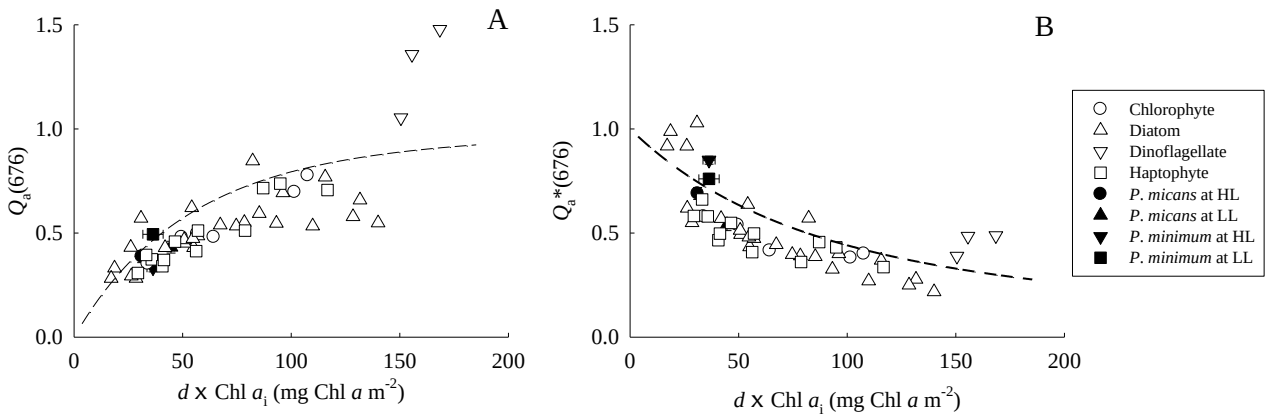

Figure 2-5. Relationships between d×Chl a_i and $Q_a(676)$ (A), and d×Chl a_i and Q_a*(676) (B). Open and closed symbols indicate literature and this study, respectively. Dashed lines indicate theoretical efficiency factor for absorption ($Q_a[\rho']$) (A) and theoretical package effect index of homogeneous spherical particles at 676nm (Q_a*[ρ']) (B), respectively. Error bars indicate one standard deviations.

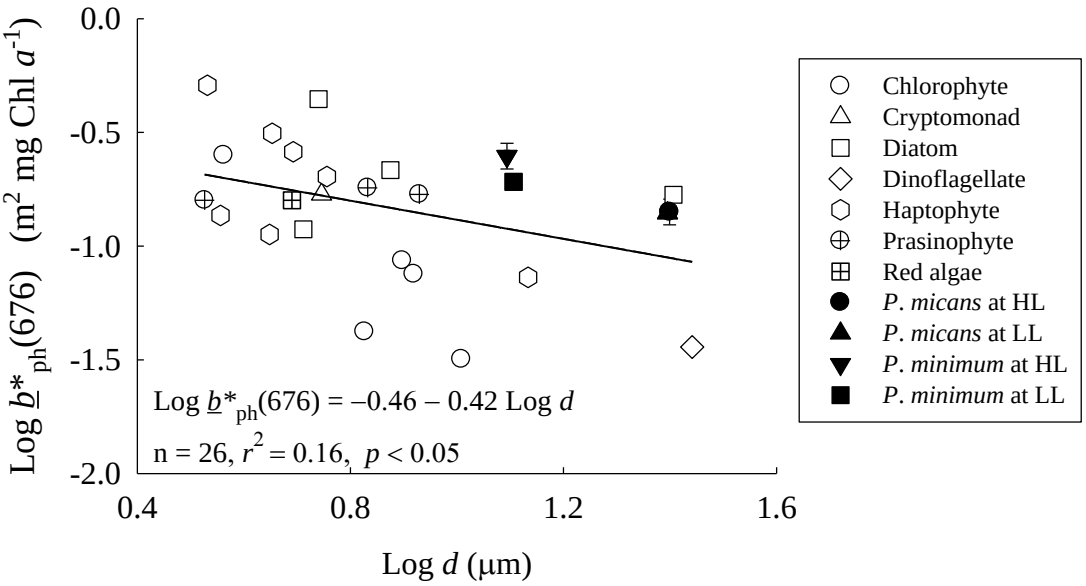

Figure 2-6. Relationship between d and $\underline{b}^*_{ph}(676)$ of and literature values (open symbols) and this study (closed symbols). Solid line indicates regression line (p<0.05). Error bars indicate one standard deviations.

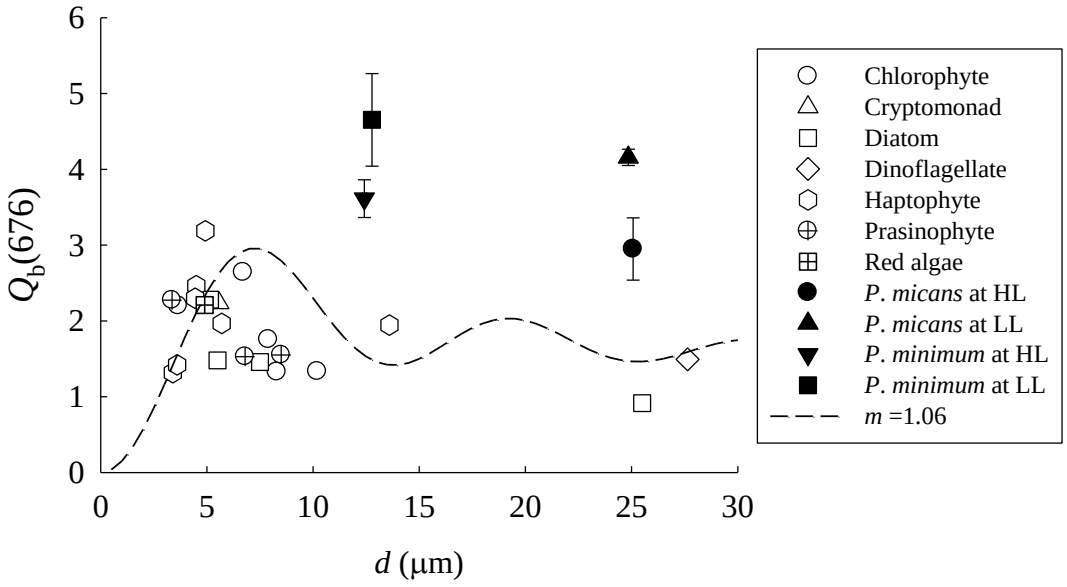

Figure 2-7. Relationship between d and $Q_b(676)$ of literature values (open symbols) and this study (closed symbols). Dashed line indicates theoretical efficiency factor for scattering of homogeneous spherical particles based on the anomalous diffraction approximation as relative refractive index to water (m) = 1.06. Error bars indicate one standard deviations.

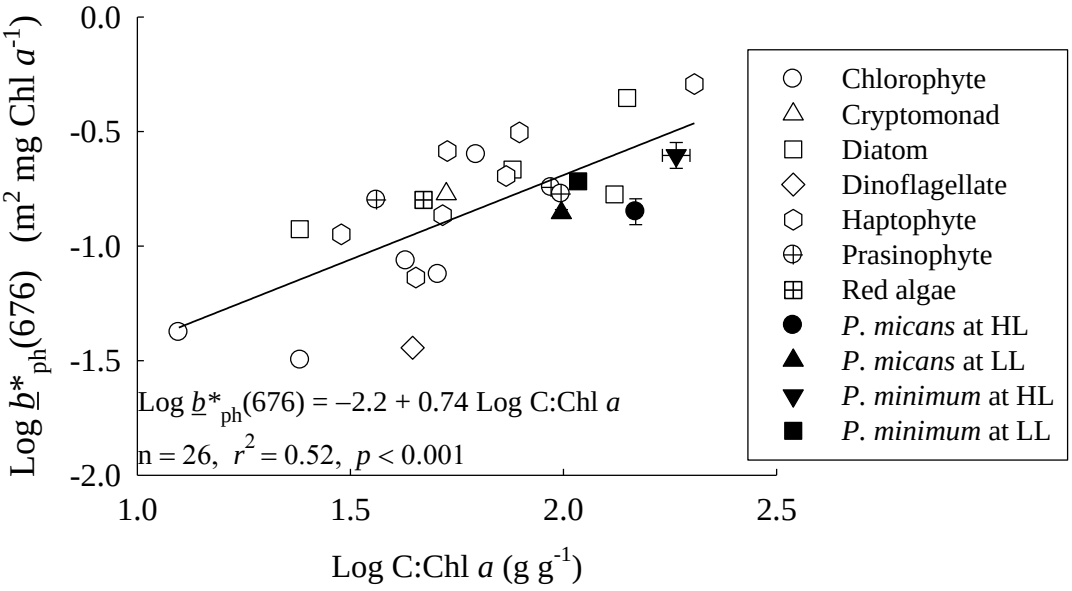

Figure 2-8. Relationship between C:Chl *a* and $\underline{b}^*_{ph}(676)$ of literature values (open symbols) and this study (closed symbols). Solid line indicates regression line (p<0.001). Error bars indicate one standard deviations.

CHAPTER III

ABSORPTION AND SCATTERING PROPERTIES OF MICRO- AND NANO-SIZE FRACTIONATED PHYTOPLANKTON ASSEMBLAGES

3.1. Introduction

Size distribution of natural assemblage of phytoplankton strongly influences marine primary production because cell size of phytoplankton influences on the photosynthesis (Banse 1976; Taguchi 1976), growth (Eppley and Sloan 1966), and sinking rate (Eppley et al. 1967). Particularly, large-cell phytoplankton, such as micro-size (20 – 200μm in diameter) and nano-size phytoplankton (2 – 20μm in diameter), can influence significantly on the production due to the occurrence of opportunistic and sporadic large blooms. To monitor the size distribution of phytoplankton or the blooms, ocean color remote sensing by satellite would be one of the most effective ways (Cullen 2008). The monitoring by satellite is based on a bio-optical relationship between phytoplankton biomass, such as chlorophyll *a* (Chl *a*), and Inherent Optical Properties (IOPs) of phytoplankton in seawater (Smith and Baker 1978). The IOPs comprise the absorption coefficient (*a*), scattering coefficient (*b*), and attenuation coefficient (*c*) which represents the sum of *a* and *b* (Preisendorfer 1976). Because the IOPs of phytoplankton are influenced by the cell size, the size distribution of phytoplankton biomass would be inversely estimated from the characteristics of IOPs as a function cell size.

Bulk IOPs of seawater is obtained as the sum of IOPs of biogeochemical constituents; pure seawater, colored dissolved organic matter (CDOM), phytoplankton, and non-phytoplankton particle. The relative contributions of the constituents to the bulk IOPs of seawater can determine

the optical type of seawater. For the ocean color remote sensing, the optical type of seawater can often separate into the two types; Case I and Case II waters (Morel and Prieur 1977). Presumably, more than 98% of the world ocean waters belong to the Case I waters (Morel 1988). In the Case I waters, phytoplankton and the associated products play a significant role in determining the IOPs of seawater. Thus the IOPS of seawater in Case I waters can be regulated by the Chl *a* concentration, and significant relationships between Chl *a* concentration and IOPs of particles can be empirically derived (Morel 1988; Liosel and Morel 1998). On the other hand, the IOPs of seawater in Case II waters can be regulated by not only phytoplankton and the associated products but also sediments and terrestrial sources, such as terrestrial CDOM or particulate matter. The bio-optical relationships between IOPs of particles and Chl *a* concentration are difficult to be derived under the presence of the terrestrial matters which may not covary with Chl *a* concentrations (D'Sa et al. 2006; Morel et al. 2006). Thus, in Case II waters, the size distribution of phytoplankton assemblage is difficult to be identified from the bulk IOPs.

Historically, the spectral characteristic of the remote sensing reflectance (R), which is estimated from the reflectance of sunlight at the sea surface (equation 1.1) or IOPs of the seawater (equation 1.2), in blue-green region (approximately from 440nm to 555nm) has been applied to monitor the phytoplankton biomass in mainly Case I waters because the region can reflect mainly the IOPs of phytoplankton in the seawater (O'Reilly et al. 1998). However the blue-green region is optically complicated due to the contributions of various biogeochemical elements in seawater. The IOPs in red region includes mostly the absorption peak by Chl *a* (676nm) and is little influenced by the CDOM or particulate matter (Kirk 1975). However accurate measurements of R at 676nm (R[676]) from space are much more subject to error due to smaller signal to noise ratio (Carder et al. 2006). Recently, substitution of the R(676) or the estimate of R(676) from the R(610-620) are

attempted (Carder et al. 2006). If an accurate $R(676)$ would be retrieved, the reliable relationships between the IOPs at 676nm and Chl *a* concentration would be utilized for monitoring the size distribution of phytoplankton.

The bio-optical relationships between phytoplankton biomass, such as Chl *a* concentration, and the IOPs would be applied to monitor the size distribution of phytoplankton. In that case, the size distribution of phytoplankton is represented as the relative Chl *a* concentrations of the size class. The monitoring of size distribution of phytoplankton is based on the assumption that an estimated Chl *a* concentration by satellite covary with the size distribution of phytoplankton (Uitz et al. 2006). The Chl *a* abundance-based approach is limited in the regions where significant relationship between the Chl *a* concentration and size distribution of phytoplankton is established (Brewin et al. 2011). On the other hand, the IOPs-based approach is alternative approach based on the characteristics of the *a* and *b* as a function of cell size, particularly spectral characteristics of *a* of phytoplankton ($a_{ph}[\lambda]$, Ciotti et al. 2002) and *b* of phytoplankton ($b_{ph}[\lambda]$, Babin et al. 2003). The spectral $a_{ph}(\lambda)$ and $b_{ph}(\lambda)$ are directly estimated from the spectral *R* measured by satellite, and then the size distribution of phytoplankton can be inversely estimated from the spectral $a_{ph}(\lambda)$ and $b_{ph}(\lambda)$ as a function of cell size. However, in Case II waters, the spectral $a_{ph}(\lambda)$ and $b_{ph}(\lambda)$ are difficult to be estimated from the *R* due to the presence of the various biogeochemical elements as mentioned above. The $a_{ph}(\lambda)$ and $b_{ph}(\lambda)$ at a single wavelength at 676nm ($a_{ph}[676]$ and $b_{ph}[676]$) would be utilized for monitoring the size distribution of phytoplankton. The relationships between $a_{ph}(676)$ and/or $b_{ph}(676)$ and size distribution of phytoplankton assemblage which are obtained by the relative Chl *a* concentration are expected to be derived in not only Case I waters but also Case II waters.

The relationships between $a_{ph}(676)$ and/or $b_{ph}(676)$ and cell size of phytoplankton can

represent the change in the Chl *a* normalized IOPs of phytoplankton, such as Chl *a* normalized absorption ($a^*_{ph}[\lambda]$) and scattering coefficient of phytoplankton ($b^*_{ph}[\lambda]$). To minimize the optical contribution of the biogeochemical constituents other than phytoplankton cell, a single wavelength at 676nm is employed to evaluate the size effect of the phytoplankton cell. The $a^*_{ph}(676)$ in natural assemblage of phytoplankton is determined by the absorptive abundance, such as phytoplankton pigments, and the absorption properties of individual cells in the assemblage, or both (Bricaud et al. 1995; Morel et al. 2006). Because of the internal geometry in the cell, such as the morphology, number, and distribution of the pigments, the variation in the $a^*_{ph}(676)$ is mainly controlled by the pigment packaging (Agustí 1991a; Fujiki and Taguchi 2002; Roy et al. 2011). The effect of the pigment packaging (package effect) is larger with increasing cells size (Finkel and Irwin 2000; Kirk 2011). To evaluate the package effect or $a^*_{ph}(676)$ as a function of cell size, the relationship between size distribution of phytoplankton assemblage, particularly the relative proportion of micro- or nano-size phytoplankton, and $a^*_{ph}(676)$ is warranted.

The $b^*_{ph}(676)$ is dependent on the amount and composition of the suspended particles in relation to their sizes, absorptive contents, such as pigments, and refractive or reflective contents, such as particulate carbon. In previous studies on the scattering efficiency of phytoplankton, the wavelength is generally employed at 555 nm or 660 nm where the absorption is very low or can be neglected. Although the *in situ* particles include not only phytoplankton but also non-phytoplankton particles in Case I waters, Chl *a* specific scattering coefficient of particle at 660nm ($b^*_p[660]$) is often shown to be non-linearly correlated with Chl *a* concentration and particulate organic carbon (POC) concentration (Loisel and Morel 1998). The non-linear relationship can be derived because the variable component of $b^*_p(660)$, such as the refractive contents, changes with the abundance of particles functionally associated with phytoplankton carbon biomass in the Case I waters (Babin et

al. 2003). However, under the presence of the terrestrial elements in Case II waters, $b^*_p(660)$ does not seem to reflect strictly the scattering efficiency of phytoplankton alone (Loisel and Morel 1998). Under the contributions of various particles to bulk $b^*_p(\lambda)$, the $b^*_p(676)$ could reflect a more accurate scattering efficiency of phytoplankton than $b^*_p(660)$ because the wavelength at 676nm is absorption peak by Chl *a*. Because the relative contribution of the $b^*_{ph}(676)$ to bulk $b^*_p(676)$ is uncertain, the scattering efficiency of phytoplankton is required to correct by comparing the substitute for the relative contribution of the abundance of the phytoplankton cell to particulate matters, such as the ratio of particulate organic carbon to Chl *a* (POC:Chl *a*) or the ratio of $a_p(\lambda)$ to $a_{ph}(\lambda)$. When the size scaling exponent of particulate organic particles as a power law is assumed as similar to the phytoplankton cells, $b^*_{ph}(676)$ as a function of cell size can assist to evaluate the size effect of phytoplankton cells.

In water column, the $a^*_{ph}(676)$ would be influenced by physiological properties of phytoplankton. In addition to the effect of the cell size on the $a^*_{ph}(676)$, the package effect can be influenced by relative proportions of accessory pigments (Bidigare et al. 1987; Hoepffner and Sathyendranath 1991). For the monitoring of the size distribution of phytoplankton using $a^*_{ph}(676)$, the evaluation of the physiological properties of phytoplankton is required with independent of the effect of cell size. Phytoplankton can alter the contents of the intracellular accessary pigments in response to the environmental conditions, such as light. In a surface mixed layer, phytoplankton can be exposed to increasing levels of light when they are transported to the surface. Thus most phytoplankton species contain photoprotective carotenoids (PPC) to protect against high light levels (Bidigare et al. 1987; Claustre et al. 1994; Brunet et al. 2011). The PPC increase with exposure to higher light levels as phytoplankton are transported vertically upwards in the surface mixed layer (MacIntyre et al. 2000), and decrease with exposure to attenuated light as phytoplankton are

transported downward in the surface mixed layer (Moline 1998; Griffith et al. 2010). The relative proportion of PPC to phytoplankton biomass, such as PPC:Chl *a*, or PPC: total carotenoid (TC), are employed to evaluate the photoprotective state of phytoplankton assemblage in a water column (Brunet et al. 1993; Fujiki et al. 2003; Alderkamp et al. 2013). The change in the PPC:Chl *a* can represent the shape of a^*_{ph} spectra, particularly spectral slope of the a^*_{ph} from 488 nm to 532 nm ($a^*_{ph}{}^{slope}$[488-532], Johnsen et al. 1994; Eisner et al. 2003). The relationship between PPC:Chl *a* or PPC:TC and the $a^*_{ph}{}^{slope}$(488-532) can be utilized to evaluate the physiological properties of phytoplankton assemblages.

In this study, I investigated the IOPs of size-fractionated phytoplankton assemblages sampled in the Indian sector of the Southern Ocean and in Sagami Bay which is located on the southern coast of main island of Japan. In the Indian sector of the Southern Ocean, the size distribution of phytoplankton assemblage spatially varied with different water mass (Odate and Fukuchi 1995). The different water mass in the area can be divided by the Antarctic Convergence (AC) (Orsi et al. 1995). Particularly, in austral summer, diatom-dominated blooms occur at near ice edge in the south of the AC (Wright et al. 1996; Chiba et al. 2000; Kopczyńska et al. 2007). Because of high macronutrient concentrations in the Indian sector of the Southern Ocean, except for low silicate concentrations at the north of the AC (Odate and Fukuchi 1995), the spatial distribution of macronutrients are likely to contribute the spatial differences in phytoplankton species. The Southern Ocean have a possibility of the large sink of atmospheric carbon dioxide, and then the investigation of the size distribution of phytoplankton can assist to evaluate the future change in the marine primary production (Boyd et al. 2008). In Sagami Bay, the size distribution of phytoplankton assemblage exhibits seasonal variability (Satoh et al. 2000; Ara et al. 2011). In the area, diatom-dominated bloom and dinoflagellate-dominated bloom occur in spring and summer,

respectively (Satoh et al. 2000; Ara et al. 2011). Thus the optical type of the two waters varied spatially or temporally between the Case I and Case II waters. The spatial investigation in the Indian sector of the Southern Ocean and temporal investigation in Sagami Bay would contribute to construct the reliable relationship IOPs and size distribution of phytoplankton assemblage.

To ensure the reliable relationship between the IOPs of phytoplankton and size distribution of phytoplankton assemblage in Case I and Case II waters, the aim of this chapter is to investigate the $a^*_{ph}(676)$ and $b^*_{ph}(676)$ as a function of cell size of natural assemblage of phytoplankton. The size distribution of phytoplankton assemblage was represented as physical size fraction of the cells (relative Chl *a* abundance), chemical size fraction of the cells (diagnostic pigment, Vidussi et al. 2001), and continuous optical size index of the cells. The optical size index was constructed by using the optical properties of phytoplankton species in the cultural experiments (Chapter II). The single wavelength at 676nm as the optical properties is applied to minimize the optical contribution of the biogeochemical constituents other than phytoplankton cell in both of the Case I and Case II waters. Furthermore, to evaluate the effect of environmental condition, such as light, on the optical properties of phytoplankton assemblage, physiological properties of phytoplankton assemblage were investigated by using the contents of photoprotective carotenoids and POC:Chl *a*. The relationships between IOPs and size distribution would assist to estimate the size distribution of phytoplankton assemblage using ocean color remote sensing as a whole.

3.2. Materials and methods

3.2.1. Cruise and sampling

Water samples were collected in the Indian sector of the Southern Ocean (SO) and Sagami Bay (SB). In SO, water samples were collected at 16 stations along the 110°E and 140°E meridians

during the cruises of the training-research vessel “Umitaka-Maru” (Tokyo University of Marine Science and Technology) in the austral summer of 2010/2011 and 2011/2012 (Table 3-1; Figure 3-1). In SB, water samples were collected at station M (35°09’47”N, 139°10’33”E, depth 120m) during the cruises of the research vessel “Tachibana” (Yokohama National University) every month during the period from July 2009 to December 2010 (Table 3-2; Figure 3-2).

In SO, vertical profiles of temperature, salinity, and density (Sigma-t) were determined using a conductivity temperature depth (CTD) rosette system (Falmouth Scientific, Inc., Cataumet, MA, USA). The position of the Antarctic Convergence (AC) was determined using the definition of Orsi et al. (1995) (Figure 3-1), where the minimum temperature above 200 m is < 2 °C. Photosynthetically available radiation (PAR) in air and under water was measured using a profiling reflectance radiometer (PRR800; Biospherical Instruments, San Diego, CA, USA). Optical depths (ζ) were defined as follows:

$$E_d(z) = E_d(0)e^{-\zeta} \quad (3.1)$$

where $E_d(z)$ and $E_d(0)$ are the values of downward PAR at z m depth and just below the surface, respectively (Kirk 2011). Water samples for nutrient, phytoplankton pigment, particulate organic carbon, and optical properties analyses were collected at three optical depths, approximately 0.39, 2.3, and 4.6, using 24-l Niskin bottles attached to the CTD rosette system (Table 3-1). The optical depth of 0.39, 2.3, and 4.6 in SO corresponded to the surface, mid-point of the euphotic zone, and lower limit of the euphotic zone, respectively (Kirk 2011).

In SB, temperature and salinity at the depth of 0, 10, 20, 30, 40, 50, 60, and 100 m were measured using a thermometer and salinometer, respectively. Sigma-t at the depth of 0, 10, 20, 30, 40, 50, 60, and 100 m were calculated from the temperature and salinity following equation of Fofonoff and Millard (1983). Photosynthetically available radiation in air and under water was

measured using a profiling UV-Visible reflectance radiometer (PUV500; Biospherical Instruments, San Diego, CA, USA). Optical depths were calculated from the equation (3.1). In SB, the optical depth of 0.0, 2.3, and 4.6 corresponded to the surface, mid-point of the euphotic zone, and lower limit of the euphotic zone, respectively (Kirk 2011). Water samples for nutrient analysis were collected at the depth of 0, 10, 20, 30, 40, 50, 60, and 100 m using 5-l Niskin bottles. Water samples for phytoplankton pigment, particulate organic carbon, and optical properties analysis were collected at three optical depths, approximately 0.0, 2.3, and 4.6 using buckets (ζ = 0.0) and 5-l Niskin bottles (ζ = 2.3 and 4.6). The water samples were prescreened through 183 μm mesh of plankton net cloth. The <183 μm fractions were defined as the bulk fraction in SB in the present study.

3.2.2. Nutrient

Subsamples for nutrient analysis were filtered through a 0.45 μm filter unit (Merck Millipore, Billerica, MA, USA). The samples were stored at −20 °C until required for nutrient analysis. Nitrate, phosphate, and silicate concentrations were measured on a nutrient auto-analyzer (SWAAT, BL TEC K. K., Osaka, Japan). The determination of nutrients was based on the modified method of Parsons et al. (1984).

3.2.3. Pigments and particulate organic carbon

Bulk fractions were size-fractionated using 20 μm mesh plankton net cloth and 2μm Millipore Isopore membrane filter (Merck Millipore, Billerica, MA, USA). The bulk fractions and the filtrates were then filtered through 47 mm glass fiber filters (Whatman type GF/F, GE healthcare UK limited, Buckinghamshire, UK) in the dark condition. Cell materials on the GF/F filters from the bulk

fractions, the < 20 μm fractions, and the < 2 μm fractions were stored at −60 °C until required for pigment analysis. The filtered samples in SO were extracted in 2 ml of *N*,*N*-dimethylformamide in the dark at −20 °C for 24 h (Suzuki and Ishimaru 1990). The filtered samples in SB were extracted in 2 ml of 90 % acetone in the dark at −20 °C for 24 hours with homogenization using an ultrasonic homogenizer (UH-50; SMT Co. Ltd., Tokyo, Japan). Those extracts were filtered through a 0.20 μm filter apparatus (Millex-LG; Merck Millipore, Billerica, MA, USA). Finally the extracts were analyzed with high performance liquid chromatography (168 Diode Array Detector, C18 reversed-phase Ultrasphere 3 mm column, Beckman Coulter Instruments, Inc., Fullerton, CA, USA) using a solvent gradient system, with solvent A (80 % methanol and 20 % 0.5 M [v/v] ammonium acetate) and solvent B (70 % methanol and 30 % ethyl acetate) as described by Wright et al. (1997). The peaks were quantified using standards for chlorophyll *a* (Chl *a*), chlorophyll c_{1+2} (Chl c_{1+2}), chlorophyll c_3 (Chl c_3), chlorophyll *b* (Chl *b*), alloxanthin (Allo), 19'-butanoyloxyfucoxanthin (But-fuco), didianoxanntin (DD), diatoxanthin (DT), fucoxanthin (Fuco), 19'-butanoyloxyfucoxanthin (But-fuco), 19'-hexanoyloxyfucoxanthin (Hex-fuco), peridinin (Peri), violaxanthin (Vio), zeaxanthin (Zea), and *beta* carotene (β-caro) from Danish Hydraulic Institute.

Total carotenoids (TC) and photoprotective carotenoid (PPC) were defined as follows:

$$TC = Allo + But\text{-}fuco + DD + DT + Fuco + Hex\text{-}fuco + Peri + Vio + Zea + \beta\text{-}caro \quad (3.2)$$

$$PPC = DD + DT + Vio + Zea + \beta\text{-}caro \quad (3.3).$$

The ratio of PPC to TC (PPC:TC) was calculated on a molar basis.

Subsamples for particulate organic carbon (POC) of bulk fraction (except St. C02-11, C07-12, D13-12, and D07-12 in SO) were filtered onto 25mm glass fiber filter (Whatman type GF/F; GE healthcare UK limited, Buckinghamshire, UK) pre-combusted at 500°C for 2 hours. Particles on filters were oven-dried at 60°C for 24 hours and stored in a desiccator until analysis.

Particulate organic carbon was measured using an elemental analyzer (FlashEA 1112, Thermo Fisher Scientific, MA, USA). The POC concentrations were determined using acetanilide as the standard (Nagao et al. 2001). The ratio of POC to Chl *a* (POC:Chl *a*) was calculated based on a weight basis.

3.2.4. Absorption properties

Bulk fractions were size-fractionated using 20 μm mesh plankton net cloth and 2μm Millipore Isopore membrane filter (Merck Millipore, Billerica, MA, USA). The bulk samples and the filtrates (< 20 μm and < 2 μm fractions) were filtered onto 25mm glass fiber filter (Whatman type GF/F; GE healthcare UK limited, Buckinghamshire, UK), and its absorption spectra were directly scanned from 300nm to 800nm by using dual beam UV-visible spectrophotometer equipped with an integrating sphere (UV-2450, Shimadzu corporation, Kyoto, Japan) following the quantitative filter technique (QFT) method of Mitchell and Kiefer (1988). Filters moistened with filtered sea water were used as the reference. The absorption spectra were normalized to absorbance between 730nm and 760nm (Babin and Stramski 2002). For conversion of the absorption (OD_f) obtained from phytoplankton particles on the filter to particles in suspension (OD_s), the following equation of Cleveland and Weidemann (1993) was employed:

$$OD_s(\lambda) = 0.378\ OD_f(\lambda) + 0.523\ (OD_f[\lambda])^2 \quad (3.4).$$

The absorption coefficient of particle ($a_p[\lambda]$) was calculated by the following equation:

$$a_p(\lambda) = 2.303\ OD_s(\lambda)\ Sf\ Vf^{-1} \quad (3.5)$$

where the factor 2.303 converts $\log_{10}$ to $\log_e$, Vf is the filtered volume, and Sf is the filtered clearance area. Following measurement of the $OD_f(\lambda)$, filters were immerged in 100% methanol for pigment extraction for 24 hours using the method of Kishino et al. (1985) and the de-colorized

filters were moistened with filtered seawater. The filter pads were used to measure the absorption spectra of non-pigmented particles ($a_d[\lambda]$). The difference between particulate and non-pigmented particles absorption coefficients was considered to be the absorption coefficient of phytoplankton pigments ($a_{ph}[\lambda]$):

$$a_{ph}(\lambda) = a_p(\lambda) - a_d(\lambda) \quad (3.6).$$

The $a_{ph}(\lambda)$ in the > 20 μm fractions (micro-size fraction) were estimated by subtracting the results for the < 20 μm fractions from the results for the bulk fraction in SO and < 183 μm fractions in SB. The $a_{ph}(\lambda)$ in the 2 – 20 μm fractions (nano-size fractions) were estimated by subtracting the results for the < 2 μm fractions (pico-size fraction) from the results for the < 20 μm fractions.

Chlorophyll *a* specific absorption coefficient of phytoplankton ($a_{ph}^*[\lambda]$) was obtained using the equation:

$$a^*_{ph}(\lambda) = a_{ph}(\lambda)\,[\text{Chl } a]^{-1} \quad (3.7)$$

where [Chl *a*] is the concentration of Chl *a* in mg m^{-3}.

The spectral slope of a^*_{ph} from 488 to 532nm was calculated as follows:

$$a^{*\,slope}_{ph} = (a^*_{ph}[488] - a^*_{ph}[532])\,(a^*_{ph}[676] \times [488 - 532])^{-1} \quad (3.8).$$

Package effect index at 676nm ($Q_a^*[676]$) was calculated as follows:

$$Q_a^*(676) = a^*_{ph}(676)\,a_{cm}(676)^{-1} \quad (3.9)$$

where $a_{cm}(676)$ is unpackaged Chl *a* specific absorption coefficient at 676nm which is assumed as 0.027 m^2 mg Chl *a* (Johnsen et al. 1994).

3.2.5. Scattering properties

The absorption and attenuation of particles ($\underline{a}_p[\lambda]$ and $\underline{c}_p[\lambda]$, where underline indicate coefficient measured by absorption and attenuation meter [ac-9; WET Labs, OR, USA]) at nine wavelengths

(412, 440, 488, 510, 532, 555, 650, 676, and 715nm) were measured using an ac-9 with a 25cm pathlength. In SO, vertical profiles of $\underline{a}_p(\lambda)$ and $\underline{c}_p(\lambda)$ of bulk sample were measured by ac-9 which was set up as a profiling instrumentation. In SB, the $\underline{a}_p(\lambda)$ and $\underline{c}_p(\lambda)$ of bulk, < 20 μm, and < 2 μm fractions at three optical depths were measured by using the ac-9 which was set up as a bench-top instrumentation in a fixed tilt position at 45°. Scattering coefficient of particle ($\underline{b}_p[\lambda]$) was calculated as the difference between absorption and attenuation of particles ($\underline{a}_p[\lambda]$ and $\underline{c}_p[\lambda]$):

$$\underline{b}_p(\lambda) = \underline{c}_p(\lambda) - \underline{a}_p(\lambda) \quad (3.10).$$

Temperature and salinity corrections were applied to account for the difference between the samples and pure water by the following equations:

$$\underline{a}_{mt}(\lambda) = \underline{a}_m(\lambda) - (\psi_t[\lambda][T - T_r] + \psi_s[\lambda][S - S_r]) \quad (3.11)$$

and

$$\underline{c}_{mt}(\lambda) = \underline{c}_m(\lambda) - (\psi_t[\lambda][T - T_r] + \psi_s[\lambda][S - S_r]) \quad (3.12)$$

where $\underline{a}_{mt}(\lambda)$ is temperature and salinity-corrected absorption, $\underline{a}_m(\lambda)$ is measured absorption, $\underline{c}_{mt}(\lambda)$ is temperature and salinity-corrected attenuation, $\underline{c}_m(\lambda)$ is measured attenuation, ψ_t is the linear temperature dependence of pure water, ψ_s is the linear salinity dependence of saltwater (Pegau et al. 1997), T is the temperature of sample, T_r is the temperature of the pure water for calibration, S is the salinity of the sample, and S_r is the salinity of the pure water (S_r = 0). The absorption was normalized to absorbance at 715nm by the following equations (Zaneveld et al. 1994):

$$\underline{a}(\lambda) = \underline{a}_{mt}(\lambda) - \underline{a}_{mt}(715) \times (\underline{c}_{mt}[\lambda] - \underline{a}_{mt}[\lambda]) (\underline{c}_{mt}[715] - \underline{a}_{mt}[715])^{-1} \quad (3.13).$$

Subsamples for the absorption and attenuation coefficient of colored dissolved organic matter ($\underline{a}_{CDOM}[\lambda]$ and $\underline{c}_{CDOM}[\lambda]$) were filtered by 0.22 μm pore size membrane filter (Merck Millipore, Billerica, MA, USA). The $\underline{a}_p(\lambda)$ and $\underline{c}_p(\lambda)$ were assumed as indicated by the following equations:

$$\underline{a}_p(\lambda) = \underline{a}(\lambda) - \underline{a}_{CDOM}(\lambda) \quad (3.14)$$

$$\underline{c}_p(\lambda) = \underline{c}_{mt}(\lambda) - \underline{c}_{CDOM}(\lambda) \quad (3.15).$$

To estimate the scattering coefficient of phytoplankton ($\underline{b}_{ph}[\lambda]$) from $\underline{b}_p(\lambda)$, the $\underline{b}_p(\lambda)$ was normalized by a ratio of $a_{ph}(555)$ to $a_p(555)$ measured by QFT as follows:

$$\underline{b}_{ph}(676) = \underline{b}_p(676) \times a_{ph}(555)\, a_p(555)^{-1} \quad (3.16).$$

Chlorophyll *a* specific scattering coefficient of phytoplankton ($\underline{b}^*_{ph}[\lambda]$) was obtained using the equation:

$$\underline{b}^*_{ph}(\lambda) = \underline{b}_{ph}(\lambda)\, [\text{Chl } a]^{-1} \quad (3.17)$$

where [Chl *a*] is the Chl *a* concentration in mg m^{-3}.

3.2.6. Size index of natural assemblage of phytoplankton

Size distribution of phytoplankton assemblage was represented as physical size fraction, chemical size fraction, and continuous size index (SI) determined by the optical properties of phytoplankton. The physical size fraction was the relative proportion of micro-size, nano-size, and pico-size fractions (%) determined by pigment concentrations of the filtrated cells. The pigment concentrations in the > 20 μm fraction (micro-size fraction) were estimated by subtracting the results for the < 20 μm fractions from the results for the bulk fraction. The pigment concentrations in the 2 – 20 μm fraction (nano-size fraction) were estimated by subtracting the results for the < 2 μm fraction (pico-size fraction) from the results for the < 20 μm fraction. The relative proportions of micro-size, nano-size, and pico-size fractions to bulk fraction were determined by the relative Chl *a* concentrations of each fractions to total Chl *a* concentrations.

The chemical size fraction was determined by the pigment composition of phytoplankton assemblages. Total diagnostic pigments (DP; in mg m^{-3}) are defined as the sum of seven diagnostic pigments from modified Vidussi et al. (2001):

$$DP = Zea + Chl\ b + Allo + Hex\text{-}fuco + But\text{-}fuco + Fuco + Peri \quad (3.18).$$

The chemical fractions (%) of micro-size (DP_{micro}), nano-size (DP_{nano}), and pico-size (DP_{pico}) were calculated as follows:

$$DP_{micro} = (Fuco + Peri) / DP \times 100 \quad (3.19)$$

$$DP_{nano} = (Allo + Hex\text{-}fuco + But\text{-}fuco) / DP \times 100 \quad (3.20)$$

$$DP_{pico} = (Zea + Chl\ b) / DP \times 100 \quad (3.21).$$

The continuous SI of the natural assemblages of phytoplankton was determined to evaluate the effect of cell size on the optical properties, particularly $a^*_{ph}(676)$ and $\underline{b}^*_{ph}(676)$, and to synthesize the equivalent spherical diameter (d) of the cultural experiments of phytoplankton species (discussed in Chapter IV). The SI was determined by the relative Chl *a* proportion of micro-size, nano-size, and pico-size fractions (%) and weighed values as follows (Bricaud et al. 2004):

$$SI\ (\mu m) = (M\times[micro\text{-}size(\%)] + N\times[nano\text{-}size(\%)] + P\times[pico\text{-}size(\%)])/100 \quad (3.22)$$

where M, N, and P are the weighted values of micro-size, nano-size, and pico-size fraction, respectively. The weighted values were assumed as the representative d ($\underline{d}$) of the each size fractions based on the association of the absorption and scattering properties with the d. The weighted values were calculated from the Chl a_{cell}, $a^*_{ph}(676)$, and $\underline{b}^*_{ph}(676)$ of cultural experiment (Chapter II).

$$Chl\ a_{cell} = C \times d^X \quad (3.23)$$

$$a^*_{ph}(676) = A \times d^Y \quad (3.24)$$

$$\underline{b}^*_{ph}(676) = B \times d^Z \quad (3.25)$$

where Chl a_{cell} is Chl *a* concentration per cell (mg Chl *a* $cell^{-1}$), A, B, C, X, Y, and Z are constants. The $a^*_{ph}(676)$ and $\underline{b}^*_{ph}(676)$ of natural assemblages of phytoplankton were reconstructed by

dividing the $a_{ph}(676)$ and $b_{ph}(676)$ by Chl *a* concentration of all cells within the assemblages as follows:

$$a^*_{ph}(676) = \frac{\sum N_i A C d_i^{X+Y}}{\sum N_i C d_i^{X}} \quad (3.26)$$

$$\underline{b}^*_{ph}(676) = \frac{\sum N_i B C d_i^{X+Z}}{\sum N_i C d_i^{X}} \quad (3.27)$$

where N is number of cell of natural assemblage of phytoplankton. The $\underline{d}$ of absorption and scattering analysis were determined by the combination of the equations (3.24) and (3.26), and the equations (3.25) and (3.27), respectively, as follows:

$$\frac{\sum N_i A C d_i^{X+Y}}{\sum N_i C d_i^{X}} = A \times \underline{d}^{Y} \quad (3.28)$$

$$\frac{\sum N_i B C d_i^{X+Z}}{\sum N_i C d_i^{X}} = B \times \underline{d}^{Z} \quad (3.29)$$

where $\underline{d}$ is representative *d* within a given range of cell size. The size range of micro-size, nano-size, and pico-size fraction were defined as from 0.7 to 2.0 μm in *d*, from 2.0 to 20 μm in *d*, and from 20 to 200 μm in *d*, respectively. To evaluate the $a^*_{ph}(676)$ of natural assemblage of phytoplankton, the weighted values (M_{abs}, N_{abs}, and P_{abs}) were calculated as follows:

$$M_{abs} = \sqrt[X]{\frac{\sum_{i=20}^{200} N_i d_i^{X+Y}}{\sum_{i=20}^{200} N_i d_i^{X}}} \quad (3.30)$$

$$N_{abs} = \sqrt[X]{\frac{\sum_{i=2.0}^{20} N_i d_i^{X+Y}}{\sum_{i=2.0}^{20} N_i d_i^{X}}} \quad (3.31)$$

$$P_{abs} = \sqrt[X]{\frac{\sum_{i=0.7}^{2.0} N_i d_i^{X+Y}}{\sum_{i=0.7}^{2.0} N_i d_i^{X}}} \quad (3.32).$$

To evaluate the $\underline{b}^*_{ph}(676)$ of natural assemblage of phytoplankton, the weighted values (M_{scat}, N_{scat}, and P_{scat}) were calculated as follows:

$$M_{scat} = \sqrt[X]{\frac{\sum_{i=20}^{200} N_i d_i^{X+Z}}{\sum_{i=20}^{200} N_i d_i^{X}}} \quad (3.33)$$

$$N_{scat} = \sqrt[X]{\frac{\sum_{i=2.0}^{20} N_i d_i^{X+Z}}{\sum_{i=2.0}^{20} N_i d_i^{X}}} \quad (3.34)$$

$$P_{scat} = \sqrt[X]{\frac{\sum_{i=0.7}^{2.0} N_i d_i^{X+Z}}{\sum_{i=0.7}^{2.0} N_i d_i^{X}}} \quad (3.35).$$

The N of natural assemblage of phytoplankton was assumed as a power function of *d* with exponent of −4 (Stramski et al. 2001) as follows:

$$N(d) = K \times d^{-4} \quad (3.36)$$

where K is constant. Finally, the SI which was determined by $a^*_{ph}(676)$ (SI_{abs}) and $\underline{b}^*_{ph}(676)$ (SI_{scat}) were calculated as follows:

$$SI_{abs}=(M_{abs}\times[\text{micro-size(\%)}]+ N_{abs}\times[\text{nano-size(\%)}] + P_{abs}\times[\text{pico-size(\%)}])/100 \quad (3.37)$$

$$SI_{scat}=(M_{scat}\times[\text{micro-size(\%)}]+ N_{scat}\times[\text{nano-size(\%)}] + P_{scat}\times[\text{pico-size(\%)}])/100 \quad (3.38).$$

3.2.7. Statistics

Differences in the pigments and the optical properties between micro-size and nano-size fractions were tested with Mann-Whitney Rank Sum Test. Analysis of covariance were carried out to compare the slopes and intercepts of regression lines of the relationships between Chl *a* and DP concentrations, bulk and size fractionated Chl *a* concentrations, Chl *a* concentration and the optical properties, POC concentration and the scattering properties, and size index and the optical properties. Two-way analysis of variance (ANOVA) was carried out to assess the effects of the threes optical depths and the two size fractions on PPC:TC.

3.3. Results

3.3.1. Abiotic factors

Investigations of size distribution of phytoplankton assemblage and the optical properties were divided into four regions according to the differences in the water mass: at the North of AC in SO (NAC), at the South of AC in SO (SAC), in SB during winter (from December to February, WSB),

and in SB from spring to autumn (from March to November, SSB).

In SO along the 110°E and 140°E meridians at NAC (north than approximately 55-58°S, St. C01-10, C02-10, C03-10, D15-11, D14-11, and C02-11), seawater temperature, salinity, and Sigma-t in the upper 100m of the water column decreased gradually from north to south in the austral summer 2010/2011 (Figure 3-3). At NAC, the temperature decreased gradually from 30m to 80m, whereas the salinity increased slightly (Figure 3-3). Thus the pycnocline was developed at about 40m mainly due to the variation in the temperature (Figure 3-3). At the area surrounding AC (approximately 55-58°S), seawater temperature, salinity, and Sigma-t in the upper 100m of the water column were approximately constant (Figure 3-3). At SAC (south than approximately 55-58°S, St. C04-10, C05-10, C06-11, C10-11, D12-11, D10-11, D07-11, C07-12, D13-12, and D07-12), seawater temperature in the upper 100m of the water column decreased with depth, and the salinity increased. Thus the Sigma-t increased with depth, and furthermore low density water observed in the upper the 10m along the 110°E and in the upper the 30m along the 140°E (Figure 3-3). And the pycnocline was developed at 10m (Figure 3-3). The spatial variation in the environmental conditions in the austral summer of 2011/2012 showed similar variation in the 2010/2011.

In SB, vertical variation in seawater temperature, salinity, and Sigma-t were approximately constant in the upper 100m of the water column during winter (from December to February, WSB) (Figure 3-4). From spring to autumn (from March to November, SSB), seawater temperature decreased gradually with depth, and the salinity increased from surface to 20m (Figure 3-4). The Sigma-t decreased gradually with depth, and seasonal pycnocline were developed from 20m to 40m (Figure 3-4).

Nitrate and phosphate concentration in upper the 100m increased gradually from north to

south in SO along the 110°E and 140°E meridians (Table 3-3). Silicate concentrations in upper the 100m in NAC were lower than 4 μM, whereas the silicate concentrations in SAC were higher than 10 μM except St. D13-12 (Table 3-3). In WSB, vertical variation in nitrate, phosphate, and silicate concentrations in the upper 100m of the water column approximately constant as well as temporal variation in Sigma-t (Table 3-4, Figure 3-5). In SSB, nitrate concentration and phosphate concentrations in the upper the pycnocline (from 20m to 40m depth) were generally low, whereas the concentrations decreased with depth in the under the pycnocline (Table 3-4, Figure 3-5). Very high silicate concentration was observed in the upper 10m in summer (Table 3-4, Figure 3-5).

At the sampling stations in SO (NAC+SAC), the depth of lower limit of the euphotic zone, which is equivalent to the optical depth of 4.6, ranged from 37m at St. D10-11 to 130m at C02-11 (Table 3-1). In SB (WSB+SSB), the depth of lower limit of the euphotic zone ranged from 16m on 12 May 2010 to 67m on 26 February 2010 (Table 3-2).

3.3.2. Chl *a* and POC concentrations

In SO along the 110°E and 140°E meridians, bulk Chl *a* concentration at NAC was lower than 0.5 mg Chl *a* m^{-3}, whereas bulk Chl *a* concentration at SAC increased from north to south (Figure 3-6). The highest bulk Chl *a* concentration was observed in 0.93 mg Chl *a* m^{-3} at ζ=2.3 of St. D10-11 (Figure 3-6). The lowest bulk Chl *a* concentration was observed in 0.15 mg Chl *a* m^{-3} at ζ=4.6 of St. D07-12 (Figure 3-6). In SB (WSB+SSB), bulk Chl *a* concentration from late autumn to spring were lower than 1 mg Chl *a* m^{-3} (Figure 3-7). High bulk Chl *a* concentrations were observed throughout the water column on 12 March 2010, and at ζ=0.0 during summer (Figure 3-7). The highest bulk Chl *a* concentration was observed in 3.8 mg Chl *a* m^{-3} on 13 September 2010 at ζ=0.0 of St. M (Figure 3-7). The lowest bulk Chl *a* concentration was observed in 0.16 mg Chl *a* m^{-3} on 22 January

2010 at ζ=4.6 of St. M (Figure 3-7).

In SO (NAC+SAC) along the 110°E and 140°E meridians, the highest bulk POC concentration was observed in 217 mg C m^{-3} at ζ=0.0 of St. D10-11. The lowest bulk POC concentration was observed in 62 mg C m^{-3} at ζ=4.6 of St. D14-11. In SB (WSB+SSB), the highest bulk POC concentration was observed in 917 mg C m^{-3} on 12 May 2010 at ζ=2.3 of St. M. The lowest bulk POC concentration was observed in 55 mg C m^{-3} on 22 January 2010 at ζ=0.0 of St. M.

In SO (NAC+SAC) along the 110°E and 140°E meridians, the highest POC:Chl *a* was observed in 793 g g^{-1} at ζ=0.0 of St. D02-10. The lowest POC:Chl *a* was observed in 169 g g^{-1} at ζ=4.6 of St. D07-11. In SB (WSB+SSB), the highest POC:Chl *a* was observed in 748 g g^{-1} on 16 October 2010 at ζ=4.6 of St. M. The lowest POC:Chl *a* was observed in 44 g g^{-1} on 13 November 2010 at ζ=2.3 of St. M.

The bulk POC concentration significantly increased with bulk Chl *a* concentration in SAC (p<0.001) and SSB (p<0.05) when the regions were divided (Table 3-5). When all stations in SO (NAC+SAC) and SB (WSB+SSB) were considered together, there was the significant positive relationship between bulk Chl *a* and bulk POC concentrations (p<0.001, Table 3-5, Figure 3-8).

3.3.3 Size distribution of phytoplankton assemblage

Physical size fractions phytoplankton assemblages were represented by the relative Chl *a* proportions of micro-size, nano-size, and pico-size fractions to bulk fractions (%) in the four regions (Figure 3-9). In NAC, the relative proportions of micro-size fractions ranged from 6.2 % at ζ=4.6 of St. C02-11 to 54% at ζ=2.3 of St. D14-11, and the relative proportion of nano-size fractions ranged from 31 % at ζ=2.3 of St. C02-11 to 54% at ζ=0.39 of St. C03-10 (Figures 3-10 and 3-11). In SAC, the relative proportions of micro-size fractions ranged from 1.5 % at ζ=4.6 of St.

D12-11 to 75% at ζ=2.3 of St. D10-11, and the relative proportion of nano-size fractions ranged from 22 % at ζ=2.3 of St. D10-11 to 87% at ζ=4.6 of St. C07-12 (Figures 3-10 and 3-11). In WSB, the relative proportions of micro-size fractions from ranged 1.3 % at ζ=2.3 on 26 February 2010 to 39% at ζ=4.6 on 14 December 2010, and the relative proportion of nano-size fractions ranged from 24 % at ζ=4.6 on 14 December 2010 to 94 % at ζ=0.0 on 18 December 2010 (Figure 3-12). In SSB, the relative proportions of micro-size fractions from ranged 3.4 % at ζ=4.6 on 23 October 2010 to 84 % at ζ=0.0 on 13 September 2010, and the relative proportions of nano-size fractions ranged from 7.8 % at ζ=0.0 on 20 October 2009 to 82 % at ζ=4.6 on 23 October 2010 (Figure 3-12).

There was the significant positive relationship (p<0.01) between micro-size fractionated and bulk Chl *a* concentration in the following three regions, such as SAC, WSB, and SSB (Table 3-6). When all stations were considered together, there was also the significant positive relationship between micro-size fractionated and bulk Chl *a* concentrations (p<0.001, Table 3-6, Figure 3-13A). The relationship between nano-size fractionated and bulk Chl *a* concentrations were significant for each region (p<0.01, Table 3-6) and for all stations (p<0.001, Figure 3-13B).

The relative proportion of micro-size fraction in bulk fractions increased significantly with bulk Chl *a* concentration (p<0.001, Figure 3-14A) when all stations were considered together, whereas the relative proportion of nano-size fraction decreased significantly with bulk Chl *a* concentration (p<0.001, Table 3-7, Figure 3-14B). Large cells contribute to the increase in the bulk biomass of Chl *a* in the sea.

Chemical size fractions of phytoplankton assemblages were represented by the relative proportion of the size class-specific pigments to the bulk DP (Diagnostic Pigments). The bulk DP concentrations increased significantly with bulk Chl *a* concentration for each region (p<0.001) and for all stations in SO (NAC+SAC) and SB (WSB+SSB) (p<0.001, Table 3-8, Figure 3-15). When

the regions were divided, the DP_{micro} increased significantly with the relative Chl *a* proportion of micro-size fraction in NAC (p<0.001), SAC (p<0.01), and SSB (p<0.001), whereas the DP_{nano} was insignificant relationship with the relative Chl *a* proportion of nano-size fraction for each region (Table 3-9, Figure 3-16). When all stations were considered together, there was the significant positive relationship between the DP_{micro} and the relative Chl *a* proportion of micro-size fraction (p<0.001), whereas there was a weak, yet significant negative relationship between DP_{nano} and the relative Chl *a* proportion of nano-size fraction (p<0.05, Table 3-9, Figure 3-16).

Continuous size index of phytoplankton assemblages in SO and SB were obtained from the relative Chl *a* proportion of micro-size, nano-size, and pico-size fractions (%) and weighed values. In cultural experiments (Chapter II), the Chl *a* concentration per cell (Chl a_{cell}) decreased significantly with the cell size of various phytoplankton species (p<0.001), and the $a^*_{ph}(676)$ and $\underline{b}^*_{ph}(676)$ increased significantly with the cell size (p<0.05, Table 3-10). The weighted values of micro-size and nano-size fractions were similar in the absorption and scattering analyses (Table 3-11). The weighted values of micro-size fractions were 10-fold higher than that of nano-size fractions. The number of the phytoplankton cell was assumed as a power function of equivalent spherical diameter (d) with the exponent of –4 (equation 3.36). When the power exponent decreased, the weighted values of three size class decreased.

The SI_{abs} and SI_{scat} at all stations were similar because the weighted value of each size class was similar between the absorption and scattering analyses (Table 3-12). The average SI_{abs} and SI_{scat} in NAC, SAC, and WSB fell in the range of the nano-size phytoplankton, whereas the average SI_{abs} and SI_{scat} in SSB fell in the range of the micro-size phytoplankton (Table 3-12).

3.3.4. Absorption properties

The $a_{ph}(676)$ of micro-size and nano-size fractions increased significantly with micro-size and nano-size fractionated Chl *a* concentrations, respectively, in NAC ($p<0.001$), SAC ($p<0.001$), and SSB ($p<0.001$) when the regions were divided (Table 3-13). When all stations were considered together, there were significant positive relationships between size fractionated Chl *a* concentrations and $a_{ph}(676)$ of two size fractions ($p<0.001$, Table 3-13, Figure 3-17A and B). The slope and intercept of the relationship between size fractionated Chl *a* concentration and $a_{ph}(676)$ were not significantly different between micro-size and nano-size fractions.

The slope of the relationship between Chl *a* concentration and $a_{ph}(676)$ was equivalent to the average $a^*_{ph}(676)$ of phytoplankton assemblage. The $a^*_{ph}(676)$ was not significantly different between micro-size and nano-size fractions for each regions and for all stations (Table 3-14). Consequently the $Q_a^*(676)$ was also not significantly different between micro-size and nano-size fractions for each regions and for all stations (Table 3-14). The similarity in $a^*_{ph}(676)$ and $Q_a^*(676)$ between micro-size and nano-size fractions suggests that the absorption efficiency may not be influenced by cell size.

The bulk $a^*_{ph}(676)$ decreased significantly with increasing SI_{abs} when all stations were considered together ($p<0.05$, Figure 3-18) although the significance was disappeared in each region (Table 3-15). The negative relationship suggests the occurrence the pigments self-shading in the cell of the natural assemblage of phytoplankton.

3.3.5. Scattering properties

The investigation of bulk $\underline{b}_{ph}(676)$ was conducted in all stations (NAC, SAC, WSB, and SSB), and that of the size-fractionated $\underline{b}_{ph}(676)$ was conducted in only SB (WSB + SSB). Average ± standard error of $a_{ph}(555):a_p(555)$, which was used to remove the scattering coefficient of the particle other

than phytoplankton cell from bulk $\underline{b}_p(\lambda)$, was 0.66 ± 0.023 (n=62) when the all regions were considered.

The $\underline{b}_{ph}(676)$ of micro-size and nano-size fractions increased significantly with micro-size and nano-size fractionated Chl *a* concentrations, respectively, when all stations of SB were considered together ($p<0.05$, Figure 3-19A and B). The slope of the relationship was not significantly different between micro-size and nano-size fractions, whereas the intercept of the relationship of nano-size fraction was higher than micro-size fraction ($p<0.05$, Table 3-16).

The slope of the relationship between Chl *a* concentration and $\underline{b}_{ph}(676)$ was equivalent to the average $\underline{b}^*_{ph}(676)$ of the natural assemblage of phytoplankton. The average $\underline{b}^*_{ph}(676)$ for the nano-size fraction was 1.5-fold lager than those for the micro-size fraction (Table 3-17).

The bulk $\underline{b}^*_{ph}(676)$ decreased significantly with increasing SI_{scat} ($p<0.05$) when all stations (n=58) were considered together (Figure 3-20) although there was insignificant relationship between the bulk $\underline{b}^*_{ph}(676)$ and SI_{scat} when the regions were divided (Table 3-18). Decreasing bulk $\underline{b}^*_{ph}(676)$ as a function of SI_{scat} suggests the scattering efficiency may be influenced by cell size.

The bulk $\underline{b}_{ph}(676)$ and bulk $\underline{b}^*_{ph}(676)$ increased significantly with the POC concentration ($p<0.001$, Figure 3-21A) and POC:Chl *a* ($p<0.001$, Figure 3-21B), respectively, when the regions were considered together. The bulk $\underline{b}_{ph}(676)$ and $\underline{b}^*_{ph}(676)$ increased significantly with the POC concentration and POC:Chl *a*, respectively, for only SSB ($p<0.001$, Table 3-19) where the maximum POC and Chl *a* concentration among four regions were observed. The POC contribute to the increase in the bulk $\underline{b}_{ph}(676)$ in the sea.

3.3.6. Physiological properties

The PPC:TC of both micro-size and nano-size fractions increased significantly with increasing light

intensity of the each depth in the water column (p<0.01, Table 3-20, Figure 3-22A). The slope of the relationship between the PPC:TC and the light intensity was not significantly different between micro-size and nano-size fractions. At each optical depth for all stations, the PPC:TC were not significantly different between micro-size and nano-size fractions (Table 3-21, Figure 3-22B). The PPC:TC exhibited the photoacclimation of phytoplankton assemblage, which is one of the physiological response of phytoplankton to the light condition, in both SO and SB, whereas the PPC:TC decreased significantly with increasing optical depth in only SO (NAC and SAC, p<0.05, Table 3-22).

The bulk $a^*_{ph}{}^{slope}$ decreased significantly with increasing the bulk PPC:TC when the all station (n=91) were considered together (p<0.01, Figure 3-23), whereas significant relations were disappeared when the individual regions were considered except for the SSB region (Table 3-23). The higher determination coefficient (r^2) was observed the SSB region, suggesting that the index of $a^*_{ph}{}^{slope}$ is likely sensitive to the biomass of pigments.

3.4. Discussion

The water stratification in water column could cause the bloom of large-cell phytoplankton in St. D10-11 (in 140^{o}E in SO), which was characterized by the high Chl *a* concentration and the high proportion of micro-size fractions (> 60 %). In the SAC region, the low density water in the upper 10m along the 110^{o}E and in the upper 30m along the 140^{o}E could be released from an ice melt water inflow in austral summer. The inflow of the ice melt water induced the formation of pycnocline at the surface layer in the water column along those lines. The ice melt water could supply macronutrient for phytoplankton growth (Kopczyńska et al. 2007), and then the bloom of large-cell phytoplankton species could occur in the surface mixed layer (Saggiomo et al. 1998;

Hashihama et al. 2008). However there were the water-mass with the low Chl *a* concentration and the low proportion of micro-size fraction in St. D07-11 (in 140^{o}E) where located near the ice edge. Compared with the distribution of the Chl *a* concentration along the 140^{o}E, the increasing Chl *a* concentrations from north to south along the 110^{o}E indicated that the water stratification in 110^{o}E was more enhanced. The enhanced water stratification could exhibit the time lag elapsed from melting ice (Sullivan et al. 1988). The difference in the biomass of micro-size fraction between St. D10-11 and St. D07-11 suggests that the occurrence of the time lag for development of the stratification or growth of phytoplankton. In Sagami Bay, there was the bloom of the large cell phytoplankton in the surface mixed layer and the extent of the bloom as the maximum Chl *a* concentration in Sagami Bay was 4-fold larger than that in the Indian sector of the Southern Ocean.

From spring to late autumn in Sagami Bay, the development of the water stratification could induce the bloom of large-cell phytoplankton because the temporal stratification could induce the nutrient supplies from deep water (Ara et al. 2011). Particularly, the high Chl *a* concentrations in the surface during summer could be provided by micro-size diatoms, such as *Nitzschia* spp. and *Thalassiosira* spp., and micro-size dinoflagellates, such as *Ceratium furca* and *C. fusus* (Fujiki et al. 2003; Baek et al. 2008). Furthermore, significant relationship between relative Chl *a* proportion of micro-size fractions and DP_{micro} in SSB confirmed that the bloom could be occurred by micro-size diatom and dinoflagellate which are characterized by accessary pigments Fuco and Peri, respectively.

Phytoplankton accessary pigments Fuco and Peri, which are used to marker pigments of micro-size fraction, could represent the index of diatom and dinoflagellate in both of the Southern Ocean (Wright et al. 1996; Takao et al. 2012) and Sagami Bay (Hashihama et al. 2008). In both regions, the micro-size phytoplankton species are almost of diatom and dinoflagellate, and therefore

the relationship between the physical size fraction and the chemical size fraction was strongly correlated in micro-size phytoplankton assemblages. Compared with micro-size fractions, the insignificant relationship between the physical size fraction and the chemical size fraction of nano-size fractions could be due to the high species diversity of nano-size cells. Since Fuco is characterized by micro-size phytoplankton species, the chemical size fraction of nano-size could be underestimated by the Fuco-containing diatoms or haptophyte with nano-size cells (Wright et al. 1996). Eventually usage of the chemical size fraction for the analysis on the size distribution of phytoplankton assemblage could be limited in the regions where the diagnostic pigment composition could have an accordance with the three size fraction of phytoplankton assemblage (Bricaud et al. 2004; Uitz et al. 2006). On the other hand, the continuous size index of natural assemblage of phytoplankton covary with the effect of cell size on the absorption and scattering properties of phytoplankton species, and therefore the continuous size index could be precisely matched with the size distribution of phytoplankton assemblage.

Increasing SI_{abs} with decreasing $a^*_{ph}(676)$ could be due to pigments self-shading in the cell (package effect, Berner et al. 1989; Bricaud et al. 1995). The slope of the relationship between Chl *a* concentration and $a_{ph}(676)$ was lower than the value in 0.027 m^2 mg Chl a^{-1} which was assumed as unpackaged absorption efficiency of Chl *a* (Johnsen et al. 1994). The low slope confirmed that the $a^*_{ph}(676)$ of micro-size and nano-size phytoplankton cell decreased due to the package effect. The similar slopes of the relationship between Chl *a* concentrations and $a_{ph}(676)$ between micro-size and nano-size fractions suggest that micro-size and nano-size cell in natural assemblage of phytoplankton could have the similar absorption efficiency per intracellular Chl *a* contents (Chl a_i). The similar efficiency could be due to the reverse relationship between the Chl a_i and cell size (Malone 1980). Accordingly the increasing SI_{abs} with decrease in $a^*_{ph}(676)$ suggests that the

package effect could be more dependent on Chl a_i but not the cell size. The effect of Chl a_i on $a^*_{ph}(676)$ is one of the reason why it is obscure to estimate the size distribution of natural phytoplankton assemblage by using absorption properties of phytoplankton (Brewin et al. 2011). On the other hand, the package effect in natural assemblages of phytoplankton could be determined by not only individual cells but also total cell volume of phytoplankton assemblage (Bricaud et al. 1995). In that case, the continuous SI_{abs} could be a better index of the representative cell size of phytoplankton assemblages because the variation in SI_{abs} was considered as the factors of the effect of Chl a_i on cell size as well as the effect of $a^*_{ph}(676)$ on cell size. Because the significant relationship between the SI_{abs} and $a^*_{ph}(676)$ for all stations in SO and SB, the relationship could be reliable at global scale.

Increasing SI_{scat} with decreasing $\underline{b}^*_{ph}(676)$ suggest that the $\underline{b}^*_{ph}(676)$ could represent the biomass of the phytoplankton assemblage but also the size distribution. The SI_{scat} is estimated by using the assumption of the size distribution of phytoplankton cell, the power exponent of –4 (Stramski et al. 2001). In previous study, the size distribution of the cells could influence on the scattering coefficient of the particles (Spinrad 1986; Babin et al. 2003). As decreasing weighted values of three size class, the SI_{scat} is shifted toward small one, whereas the slope of the relationship between the $\underline{b}^*_{ph}(676)$ and SI_{scat} does not change because the change in the weighted values of three size class is similar. The approximately constant slope of the relationship suggests that the scattering efficiency of particles other than phytoplankton cell, such as detritus, was similar to that of phytoplankton, and then the slope of the relationship can assist to evaluate the size effect of phytoplankton cells and monitoring of the size distribution of phytoplankton assemblage.

In the Indian sector of the southern ocean, decreasing PPC:TC with increasing optical depth suggests that the photoprotective response of natural phytoplankton assemblage to high light

(Motokawa et al. 2014). Photoprotective acclimation of natural phytoplankton assemblages can be indexed by the change in photoprotecitve carotenoid normalized phytoplankton biomass (MacIntyre et al. 2002). The composition of PPC and TC in phytoplankton cell is different among species (Brunet et al. 2011), however the PPC:TC of natural assemblage of phytoplankton as a function of light intensity was similar between micro-size and nano-size fractions. Therefore the $a^*_{ph}{}^{slope}$ could be utilized to evaluate the photoprotective acclimation of phytoplankton without the size effect on the $a^*_{ph}{}^{slope}$ because the slope of the relationship between the $a^*_{ph}{}^{slope}$ and PPC:TC was similar between micro-size and nano-size fractions.

The high intercept of the relationship between the $a^*_{ph}{}^{slope}$ and PPC:TC in SSB could be due to the high proportion of micro-size phytoplankton. The high intercept indicates the flat spectra of $a^*_{ph}{}^{slope}$ as a function of PPC:TC (Eisner et al. 2003). The large-cell phytoplankton could be influenced on large package effect by intracellular PPC and TC (Johnsen and Sakshaug 1993). The package effect by TC in the cell could larger than those by PPC because of the higher concentration of TC than PPC. Thus, under the similar light condition, the package effect as a function of PPC:TC of large-cell could be higher than that of small-cells, and then the $a^*_{ph}{}^{slope}$ could become flatter.

Furthermore the high proportion of micro-size phytoplankton in SSB could induce the flat slope of the relationship between the $\underline{b}^*_{ph}(676)$ and POC:Chl *a*. The flat slope indicates little change in the $\underline{b}^*_{ph}(676)$ as a function of POC:Chl *a*. The $b^*_{ph}(676)$ decreased with increasing cell size (Chapter II), and the cell size decreased with the intracellular carbon contents of phytoplankton cell (Vaillancourt et al. 2004). Thus the compensation effect of carbon and cell size on the $\underline{b}^*_{ph}(676)$ could induce small change in the $\underline{b}^*_{ph}(676)$ as a function of POC:Chl *a*. On the other hand, the *in situ* POC:Chl *a* is one of the index of the physiology in phytoplankton assemblage to be utilized to monitor the phytoplankton growth (Behrenfeld and Boss 2003). Therefore the relationship between

POC:Chl *a* and $\underline{b}^*_{ph}(676)$ could assist to evaluate the phytoplankton physiology in water column and estimate the size distribution of phytoplankton assemblage using $\underline{b}^*_{ph}(676)$.

The present study confirms that the size distribution of phytoplankton assemblage is estimated by using $a^*_{ph}(676)$ and $\underline{b}^*_{ph}(676)$ in both of Case I and II waters. The optical continuous size index could most assist to evaluate the size effect of cells in natural assemblage of phytoplankton. Decreasing $a^*_{ph}(676)$ with increasing SI_{abs} could indicate the direct effects of Chl a_i and indirect effect of cell size on the $a^*_{ph}(676)$, whereas decreasing $\underline{b}^*_{ph}(676)$ with increasing SI_{scat} could indicate direct effect of cell size on the $\underline{b}^*_{ph}(676)$. The significant relationships between SI_{abs} and $a^*_{ph}(676)$ and/or SI_{scat} and $\underline{b}^*_{ph}(676)$ suggest that the optical characteristics of phytoplankton at 676nm could be reliable for the estimation of size distribution of phytoplankton in not only Case I waters but also Case II waters. Furthermore the present study suggests that PPC:TC of phytoplankton assemblage and POC:Chl *a* could assist to interpret the variation in the intercept of the relationships between SI_{abs} and $a^*_{ph}(676)$ and/or SI_{scat} and $\underline{b}^*_{ph}(676)$.

Table 3-1. Sampling date and depth in Southern Ocean at the optical depths of 0.39, 2.3, and 4.6. Sampling depth with a hyphen indicates no data available. Sampling depth with an asterisk indicates ζ= 3.9.

Station	Samling date	Sampling depth (m)		
	Local time	ζ = 0.39	ζ = 2.3	ζ = 4.6
C01-10	Dec. 26 2010	1	25	52
C02-10	Dec. 27 2010	3	35	67
C03-10	Dec. 28 2010	3	28	75*
C04-10	Dec. 29 2010	3	30	65
C05-10	Dec. 30 2010	3	25	55
C06-11	Dec. 31 2010	3	40	60
C10-11	Jan. 2 2011	3	17	43
D15-11	Jan. 18 2011	3	33	68
D14-11	Jan. 17 2011	3	25	63
D12-11	Jan. 15 2011	3	25	65
D10-11	Jan. 14 2011	3	20	37
D07-11	Jan. 11 2011	5	30	60
C02-11	Dec. 30 2011	—	60	130
C07-12	Jan. 3 2012	—	28	64
D13-12	Jan. 27 2012	5	34	75
D07-12	Jan. 21 2012	5	28	120

Table 3-2. Sampling date and depth in Sagami Bay at the optical depths of 0.0, 2.3, and 4.6.

Station	Samling date	Sampling depth (m)		
	Local time	$\zeta = 0.0$	$\zeta = 2.3$	$\zeta = 4.6$
M	Jul. 16 2009	0	15	45
M	Aug. 20 2009	0	15	45
M	Sep. 10 2009	0	14	40
M	Oct. 23 2009	0	10	23
M	Dec. 1 2009	0	9	17
M	Dec. 18 2009	0	19	55
M	Jan. 22 2010	0	20	55
M	Feb. 26 2010	0	37	67
M	Mar. 15 2010	0	10	24
M	Apr. 14 2010	0	20	47
M	May. 12 2010	0	5	16
M	Jun. 19 2010	0	16	46
M	Jul. 21 2010	0	27	50
M	Aug. 18 2010	0	16	36
M	Sep. 13 2010	0	15	32
M	Oct. 16 2010	0	20	45
M	Nov. 13 2010	0	14	29
M	Dec. 14 2010	0	25	65

Table 3-3. Spatial variations in nitrate, phosphate, and silicate concentrations at the optical depths of 0.39, 2.3, and 4.6 of the Indian sector of the Southern Ocean. Sampling depth with a hyphen indicates no data available. N.D. indicates not detect.

Station	Nitrate (μM)			Phosphate (μM)			Silicate (μM)		
	ζ = 0.39	ζ = 2.3	ζ = 4.6	ζ = 0.39	ζ = 2.3	ζ = 4.6	ζ = 0.39	ζ = 2.3	ζ = 4.6
C01-10	0.1	0.2	0.2	N.D.	0.01	N.D.	0.1	0.1	0.3
C02-10	2.0	2.1	2.4	0.25	0.29	0.33	0.2	0.2	1.2
C03-10	4.8	4.5	4.5	0.61	0.59	0.64	3.4	3.0	3.1
C04-10	6.1	4.4	6.0	0.97	0.88	1.09	13.7	10.6	15.2
C05-10	5.5	6.5	6.3	0.73	1.01	1.24	10.7	15.6	19.6
C06-11	5.2	5.7	5.7	1.04	1.15	1.22	18.8	20.8	21.9
C10-11	4.1	5.0	5.4	0.64	0.62	0.85	37.0	37.3	43.5
D15-11	4.5	4.0	4.5	0.84	0.69	0.81	0.8	0.2	1.9
D14-11	5.7	5.7	5.5	0.82	1.08	0.83	0.1	0.1	0.1
D12-11	4.6	5.7	5.5	1.08	1.08	1.10	12.7	0.1	14.9
D10-11	5.7	4.9	5.3	0.99	0.83	0.92	22.0	18.3	19.7
D07-11	5.7	5.1	5.3	1.13	0.97	1.19	32.6	33.5	37.5
C02-11	—	3.3	3.1	—	0.50	0.44	—	0.6	1.6
C07-12	—	5.7	6.9	—	0.61	1.11	—	12.3	20.1
D13-12	5.8	6.3	7.0	0.63	0.49	0.57	5.9	3.3	4.6
D07-12	6.7	5.0	5.9	0.90	0.81	0.86	20.3	21.6	30.7

Table 3-4. Temporal variations in nitrate, phosphate, and silicate concentrations at the optical depths of 0.0, 2.3, and 4.6 of Sagami Bay. Sampling depth with a hyphen indicates no data available. N.D. indicates not detect.

Station	Samling date	Nitrate (μM)			Phosphate (μM)			Silicate (μM)		
	Local time	ζ = 0.0	ζ = 2.3	ζ = 4.6	ζ = 0.0	ζ = 2.3	ζ = 4.6	ζ = 0.0	ζ = 2.3	ζ = 4.6
M	Jul. 16 2009	—	—	—	—	—	—	—	—	—
M	Aug. 20 2009	6.1	1.5	3.5	0.10	0.00	0.10	8.0	4.8	7.9
M	Sep. 10 2009	7.6	4.1	1.9	0.20	0.10	0.10	14.8	9.8	7.4
M	Oct. 23 2009	5.6	20.3	5.5	0.20	0.50	0.20	13.8	18.0	12.1
M	Dec. 1 2009	14.3	15.4	17.6	0.35	0.50	0.50	12.1	14.6	15.1
M	Dec. 18 2009	—	—	—	—	—	—	—	—	—
M	Jan. 22 2010	24.4	18.3	24.3	0.70	0.80	0.80	17.0	25.3	19.8
M	Feb. 26 2010	14.1	14.8	19.3	0.50	0.50	0.60	14.3	13.6	15.8
M	Mar. 15 2010	13.6	8.8	9.8	0.40	0.50	0.40	14.4	14.3	10.0
M	Apr. 14 2010	9.6	11.0	6.7	0.60	0.40	0.30	16.5	14.5	9.2
M	May. 12 2010	1.2	1.3	13.6	0.20	0.20	0.40	11.5	8.7	14.4
M	Jun. 19 2010	2.3	7.5	10.4	0.55	0.65	0.45	14.9	17.3	14.3
M	Jul. 21 2010	1.5	2.4	4.1	0.03	N.D.	0.07	17.8	5.2	10.8
M	Aug. 18 2010	2.6	0.6	4.1	1.18	1.33	1.34	37.6	6.6	9.3
M	Sep. 13 2010	0.8	0.8	0.9	N.D.	N.D.	N.D.	2.9	2.6	4.7
M	Oct. 16 2010	1.6	3.5	8.1	N.D.	N.D.	N.D.	12.6	5.2	9.9
M	Nov. 13 2010	1.0	1.4	1.7	N.D.	N.D.	N.D.	5.7	4.7	5.6
M	Dec. 14 2010	6.0	5.6	7.5	0.03	0.08	0.11	11.2	9.1	8.9

Table 3-5. Regression analysis between bulk Chl *a* and bulk POC concentrations. N. S. indicates not significant. n, S.E., r^2, and *p* indicate the number of sample, determination coefficient, standard error, and probability, respectively.

Regression equation	Region	n	Y_{int} ± S.E.	Slope ± S.E.	r^2	*p*
POC	NAC	15	90 ± 20	80 ± 77	0.08	N.S.
= Y_{int} + Slope × Chl *a*	SAC	21	72 ± 16	145 ± 33	0.50	<0.001
	WSB	13	76 ± 23	61 ± 49	0.12	N.S.
	SSB	39	155 ± 39	53 ± 22	0.13	<0.05
	All	88	108 ± 15	73 ± 13	0.28	<0.001

Table 3-6. Regression analyses between micro-size and nano-size fractionated Chl *a* concentrations and bulk Chl *a* concentration. N. S. indicates not significant. n, S.E., r^2, and *p* indicate the number of sample, determination coefficient, standard error, and probability, respectively.

Regression equation	Region	n	Y_{int} ± S.E.	Slope ± S.E.	r^2	*p*
Bulk Chl *a*	NAC	15	0.06 ± 0.03	0.01 ± 0.120	0.00	N.S.
= Y_{int} + Slope × Micro-size Chl *a*	SAC	29	–0.13 ± 0.03	0.72 ± 0.076	0.77	<0.001
	WSB	14	–0.04 ± 0.03	0.24 ± 0.072	0.49	<0.01
	SSB	34	–0.27 ± 0.10	0.71 ± 0.055	0.84	<0.001
	All	92	–0.16 ± 0.03	0.66 ± 0.028	0.87	<0.001
Bulk Chl *a*	NAC	15	–0.01 ± 0.02	0.50 ± 0.071	0.79	<0.001
= Y_{int} + Slope × Nano-size Chl *a*	SAC	29	0.08 ± 0.03	0.30 ± 0.077	0.36	<0.001
	WSB	14	0.07 ± 0.03	0.22 ± 0.062	0.50	<0.01
	SSB	34	0.13 ± 0.08	0.21 ± 0.042	0.44	<0.001
	All	92	0.09 ± 0.02	0.22 ± 0.020	0.58	<0.001

Table 3-7. Regression analyses between relative Chl *a* proportions of micro-size and nano-size fractions to bulk fraction and log bulk Chl *a* concentration. N. S. indicates not significant. n, S.E., r^2, and *p* indicate the number of sample, determination coefficient, standard error, and probability, respectively.

Regression equation	Region	n	Y_{int} ± S.E.	Slope ± S.E.	r^2	*p*
Log bulk Chl *a*	NAC	15	2.2 ± 20.4	−37.5 ± 32.3	0.09	N.S.
= Y_{int} + Slope × Micro-size (%)	SAC	29	62.0 ± 7.0	65.1 ± 14.3	0.43	<0.001
	WSB	14	15.5 ± 7.8	0.3 ± 17.6	0.00	N.S.
	SSB	34	42.2 ± 3.4	31.9 ± 8.8	0.29	<0.05
	All	92	41.9 ± 2.5	31.2 ± 5.2	0.28	<0.001
Log bulk Chl *a*	NAC	15	44.8 ± 12.0	−2.2 ± 19.0	0.00	N.S.
= Y_{int} + Slope × Nano-size (%)	SAC	29	37.5 ± 7.9	−33.0 ± 16.0	0.14	<0.05
	WSB	14	33.2 ± 7.1	−15.3 ± 16.0	0.07	N.S.
	SSB	34	32.6 ± 2.5	−6.5 ± 6.4	0.03	N.S.
	All	92	36.4 ± 2.1	−19.1 ± 36.4	0.18	<0.001

Table 3-8. Regression analysis between bulk Chl *a* and bulk DP concentrations. N. S. indicates not significant. n, S.E., r^2, and *p* indicate the number of sample, determination coefficient, standard error, and probability, respectively.

Regression equation	Region	n	Y_{int} ± S.E.	Slope ± S.E.	r^2	*p*
DP	NAC	17	–0.07 ± 0.07	1.57 ± 0.26	0.71	<0.001
= Y_{int} + Slope × Chl *a*	SAC	29	–0.15 ± 0.05	1.50 ± 0.11	0.87	<0.001
	WSB	14	0.09 ± 0.04	0.59 ± 0.08	0.82	<0.001
	SSB	39	0.16 ± 0.15	0.87 ± 0.09	0.73	<0.001
	All	99	0.08 ± 0.05	0.90 ± 0.04	0.81	<0.001

Table 3-9. Regression analyses between the relative Chl *a* proportion of micro-size and DP_{micro}, the relative Chl *a* proportion of nano-size fraction and DP_{nano}. N. S. indicates not significant. n, S.E., r^2, and *p* indicate the number of sample, determination coefficient, standard error, and probability, respectively.

Regression equation	Region	n	Y_{int} ± S.E.	Slope ± S.E.	r^2	*p*
DP_{micro}(%)	NAC	15	12 ± 5.6	0.97 ± 0.183	0.83	<0.001
= Y_{int} + Slope × Micro-size (%)	SAC	28	58 ± 4.6	0.34 ± 0.121	0.23	<0.01
	WSB	14	30 ± 3.3	0.01 ± 0.176	0.00	N.S.
	SSB	34	45 ± 5.7	0.65 ± 0.117	0.49	<0.001
	All	91	34 ± 3.4	0.77 ± 0.088	0.46	<0.001
DP_{nano}(%)	NAC	15	36 ± 20.4	0.46 ± 0.433	0.08	N.S.
= Y_{int} + Slope × Nano-size (%)	SAC	28	31 ± 9.4	–0.06 ± 0.169	0.00	N.S.
	WSB	14	39 ± 9.5	–0.16 ± 0.233	0.04	N.S.
	SSB	34	5 ± 3.2	0.20 ± 0.091	0.14	N.S.
	All	91	14 ± 5.4	0.32 ± 0.120	0.07	<0.05

Table 3-10. Regression equations of (3.23), (3.24), and (3.25) which were derived from cultural experiments (Chapter II). n, r^2, and p indicate the number of sample, determination coefficient, and probability, respectively.

	Regression equation	n	r^2	p
(3.23)	Chl $a_{cell} = 1.02\times10^{-11} \times d^{2.33}$	72	0.89	<0.001
(3.24)	$a^*_{ph}(676) = 0.0165 \times d^{-0.0940}$	50	0.08	<0.05
(3.25)	$\underline{b}^*_{ph}(676) = 0.343 \times d^{-0.419}$	26	0.16	<0.05

Table 3-11. Weighted values of micro-size, nano-size, and pico-size fractions for absorption and scattering analyses.

Analysis	Size fraction		
	Micro-size	Nano-size	Pico-size
Absorption	47	4.7	1.1
Scattering	44	4.4	1.1

Table 3-12. Average ± standard error of SI_{abs} and SI_{scat} in NAC, SAC, WSB, SSB, and all stations.

Region	n	SI_{abs}	SI_{scat}
NAC	15	14.4 ± 2.02	13.5 ± 1.88
SAC	29	18.1 ± 1.66	16.9 ± 1.55
WSB	14	8.9 ± 1.38	8.4 ± 1.29
SSB	34	21.9 ± 1.76	20.5 ± 1.65
All	92	17.6 ± 1.01	16.5 ± 0.95

Table 3-13. Regression analyses between micro-size fractionated Chl *a* and $a_{ph}(676)$, and nano-size fractionated Chl *a* and $a_{ph}(676)$. N. S. indicates not significant. n, S.E., r^2, and *p* indicate the number of sample, determination coefficient, standard error, and probability, respectively.

Regression equation	Region	n	Y_{int} ± S.E.	Slope ± S.E.	r^2	*p*
Micro-size $a_{ph}(676)$	NAC	15	0.0002 ± 0.0003	0.023 ± 0.0043	0.69	<0.001
$=Y_{int}$ + Slope × Micro-size Chl *a*	SAC	28	–0.0004 ± 0.0005	0.026 ± 0.0020	0.86	<0.001
	WSB	9	0.0014 ± 0.0003	–0.001 ± 0.0003	0.03	N.S.
	SSB	29	0.0049 ± 0.0049	0.020 ± 0.0040	0.49	<0.001
	All	82	0.0012 ± 0.0014	0.022 ± 0.0019	0.63	<0.001
Nano-size $a_{ph}(676)$	NAC	15	0.0002 ± 0.0005	0.023 ± 0.0036	0.76	<0.001
$=Y_{int}$ + Slope × Nano-size Chl *a*	SAC	28	–0.0003 ± 0.0003	0.027 ± 0.0015	0.92	<0.001
	WSB	9	0.0001 ± 0.0019	0.017 ± 0.0108	0.24	N.S.
	SSB	29	0.0016 ± 0.0019	0.020 ± 0.0033	0.58	<0.001
	All	82	0.0005 ± 0.0006	0.022 ± 0.0016	0.69	<0.001

Table 3-14. Average ± standard error of the $a^*_{ph}(676)$ and $Q^*_a(676)$ of micro-size and nano-size fractions in NAC, SAC, WSB, SSB, and all stations.

Region	n	$a^*_{ph}(676)$		$Q^*_a(676)$	
		Micro-size fraction	Nano-size fraction	Micro-size fraction	Nano-size fraction
NAC	15	0.029 ± 0.0043	0.025 ± 0.0015	1.08 ± 0.16	0.92 ± 0.06
SAC	28	0.026 ± 0.0031	0.026 ± 0.0010	0.96 ± 0.12	0.95 ± 0.04
WSB	9	0.029 ± 0.0081	0.019 ± 0.0032	1.08 ± 0.30	0.72 ± 0.12
SSB	29	0.036 ± 0.0073	0.025 ± 0.0030	1.17 ± 0.26	0.92 ± 0.10
All	81	0.030 ± 0.0033	0.025 ± 0.0012	1.09 ± 0.11	0.90 ± 0.05

Table 3-15. Regression analysis between log $a^*_{ph}(676)$ and log SI_{abs}. N. S. indicates not significant. n, S.E., r^2, and p indicate the number of sample, determination coefficient, standard error, and probability, respectively.

Regression equation	Region	n	Y_{int} ± S.E.	Slope ± S.E.	r^2	p
Log $a^*_{ph}(676)$	NAC	13	−1.50 ± 0.08	−0.06 ± 0.07	0.06	N.S.
= Y_{int} + Slope × Log SI_{abs}	SAC	21	−1.44 ± 0.08	−0.12 ± 0.07	0.15	N.S.
	WSB	13	−1.40 ± 0.13	−0.21 ± 0.13	0.18	N.S.
	SSB	30	−1.44 ± 0.18	−0.13 ± 0.13	0.03	N.S.
	All	77	−1.46 ± 0.06	−0.11 ± 0.05	0.06	<0.05

Table 3-16. Regression analyses between micro-size fractionated Chl *a* and $\underline{b}_{ph}(676)$, and nano-size fractionated Chl *a* and $\underline{b}_{ph}(676)$. N. S. indicates not significant. n, S.E., r^2, and *p* indicate the number of sample, determination coefficient, standard error, and probability, respectively.

Regression equation	Region	n	Y_{int} ± S.E.	Slope ± S.E.	r^2	*p*
Micro-size $\underline{b}_{ph}(676)$	NAC	0				
$=Y_{int}$ + Slope × Micro-size Chl *a*	SAC	0				
	WSB	6	0.020 ± 0.01	0.050 ± 0.107	0.05	N.S.
	SSB	26	0.065 ± 0.06	0.070 ± 0.043	0.10	N.S.
	SB	32	0.050 ± 0.04	0.077 ± 0.036	0.13	<0.05
Nano-size $\underline{b}_{ph}(676)$	NAC	0				
$=Y_{int}$ + Slope × Nano-size Chl *a*	SAC	0				
	WSB	6	0.068 ± 0.12	0.270 ± 0.688	0.04	N.S.
	SSB	26	0.067 ± 0.02	0.099 ± 0.030	0.31	<0.01
	SB	32	0.077 ± 0.02	0.089 ± 0.032	0.20	<0.05

Table 3-17. Average ± standard error of the $\underline{b}^*_{ph}(676)$ of micro-size and nano-size fractions in WSB, SSB, and all stations. n indicates number of sample.

Region	n	$\underline{b}^*_{ph}(676)$	
		Micro-size fraction	Nano-size fraction
NAC	0		
SAC	0		
WSB	6	0.49 ± 0.129	0.75 ± 0.234
SSB	26	0.21 ± 0.067	0.32 ± 0.044
SB	32	0.27 ± 0.062	0.40 ± 0.062

Table 3-18. Regression analyses between log SI_{scat} and log $\underline{b}^*_{ph}(676)$. N. S. indicates not significant. n, S.E., r^2, and p indicate the number of sample, determination coefficient, standard error, and probability, respectively.

Regression equation	Region	n	Y_{int} ± S.E.	Slope ± S.E.	r^2	p
Log $\underline{b}^*_{ph}(676)$	NAC	5	–0.57 ± 0.32	0.26 ± 0.29	0.21	N.S.
= Y_{int} + Slope × Log SI_{scat}	SAC	13	0.00 ± 0.16	–0.19 ± 0.13	0.16	N.S.
	WSB	8	–0.68 ± 0.65	0.05 ± 0.75	0.00	N.S.
	SSB	32	–0.33 ± 0.29	–0.44 ± 0.23	0.11	N.S.
	All	58	–0.20 ± 0.23	–0.39 ± 0.19	0.07	<0.05

Table 3-19. Regression analyses between log POC concentration and log $\underline{b}_{ph}(676)$, and log POC:Chl *a* and log $\underline{b}^*_{ph}(676)$. N. S. indicates not significant. n, S.E., r^2, and *p* indicate the number of sample, determination coefficient, standard error, and probability, respectively.

Regression equation	Region	n	Y_{int} ± S.E.	Slope ± S.E.	r^2	*p*
Log $\underline{b}_{ph}(676)$	NAC	8	−1.26 ± 0.52	0.21 ± 0.26	0.10	N.S.
= Y_{int} + Slope × Log POC	SAC	14	−1.06 ± 0.74	0.17 ± 0.36	0.02	N.S.
	WSB	7	−4.27 ± 1.83	1.62 ± 0.93	0.38	N.S.
	SSB	33	−3.67 ± 0.46	1.24 ± 0.20	0.56	<0.001
	All	62	−2.62 ± 0.32	0.83 ± 0.15	0.34	<0.001
Log $\underline{b}^*_{ph}(676)$	NAC	8	−1.87 ± 0.73	0.63 ± 0.28	0.47	N.S.
= Y_{int} + Slope × Log POC:Chl *a*	SAC	14	−0.97 ± 0.46	0.30 ± 0.18	0.18	N.S.
	WSB	7	−2.32 ± 2.15	0.70 ± 0.89	0.11	N.S.
	SSB	33	−2.09 ± 0.35	0.54 ± 0.15	0.29	<0.01
	All	62	−2.85 ± 0.31	0.94 ± 0.13	0.47	<0.001

Table 3-20. Regression analyses between light intensity (Light Int.) and PPC:TC. N. S. indicates not significant. n, S.E., r^2, and p indicate the number of sample, determination coefficient, standard error, and probability, respectively.

Regression equation	Size	n	Y_{int} ± S.E.	Slope ± S.E.	r^2	p
PPC:TC	Micro-size	64	−0.94 ± 0.07	0.10 ± 0.04	0.11	<0.01
$= Y_{int}$ + Slope × Light Int.	Nano-size	64	−1.01 ± 0.06	0.16 ± 0.03	0.33	<0.001
	Micro+Nano size	128	−0.98 ± 0.05	0.13 ± 0.02	0.20	<0.001

Table 3-21. Average ± standard error of the PPC:TC at the optical depths of 0.0, 2.3, and 4.6. n indicates number of sample.

Optical depth	n	PPC:TC	
		Micro-size fraction	Nano-size fraction
$\zeta = 0.0$	31	0.21 ± 0.031	0.25 ± 0.018
$\zeta = 2.3$	31	0.21 ± 0.021	0.21 ± 0.014
$\zeta = 4.6$	29	0.16 ± 0.021	0.13 ± 0.019
All	91	0.19 ± 0.015	0.20 ± 0.011

Table 3-22. Results of two-way analysis of variance of the optical properties and size fraction on PPC:TC in NAC, SAC, WSB, and SSB. DF, SS, MS, F, and *p* indicate degrees of freedom, sum of squares, mean of squares, F value, and probability, respectively.

Region	Source of Variation	PPC:TC				
		DF	SS	MS	F	*p*
NAC	Optical depth (A)	2	0.117	0.0585	3.494	0.045
	Size fraction (B)	1	0.0167	0.0167	0.998	0.327
	A x B	2	0.00126	0.00063	0.0376	0.963
	Residual	26	0.435	0.0167		
	Total	31	0.570	0.0184		
SAC	Optical depth (A)	2	0.215	0.107	8.648	<0.001
	Size fraction (B)	1	0.00516	0.00516	0.415	0.522
	A x B	2	0.0163	0.00816	0.656	0.523
	Residual	54	0.671	0.00124		
	Total	59	0.907	0.0154		
WSB	Optical depth (A)	2	0.00272	0.00136	0.0644	0.938
	Size fraction (B)	1	0.00002	0.00002	0.000948	0.976
	A x B	2	0.0475	0.0238	1.125	0.346
	Residual	18	0.380	0.0211		
	Total	23	0.439	0.0191		
SSB	Optical depth (A)	2	1.995	0.997	1.061	0.353
	Size fraction (B)	1	1.063	1.063	1.130	0.292
	A x B	2	2.445	1.222	1.3	0.280
	Residual	58	54.528	0.940		
	Total	63	59.893	0.951		

Table 3-23. Regression analyses between bulk PPC:TC (mol mol^{-1}) and bulk $a^*_{ph}{}^{slope}$ from 488 to 532nm. N. S. indicates not significant. n, S.E., r^2, and p indicate the number of sample, determination coefficient, standard error, and probability, respectively.

Regression equation	Region	n	Y_{int} ± S.E.	Slope ± S.E.	r^2	p
$a^*_{ph}{}^{slope}(488\text{-}532)$	NAC	17	−0.025 ± 0.004	−0.023 ± 0.019	0.09	N.S.
$= Y_{int} + Slope \times PPC:TC$	SAC	28	−0.019 ± 0.005	−0.035 ± 0.020	0.11	N.S.
	WSB	11	−0.017 ± 0.002	−0.007 ± 0.009	0.07	N.S.
	SSB	35	−0.009 ± 0.001	−0.032 ± 0.006	0.50	<0.001
	All	91	−0.016 ± 0.002	−0.030 ± 0.010	0.09	<0.01

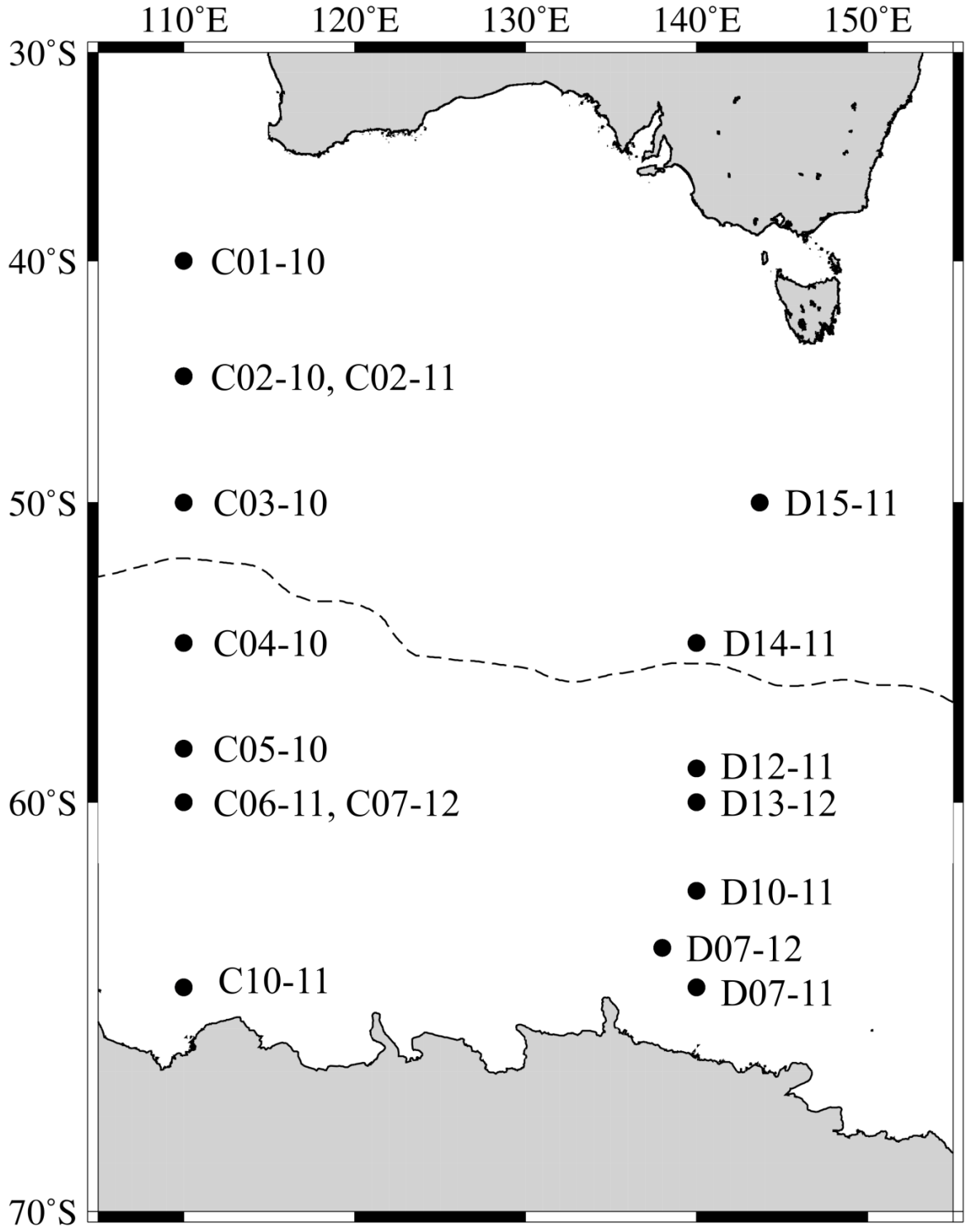

Figure 3-1. Location of sampling stations in the Indian sector of the Southern Ocean. Circles represent the sampling stations. Broken line indicates the approximate position of the Antarctic convergence.

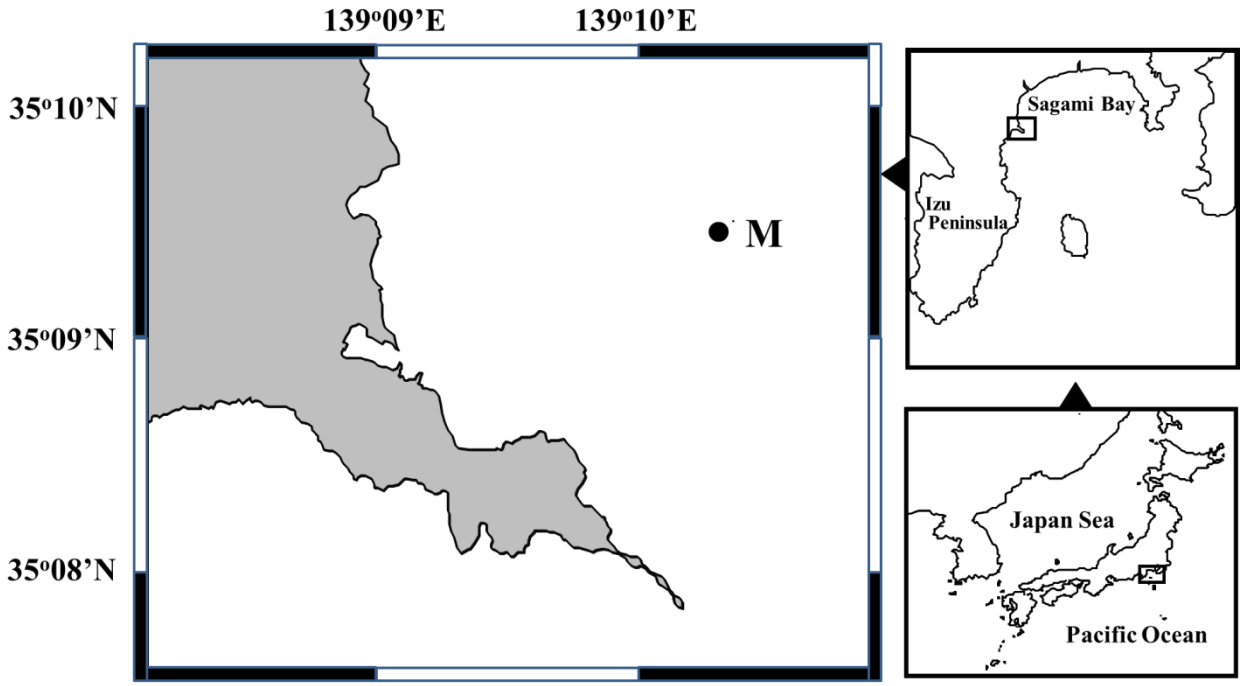

Figure 3-2. Location of sampling station M off the Manazuru Peninsula in Sagami Bay. Circle represents the sampling station.

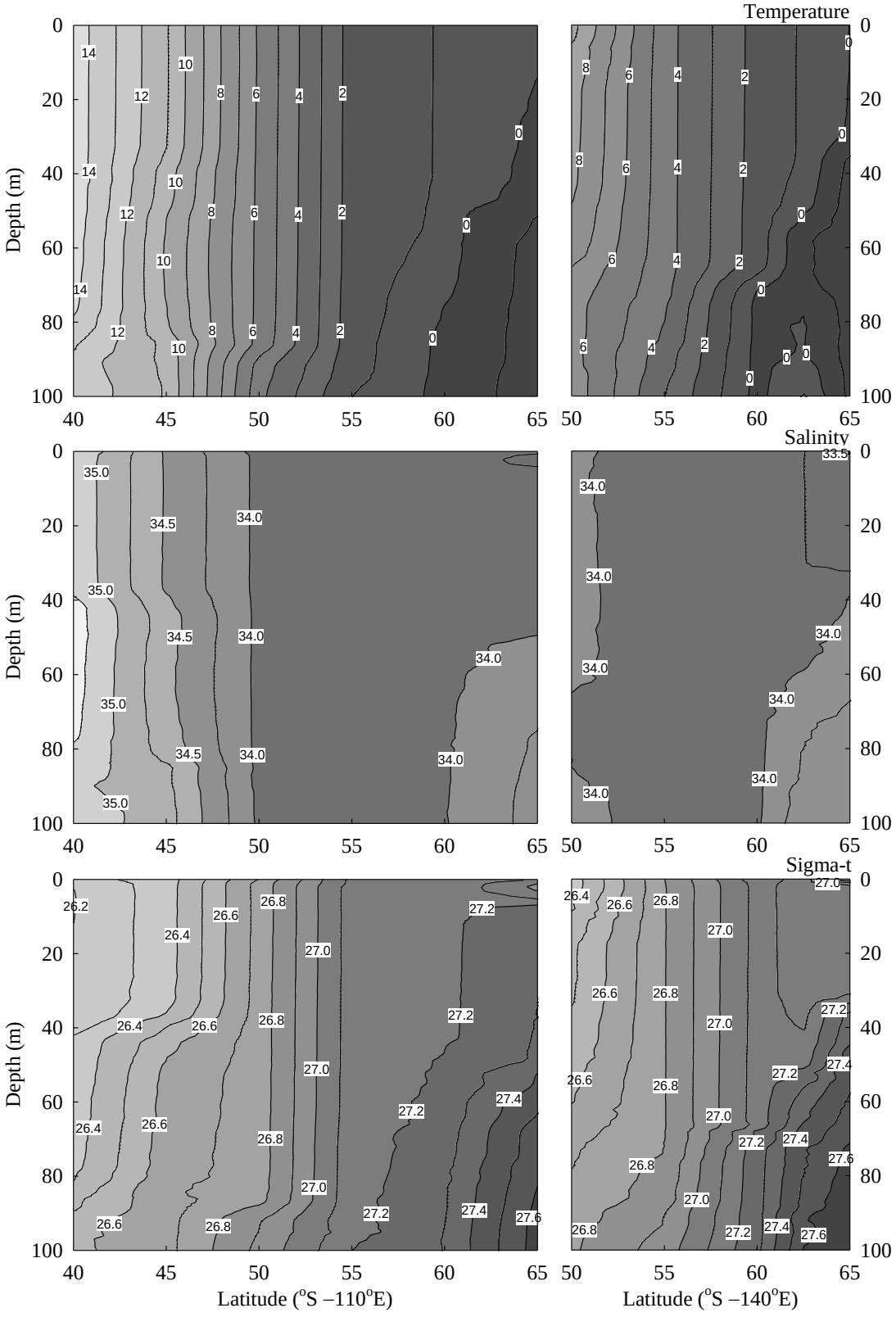

Figure 3-3. Spatial variations in seawater temperature, salinity, and Sigma-t in the Indian sector of the Southern Ocean in the austral summer of 2011/2012.

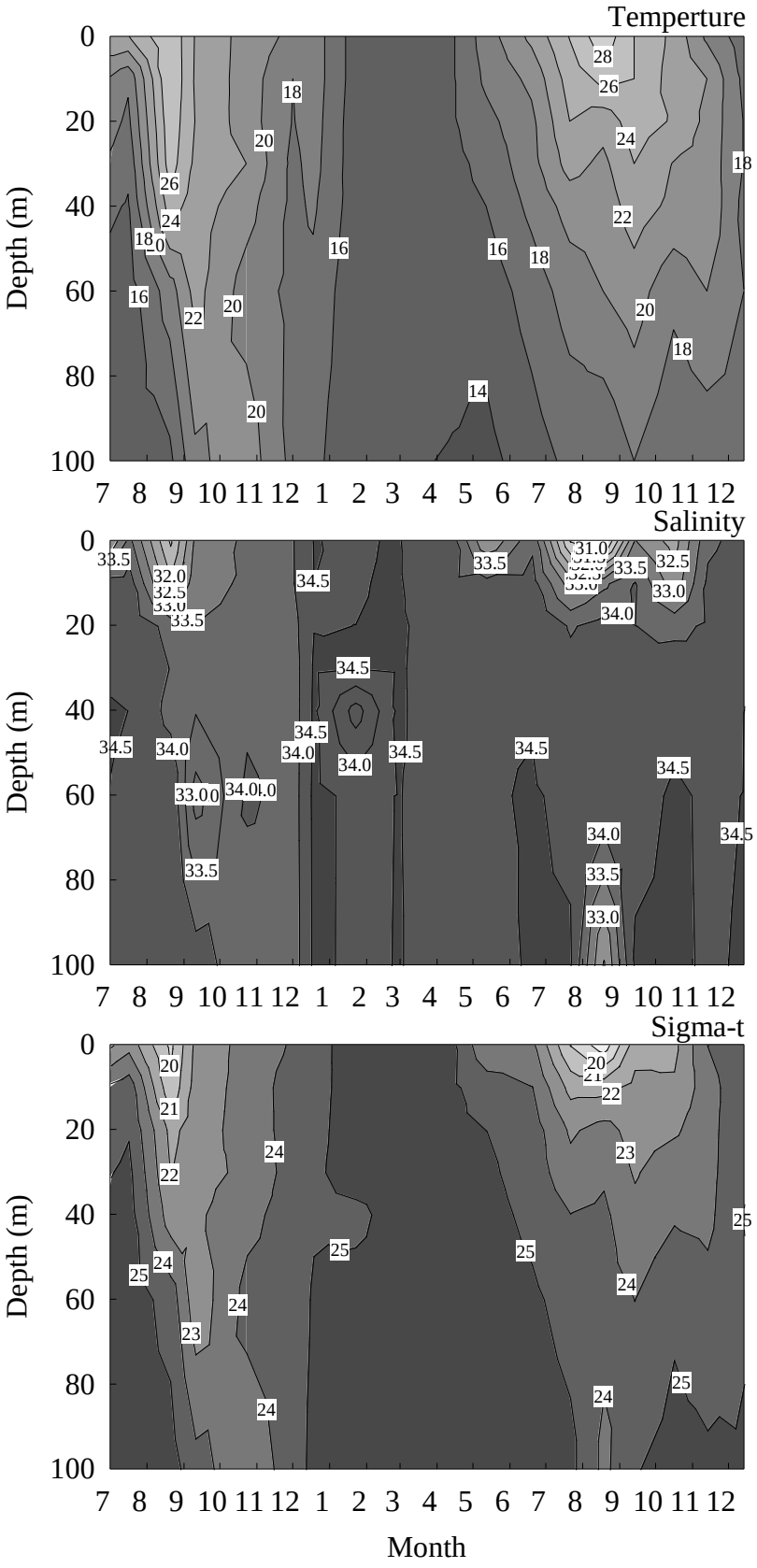

Figure 3-4. Temporal variations in seawater temperature, salinity, and Sigma-t at Station M in Sagami Bay from July 2009 to December 2010.

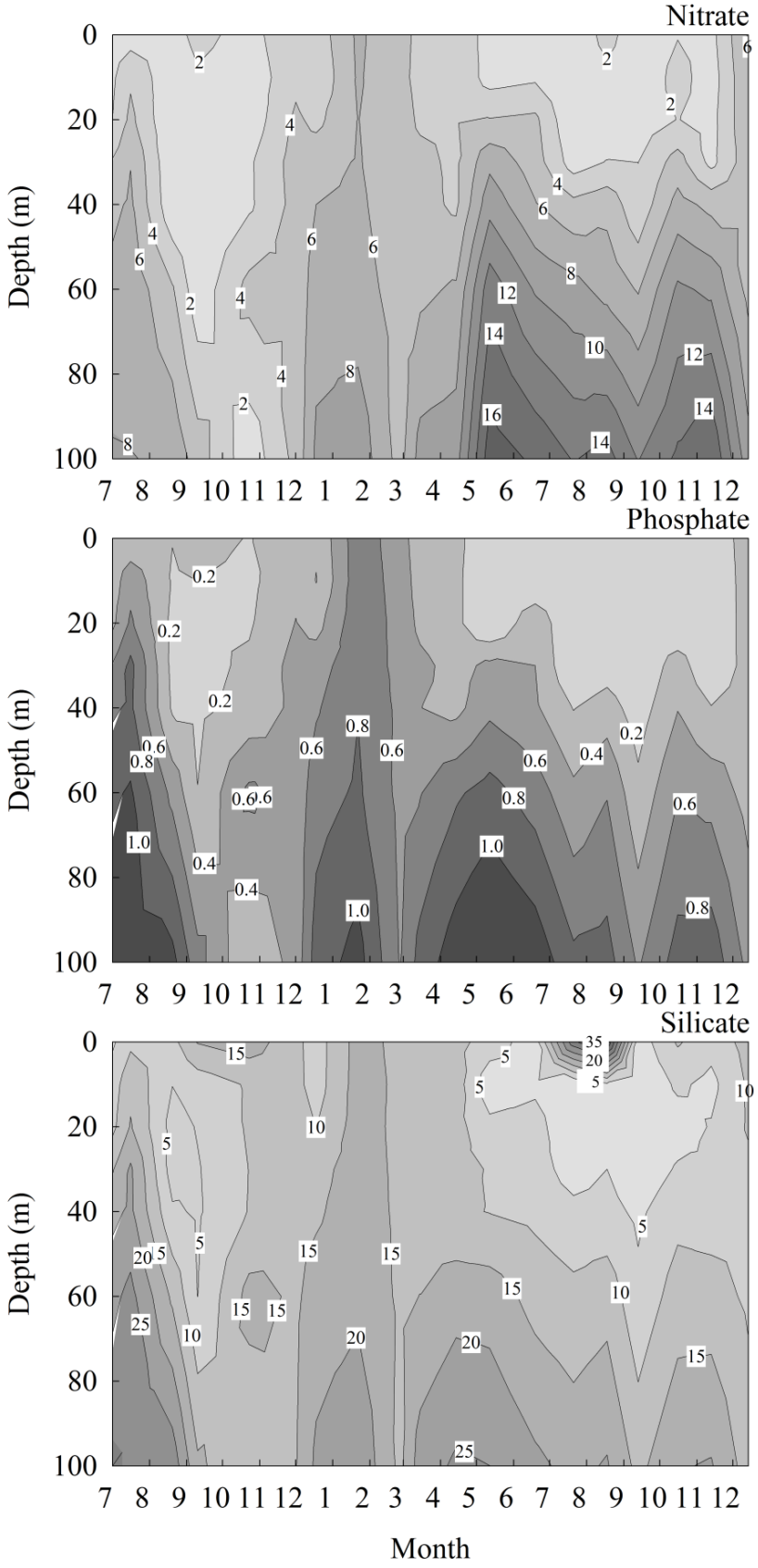

Figure 3-5. Temporal variations in nitrate, phosphate and silicate concentrations at Station M in Sagami Bay from July 2009 to December 2010.

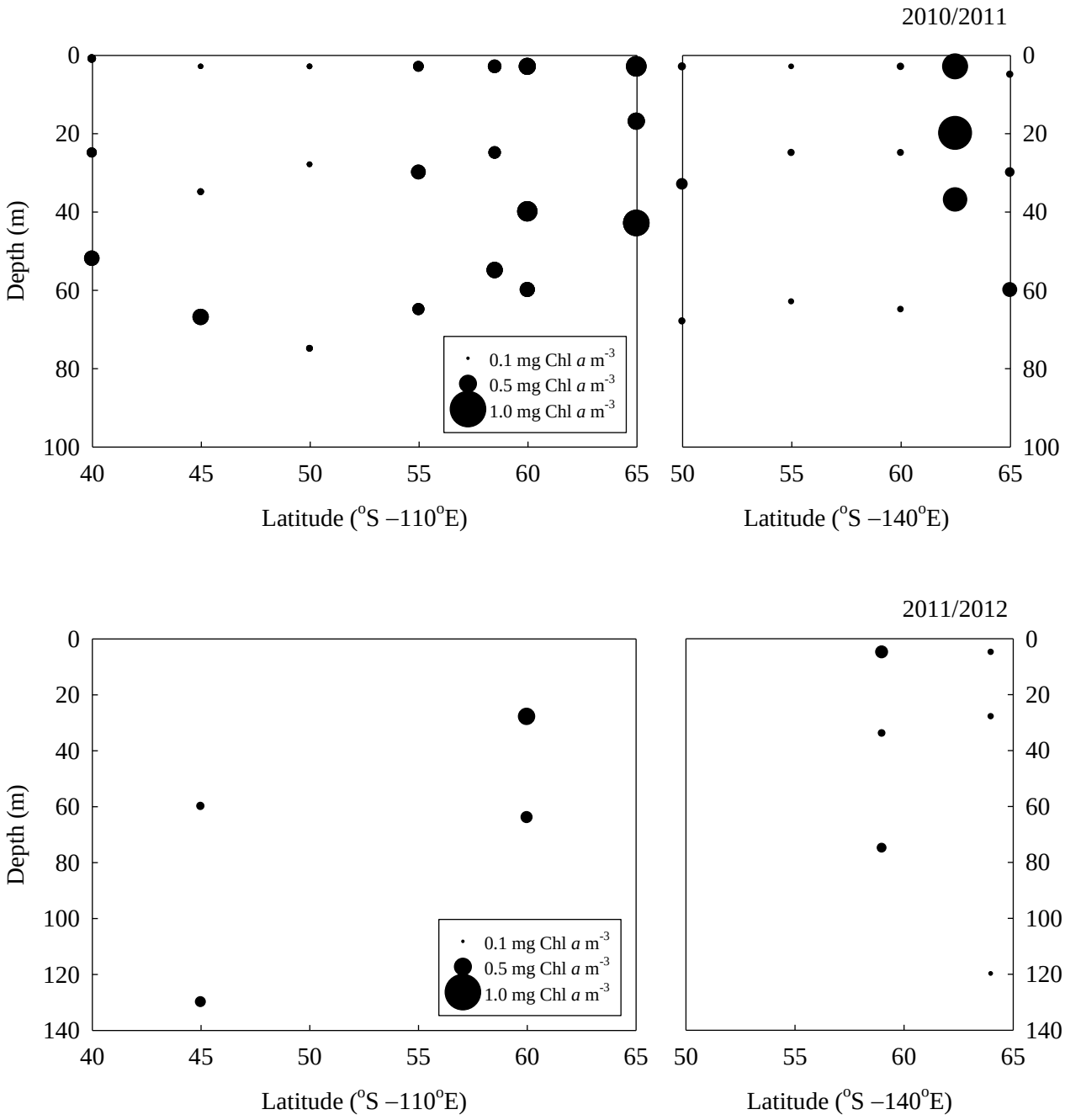

Figure 3-6. Spatial variation in bulk Chl *a* concentrations at the optical depths of 0.39, 2.3, and 4.6 in the Indian sector of the Southern ocean in the austral summer of 2010/2011 and 2011/2012.

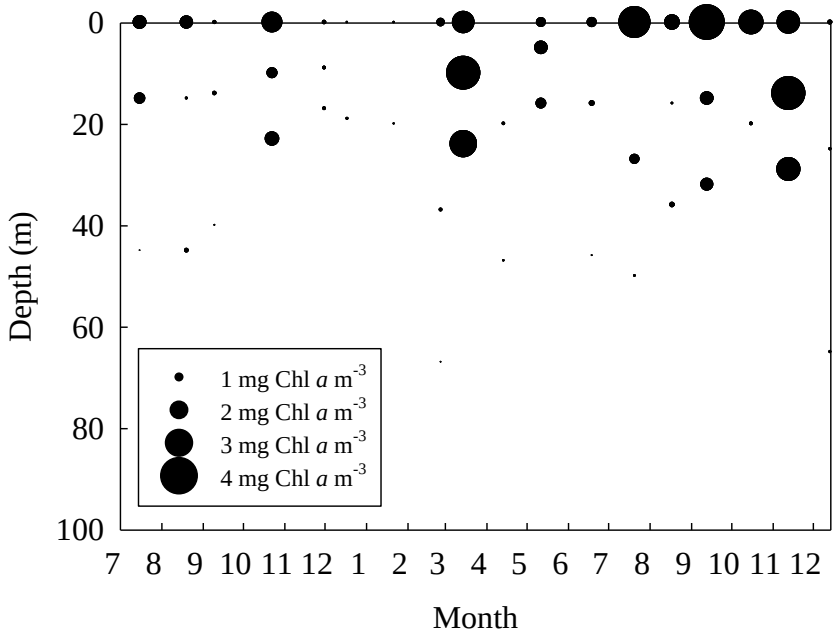

Figure 3-7. Temporal variations in bulk Chl *a* concentrations at the optical depths of 0.0, 2.3, and 4.6 at Station M in Sagami Bay from July 2009 to December 2010.

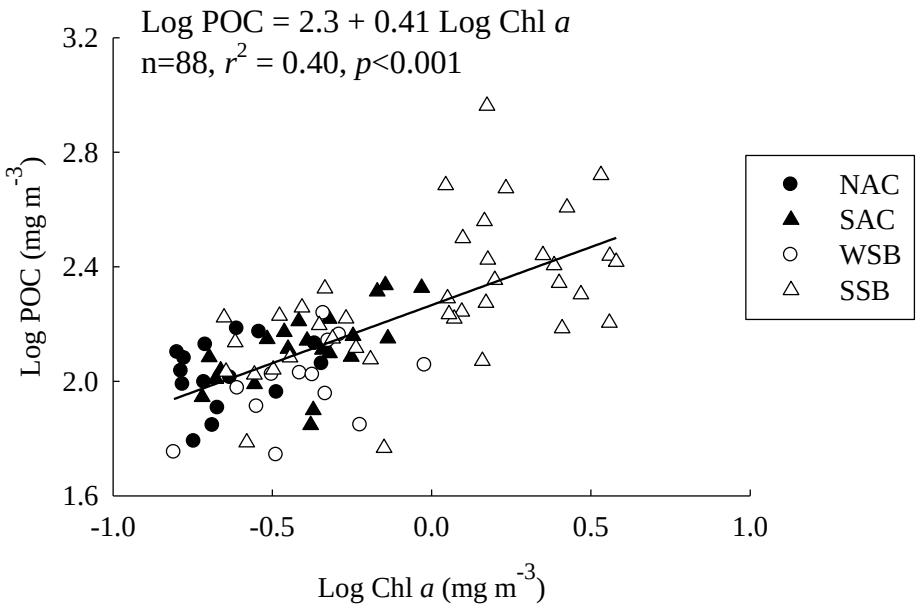

Figure 3-8. Relationship between log bulk Chl *a* and log bulk POC concentrations. Closed and open symbols indicate the Southern Ocean and Sagami Bay, respectively. Solid line indicates regression line for all regions.

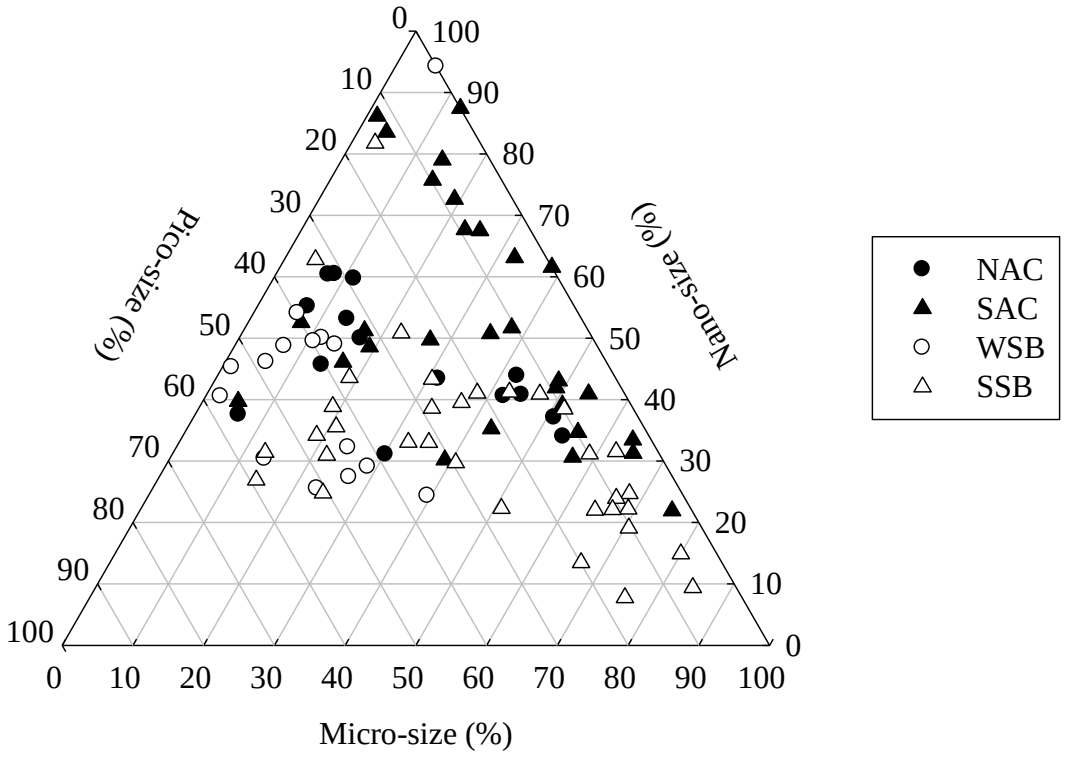

Figure 3-9. Ternary plot illustrating the relative Chl *a* proportions of micro-size, nano-size, and pico-size fractions to bulk fraction (%) in NAC, SAC, WSB, and SSB. Closed and open symbols indicate the Southern Ocean and Sagami Bay, respectively.

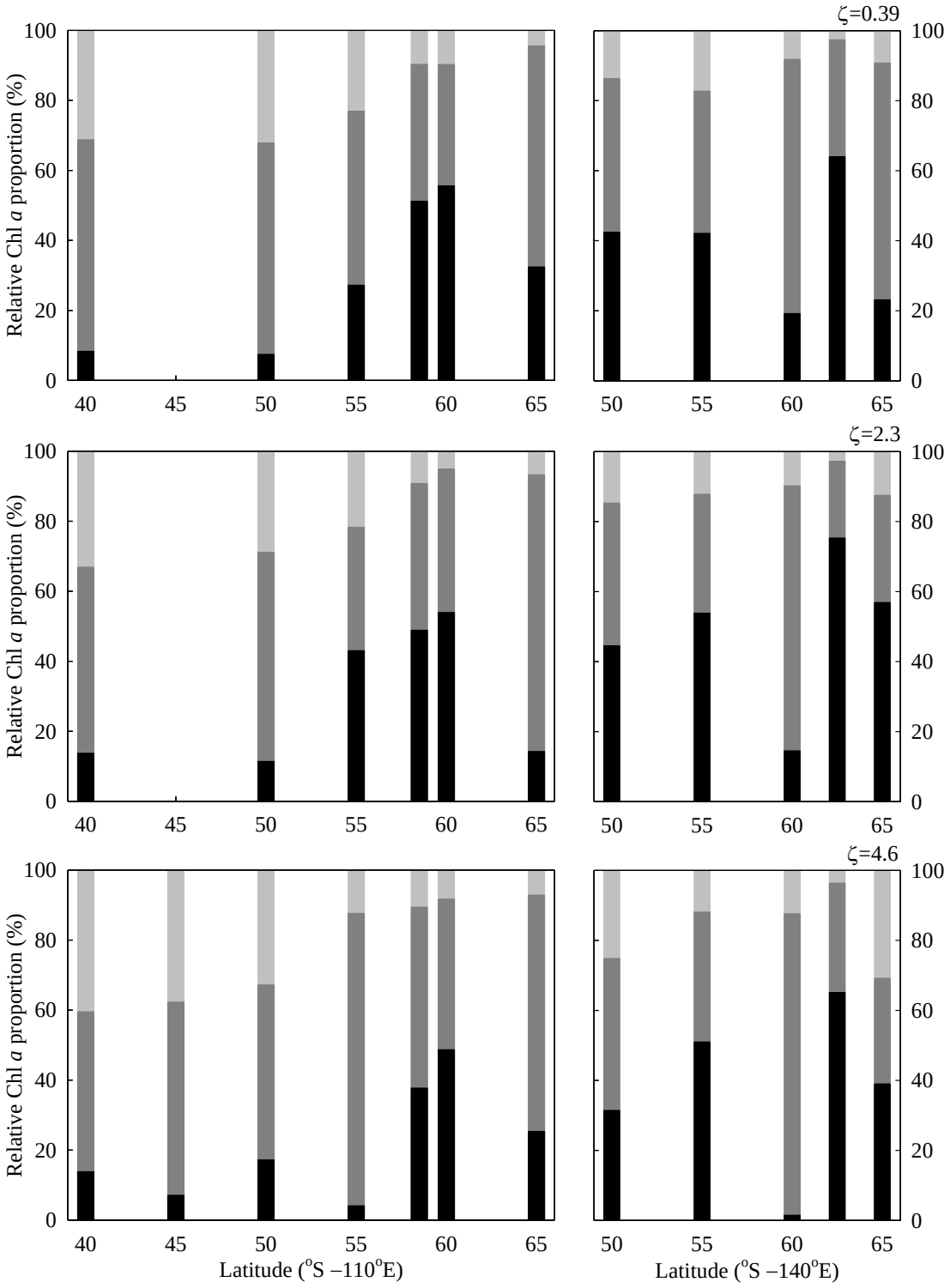

Figure 3-10. Spatial variation in relative Chl *a* proportions of micro-size (black), nano-size (dark gray), and pico-size fractions (gray) to bulk fractions at the optical depths of 0.39, 2.3, and 4.6 in the Indian sector of the Southern Ocean in the austral summer of 2010/2011.

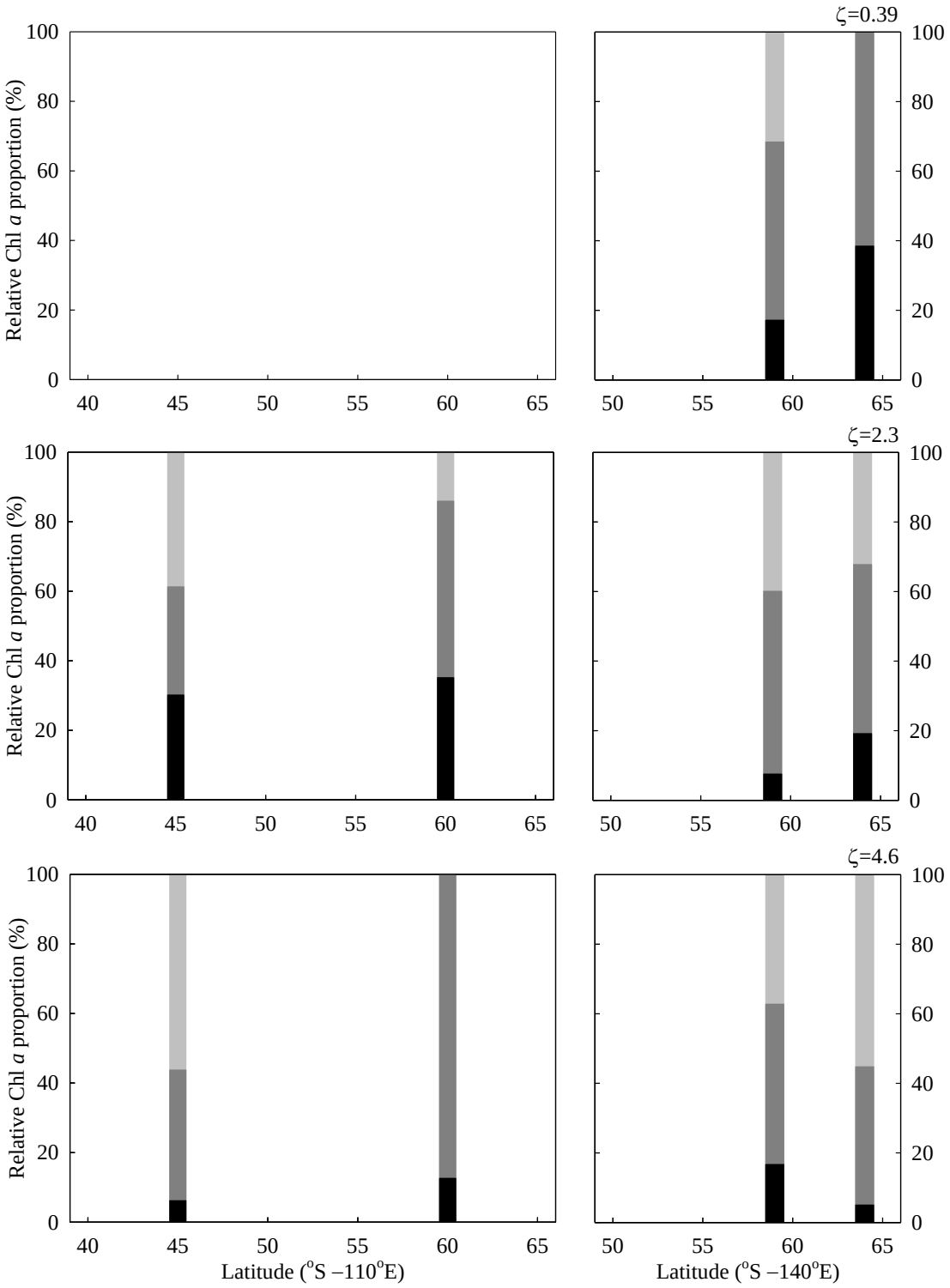

Figure 3-11. Spatial variation in relative Chl *a* proportions of micro-size (black), nano-size (dark gray), and pico-size fractions (gray) to bulk fractions at the optical depths of 0.39, 2.3, and 4.6 in the Indian sector of the Southern Ocean in the austral summer of 2011/2012.

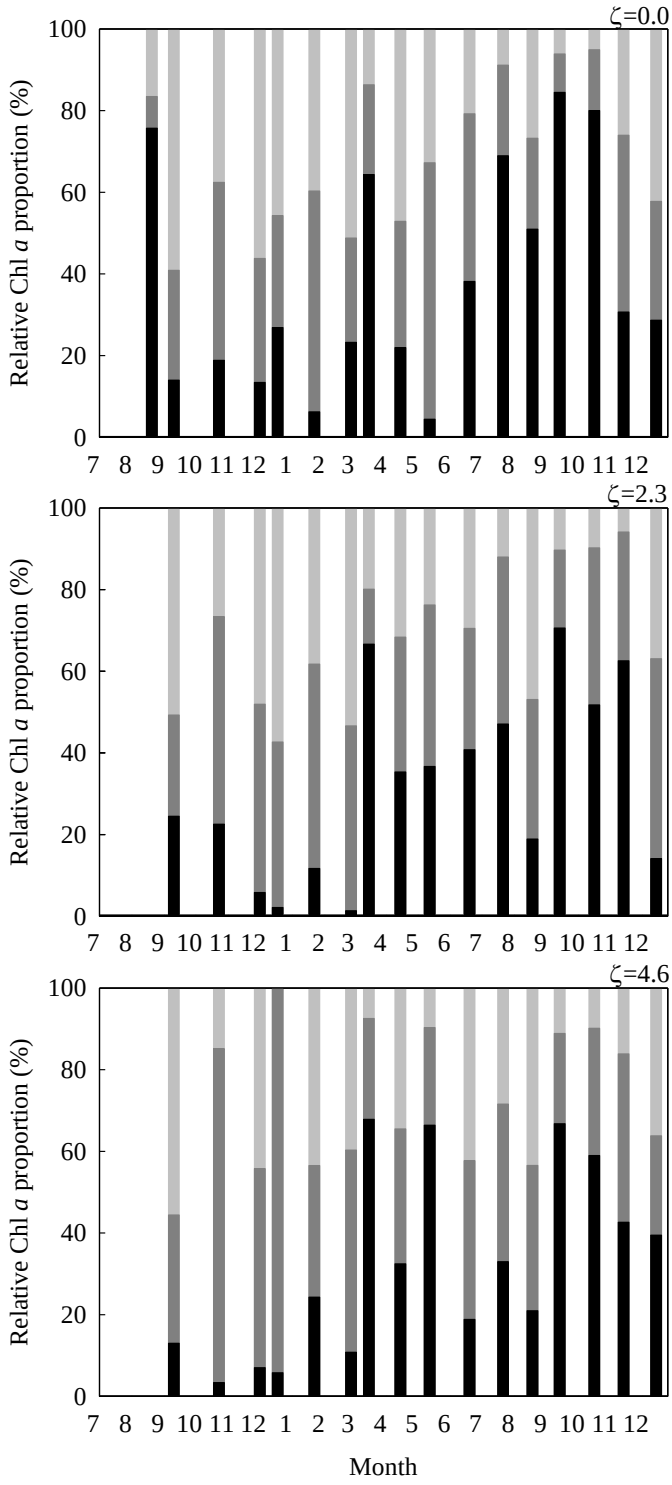

Figure 3-12. Temporal variation in relative Chl *a* proportions of micro-size (black), nano-size (dark gray), and pico-size fractions (gray) to bulk fractions from September 2009 to December 2010 at the optical depths of 0.0, 2.3, and 4.6 of Station M in Sagami Bay.

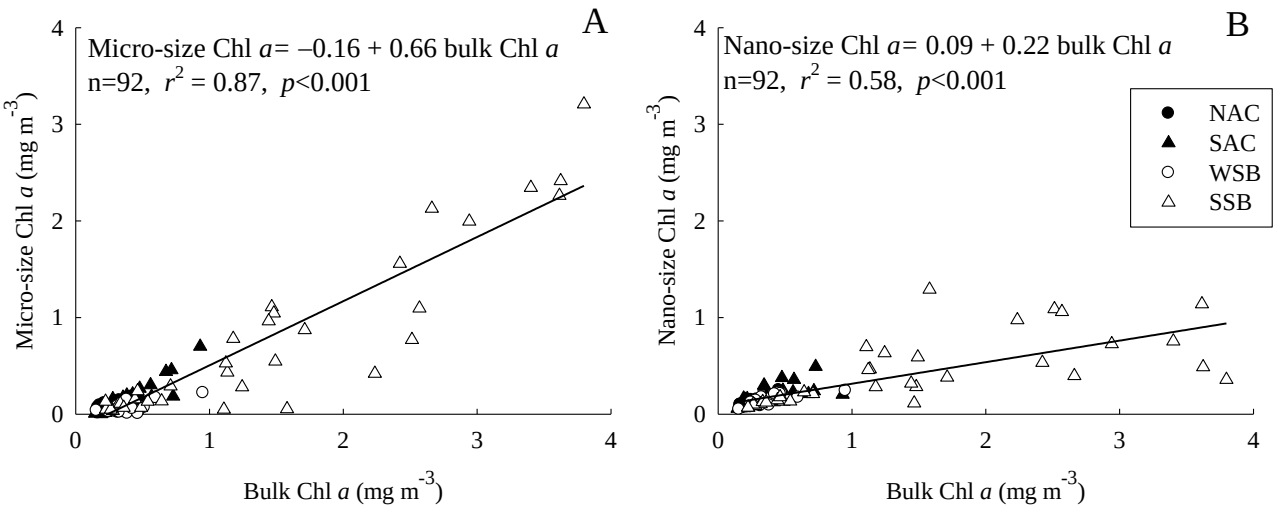

Figure 3-13. Relationships between bulk Chl *a* concentration and micro-size fractionated Chl *a* (A) and nano-size fractionated Chl *a* concentration (B). Closed and open symbols indicate the Southern Ocean and Sagami Bay, respectively. Solid lines indicate regression lines of all regions.

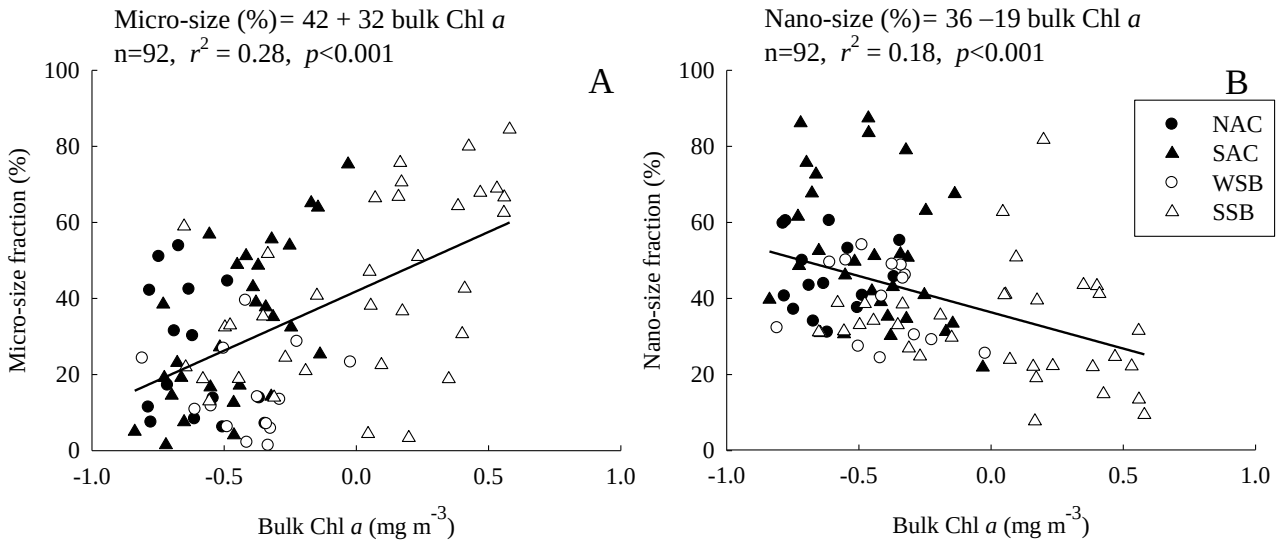

Figure 3-14. Relationships between bulk Chl *a* concentration and the relative proportions of micro-size fraction (A) and nano-size fraction (B) to bulk fractions. Closed and open symbols indicate the Southern Ocean and Sagami Bay, respectively. Solid lines indicate regression lines for all regions.

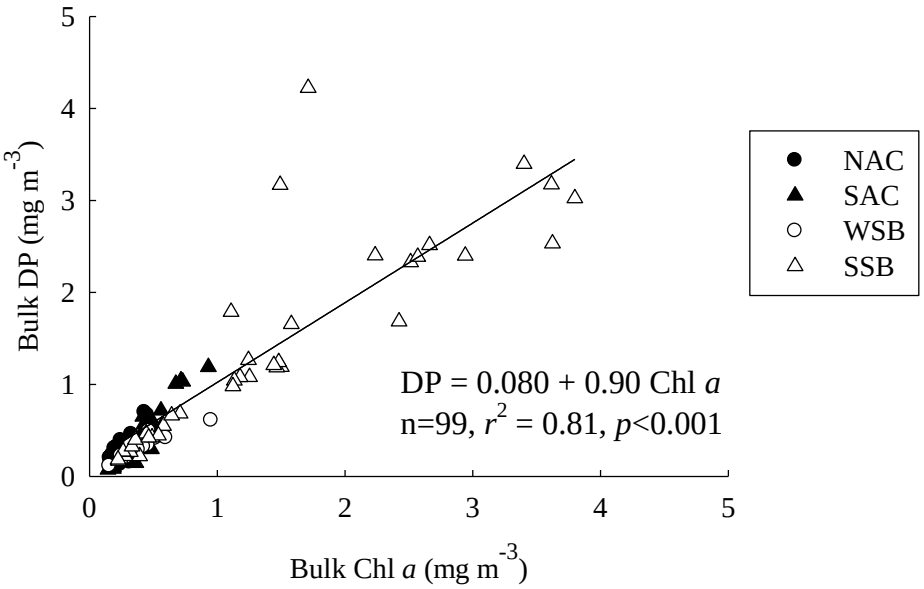

Figure 3-15. Relationship between bulk Chl *a* concentration and bulk DP concentration. Closed and open symbols indicate the Southern Ocean and Sagami Bay, respectively. Solid line indicates regression line.

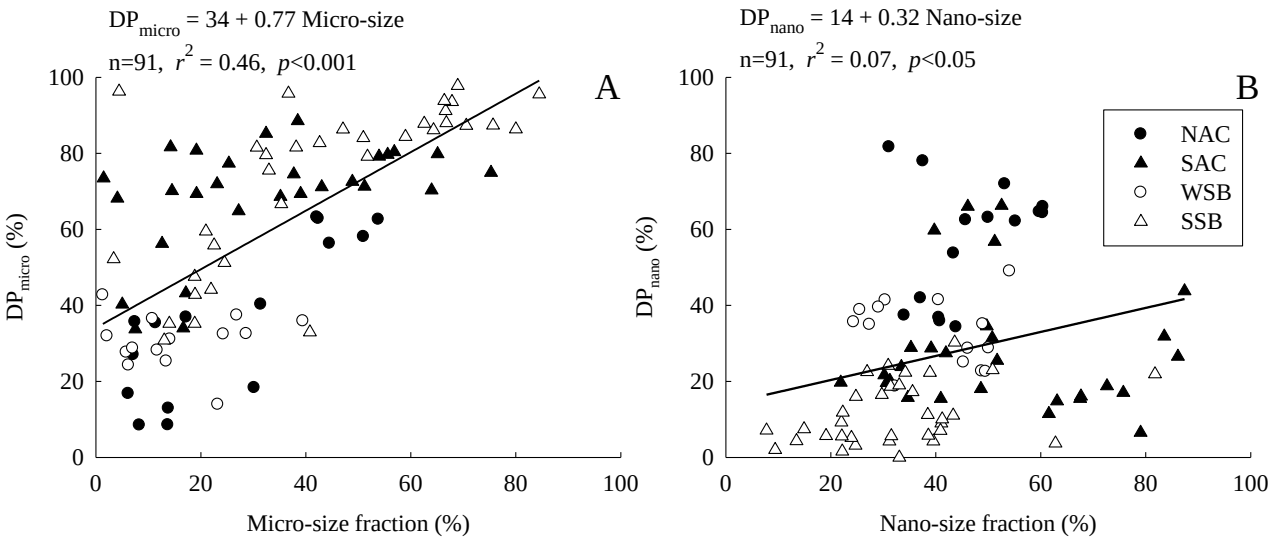

Figure 3-16. Relationships between relative Chl *a* proportion of micro-size fraction and DP_{micro} (A), and relative Chl *a* proportion of nano-size fraction and DP_{nano} (B). Closed and open symbols indicate the Southern Ocean and Sagami Bay, respectively. Solid lines indicate regression lines.

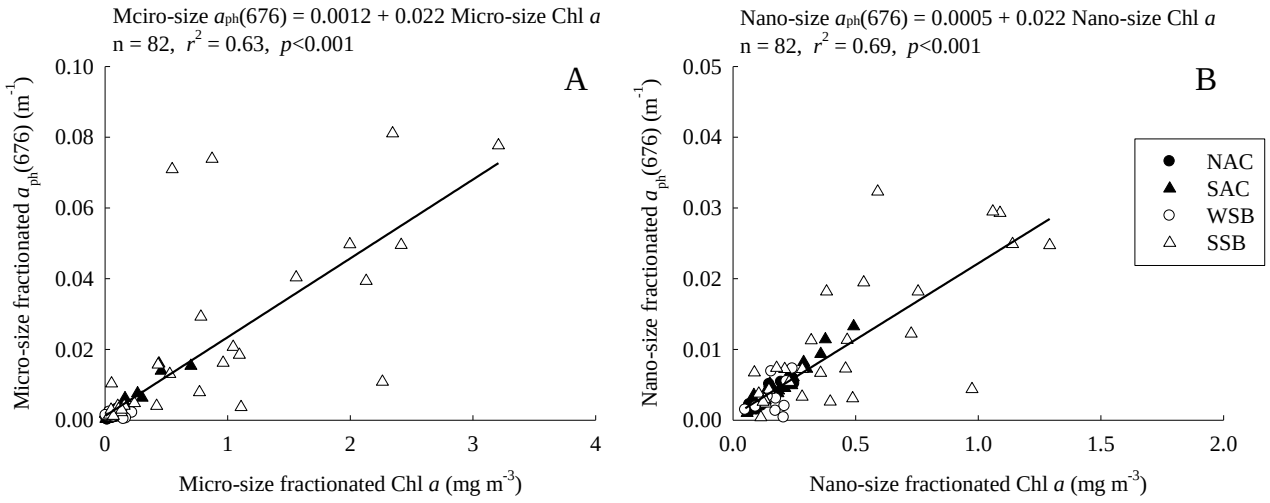

Figure 3-17. Relationships between micro-size fractionated Chl *a* and $a_{ph}(676)$ (A), and nano-size fractionated Chl *a* and $a_{ph}(676)$ (B). Closed and open symbols indicate the Southern Ocean and Sagami Bay, respectively. Solid lines indicate regression lines.

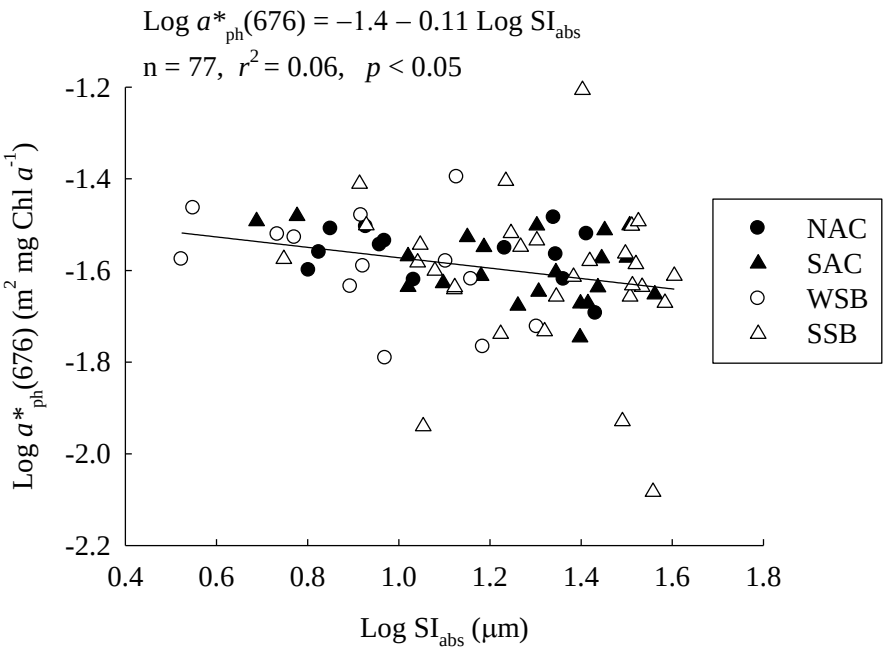

Figure 3-18. Relationship between log SI_{abs} and log bulk $a^*_{ph}(676)$. Closed and open symbols indicate the Southern Ocean and Sagami Bay, respectively. Solid line indicates regression line.

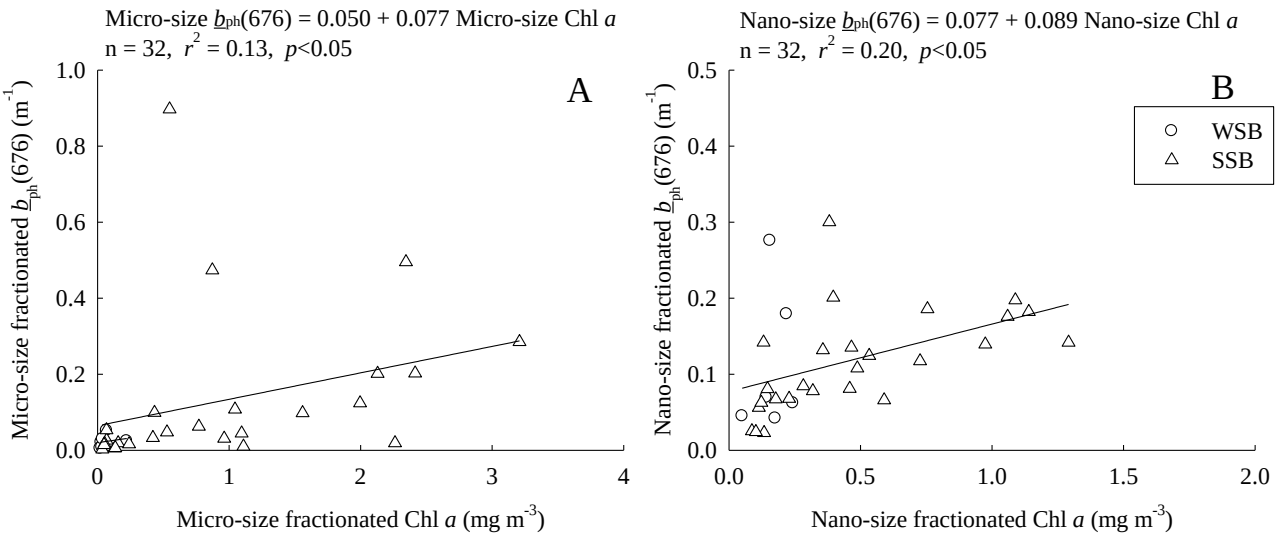

Figure 3-19. Relationships between micro-size fractionated Chl *a* and $\underline{b}_{ph}(676)$ (A), and nano-size fractionated Chl *a* and $\underline{b}_{ph}(676)$ (B) in the WSB (open circle) plus SSB regions (open triangle). Solid lines indicate regression lines.

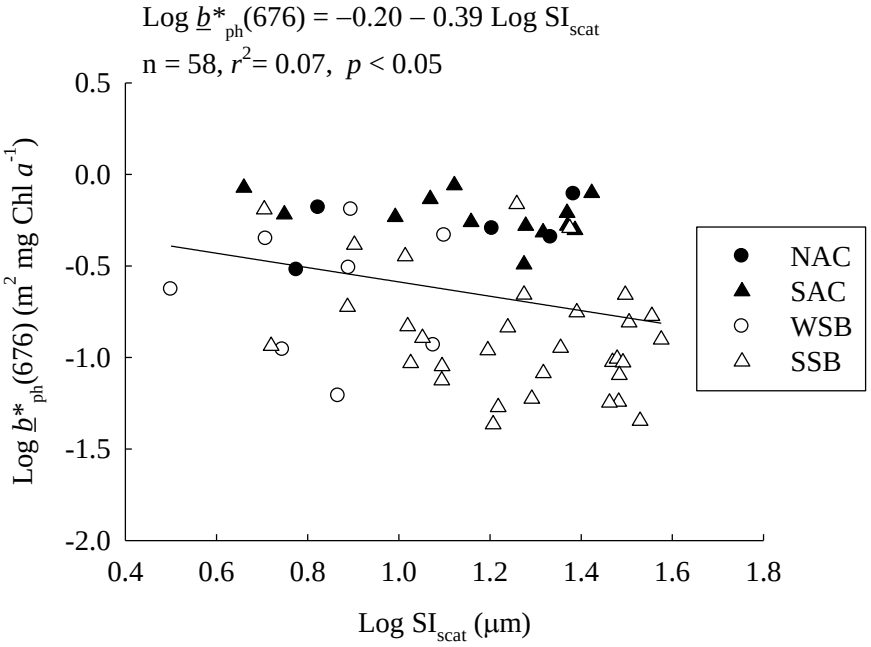

Figure 3-20. Relationship between log SI_{scat} and log bulk $\underline{b}^*_{ph}(676)$. Closed and open symbols indicate the Southern Ocean and Sagami Bay, respectively. Solid line indicates regression line.

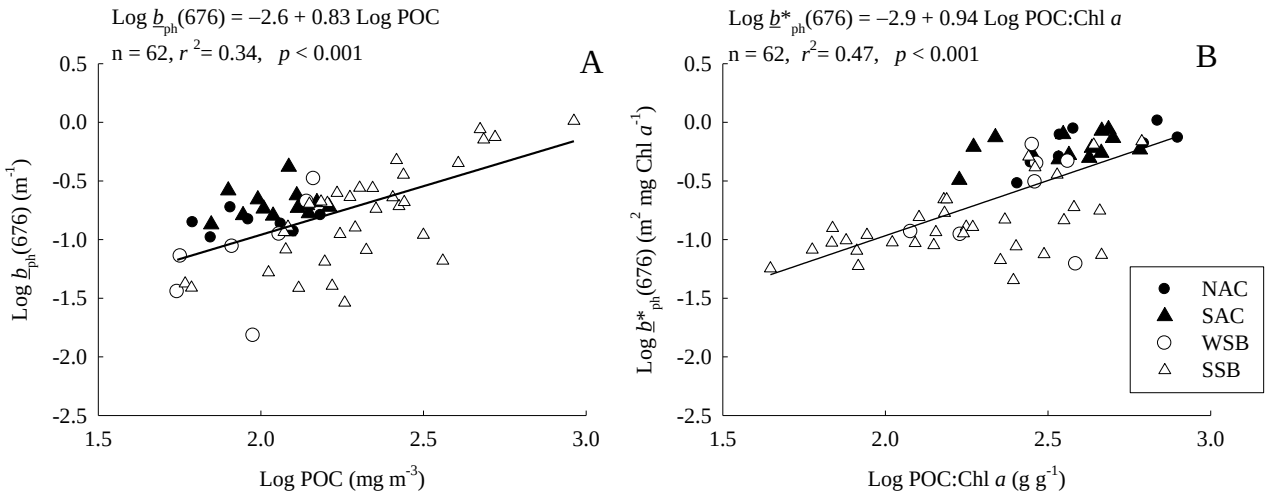

Figure 3-21. Relationships between log POC concentration and log bulk $\underline{b}_{ph}(676)$ (A), and log POC:Chl *a* and log bulk $\underline{b}^*_{ph}(676)$ (B). Closed and open symbols indicate the Southern Ocean and Sagami Bay, respectively. Solid line indicates regression lines for all stations.

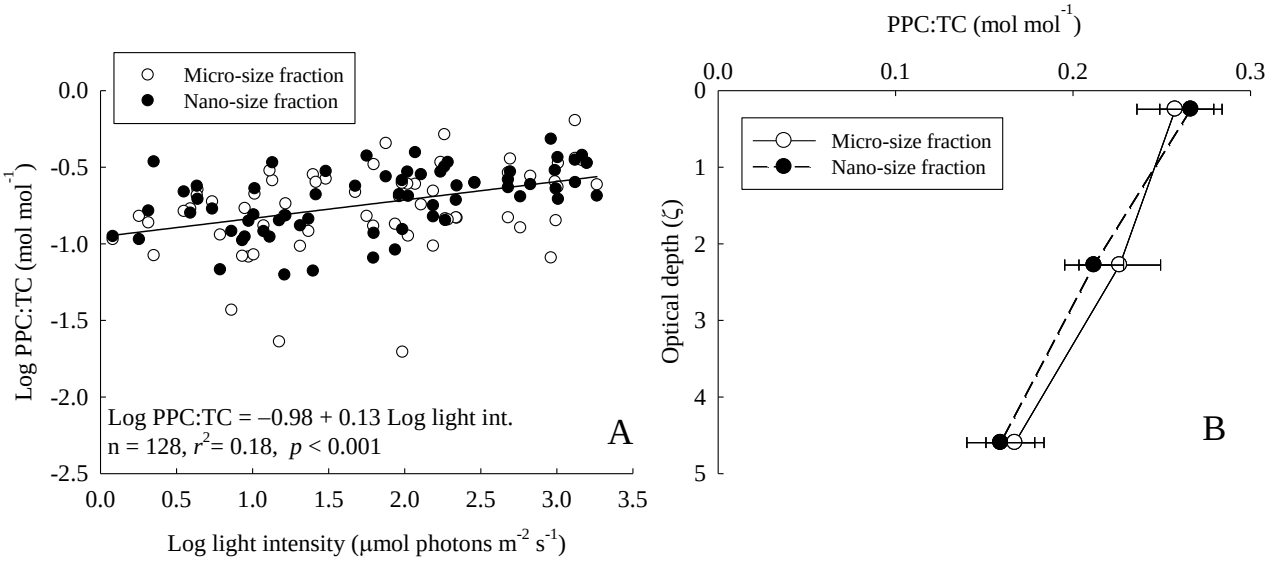

Figure 3-22. Relationship between light intensity and PPC:TC (A). Solid line indicates regression line. Vertical distribution of the average PPC:TC for all stations (B). Open and closed symbols indicate micro- and nano-size fractions. Error bars indicate standard errors.

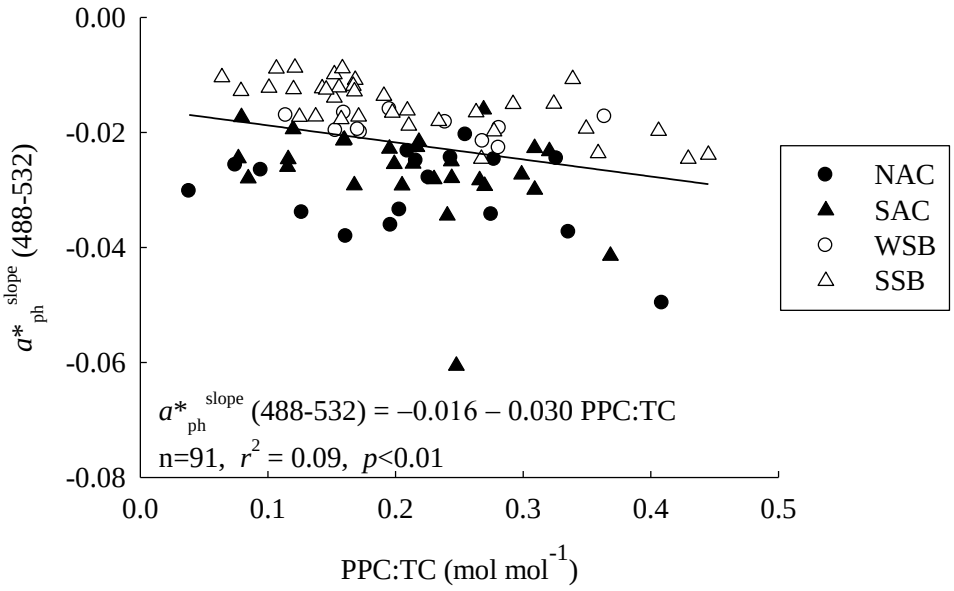

Figure 3-23. Relationships between bulk PPC:TC (mol mol^{-1}) and bulk $a^*_{ph}{}^{slope}$ from 488 to 532nm. Closed and open symbols indicate the Southern Ocean and Sagami Bay, respectively. Solid indicates regression line for all stations.

CHAPTER IV

GENERAL DISCUSSION

4.1. Absorption properties of phytoplankton as a function of cell size

Light absorption by phytoplankton in water column can be used to analyze the primary production (Kiefer and Mitchell 1983). The primary production rate of phytoplankton exhibits an allometric scaling of cell size (Banse 1976; Taguchi 1976). The absorption coefficient as a function of cell size is fundamental for monitoring the primary production (Finkel 2001). The absorption coefficient of phytoplankton ($a_{ph}[\lambda]$) can be directly estimated from water leaving reflectance (R) which are measured by ocean color remote sensing (Carder et al. 1999). The estimated $a_{ph}(\lambda)$ could be applied to monitor the size distribution of *in situ* phytoplankton assemblage (Ciotti et al. 2002; Hirata et al. 2008; Brewin et al. 2011). The continuous size index of phytoplankton assemblage can be appropriate to monitor the size distribution by ocean color remote sensing (Bricaud et al. 2004). In this study, continuous size index for absorption analysis (SI_{abs}) is validated by the similar negative slope of the *in situ* relationship between $a^*_{ph}(676)$ and SI_{abs} compared with the slope of the cultural relationship between $a^*_{ph}(676)$ and equivalent spherical diameter (d, Table 4-1). The similarity confirm that the decrease in $a^*_{ph}(676)$ could be determined by not only the size distribution of cells, but also cumulative cell volume in phytoplankton assemblage (Bricaud et al. 2004). The decrease in $a^*_{ph}(676)$ is caused by the package effect of phytoplankton cell (Duysens 1956; Morel and Bricaud 1981; Berner et al. 1989; Kirk 2011). Thus the similarity also suggests that the package effect in natural assemblage of phytoplankton could be evaluated by SI_{abs}. The estimation of the package effect in natural assemblage of phytoplankton could assist to estimate the change in the primary production.

On the other hand, the higher intercept of the *in situ* relationships between $a^*_{ph}(676)$ and SI_{abs} compared with that of the cultural relationship (Table 4-1) suggests that the *in situ* relationship could be influenced by the physiological properties of phytoplankton which could co-vary with the environmental conditions (Brewin et al. 2011). The large intercepts of the relationship between the cell size and $a^*_{ph}(676)$ was induced in the high light conditions (Fujiki and Taguchi 2002), whereas the difference of the intercept of the *in situ* relationship between SI_{abs} and $a^*_{ph}(676)$ in the three optical depths in the water column was not observed even though the light intensity indicated 10^3 fold variation. However decreasing PPC:TC with increasing optical depth suggests that the natural assemblage of phytoplankton could acclimate to the surrounding light regime in water column. Although the natural assemblage of phytoplankton might be acclimated uniformly to the light fluctuation in surface mixed layer, the similar slope of the *in situ* relationship compared to the cultural relationship suggest that the variation in a^*_{ph} as a function of cell size could be appreciated by using wavelength 676nm (red region) because blue or green region could be largely influenced the variation in phytoplankton size, species and the pigment composition. Remote sensing reflectance at 676nm (R[676]) for remote sensing can be used to Chl *a* specific IOPs, however accurate measurements of the $R(676)$ from ocean color remote sensing are much more subject to correct due to smaller signal to noise ratio (Carder et al. 2006). The relationship between $a^*_{ph}(676)$ and SI_{abs} would provide the understanding of the variation in the $R(676)$ as a function of cell size.

4.2. Scattering properties of phytoplankton as a function of cell size

The continuous size index for scattering analysis (SI_{scat}) is validated by the similar negative slope of the *in situ* relationship between $\underline{b}^*_{ph}(676)$ and SI_{scat} to the slope of the cultural relationship between $\underline{b}^*_{ph}(676)$ and d (Table 4-1). This similarity confirm that decrease in $\underline{b}^*_{ph}(676)$ could be

determined by not only size distribution of cells, but also cumulative cell volume of phytoplankton assemblage, as suggested by Pak et al. (1970) and Spinrad (1986). Furthermore the similarity suggest that the effect of cell size on the $\underline{b}^*_{ph}(676)$ could be similar although the relative contribution of $\underline{b}^*_{ph}(676)$ to the Chl *a* specific scattering coefficient of particles ($\underline{b}^*_p[676]$) is variable. When the power exponent of the number of the particles is decreasing, and the intercept of the *in situ* relationship between $\underline{b}^*_{ph}(676)$ and SI_{abs} was getting close to that of the cultural experiment. It is indicated that the effect of the cultural $\underline{b}^*_{ph}(676)$ on cell size could be similar to that of *in situ* $\underline{b}^*_{ph}(676)$. The higher intercept of the *in situ* relationship between $\underline{b}^*_{ph}(676)$ and SI_{scat} could be due to the high light conditions (Befrenfeld and Boss 2003) because the high light conditions could induce the decreasing Chl *a* per cell, and the $\underline{b}^*_{ph}(676)$ increased consequently. In addition, the difference in $\underline{b}^*_{ph}(676)$ could be due to the carbon content in natural assemblages of phytoplankton (Behrenfeld and Boss 2003). The significant positive intercept of the *in situ* relationships could be due to the carbon contents of particles other than phytoplankton, such as detritus (Morel and Ahn 1991). The carbon content in natural assemblages of phytoplankton could be evaluated by the POC:Chl *a*.

The slope and intercept of the *in situ* relationship between $\underline{b}^*_{ph}(676)$ and POC:Chl *a* were similar to the cultural relationship between $\underline{b}^*_{ph}(676)$ and C:Chl *a* (Table 4-2) although the *in situ* POC included particulate carbon contents other than the carbon contents of phytoplankton. The relative proportion of scattering coefficient of phytoplankton to total scattering coefficient of particles (b_{ph}:b_p) is difficult to quantify in the ocean because various particles other than phytoplankton, such as detritus are present (Stramski 1991). In the present study, $b_{ph}(676)$:$b_p(676)$ is assumed to be equivalent to $a_{ph}(555)$:$a_p(555)$, which is determined with the QFT method. The average $a_{ph}(555)$:$a_p(555)$ was 0.66, which was higher than the previously observed ratio of the

carbon content of phytoplankton to bulk carbon content in the surface water, approximately from 0.25 to 0.40 (DuRand and Olson 1996; Behrenfeld and Boss 2006). However the estimation of $b_{ph}(676)$:$b_p(676)$ by the $a_{ph}(555)$:$a_p(555)$ could be appropriate because the slope of *in situ* relationship between $\underline{b}^*_{ph}(676)$ and POC:Chl *a* was similar to the cultural relationship between $\underline{b}^*_{ph}(676)$ and C:Chl *a*. Assuming that the scattering efficiency of detritus is similar to that of phytoplankton, the similar slopes between the *in situ* and the cultural relationships suggest that the carbon contents of particles other than phytoplankton could covary with that of phytoplankton cell, and the $b_p(676)$ could covary with $b_{ph}(676)$.

4.3. Implications for ocean color remote sensing

The Chl *a* is a standard parameter as phytoplankton biomass from ocean color remote sensing (Gordon and Morel 1983). The Chl *a* concentration is directly estimated from the water leaving reflectance ratio (Gordon and Morel 1983; O'Reilly et al. 1998). The spatial distribution of Chl *a* concentration exhibited different patterns from that of backscattering coefficient of particles (Loisel and Stramski 2000). The difference was due to the different particle composition, particularly coccolithophorid, which are characterized by a high backscattering. The algorithm for the estimation of Chl *a* concentration was constructed by the spectral ratio of the reflectance, which was determined only by the characteristics of the absorption spectra of phytoplankton pigments but not scattering efficiency of phytoplankton. This study indicates both absorption and scattering properties could be utilized for the estimation of the size distribution of phytoplankton assemblage. Simultaneous approach of absorption and scattering of phytoplankton induce not only the estimation of the size distribution but also particulate composition, particularly POC:Chl *a*.

The change in marine POC standing stock is fundamental for evaluating the marine carbon

cycle. The export flux of organic carbon from the euphotic zone is a relatively small proportion of total production, amounting to between 5 and 10% of the total carbon fixed per annum in the central ocean basin (Laws et al. 2000), whereas the flux at high latitude and at nutrient rich area can account for 50% of the total carbon fixation (Sancetta et al. 1991; Campbell and Aarup 1992). The large flux could be due to the sinking of the diatoms, dinoflagellates, and other large dence cells, and subsequently the large bloom of large cell phytoplankton is likely removed from the sea surface. Therefore, the size distribution of phytoplankton assemblage in the surface estimated by the optical size index could assist to understand the dynamics of marine carbon cycle, although the observation by ocean color remote sensing is limited in the one optical depth.

4.4. Conclusions

The quantitative analysis of the effect of cell size on the IOPs of phytoplankton could assist to monitor the size distribution of phytoplankton assemblage by ocean color remote sensing. Both $a^*_{ph}(676)$ and $b^*_{ph}(676)$ of phytoplankton species including dinoflagellates decrease with increase in the average *d*. For evaluating the cell size effect on the IOPs, the weighted values of micro-size, nano-size, and pico-size cell should be calculated from the IOPs as a function of cell size. Then the continuous size indies of phytoplankton cell should be derived from the weighted values and the relative size-fractionated Chl *a* concentration to bulk Chl *a* concentration of natural assemblage of phytoplankton. In Case I and II waters, there are the significant relationships between the $a^*_{ph}(676)$ and the SI_{abs}, and the $b^*_{ph}(676)$ and the SI_{scat}. The relationships can be used to invert the size distribution of natural assemblage of phytoplankton from remotely sensed data. However, the difference in the intercepts of the relationships between the IOPs and *d* and/or size index suggests that the more accurate evaluation of the effect of cell size on the IOPs would require the knowledge

of physiological state of natural assemblage of phytoplankton. The present study suggests that the physiological state of phytoplankton can be estimated based on the significant relationships between $a^*_{ph}{}^{slope}$ and PPC:TC and between $b^*_{ph}(676)$ and POC:Chl *a*. The estimated size distribution of natural assemblage of phytoplankton from remotely sensed data could contribute to the understanding marine carbon cycle.

Table 4-1. Regression analyses between $a^*_{ph}(676)$ and d and SI_{abs}, $\underline{b}^*_{ph}(676)$ and d and SI_{scat} from cultural experiment (Chapter II) and *in situ* experiment (Chapter III). n, S.E., r^2, and p indicate the number of sample, standard error, determination coefficient, and probability, respectively. Alphabets indicate significant difference at $p<0.01$.

Population	Equation	n	Y_{int} ± S.E.	Slope ± S.E.	r^2	p
Culture	$\text{Log } a^*_{ph}(676) = Y_{int} + \text{Slope} \times \text{Log } d$	50	−1.78 ± 0.05 [a]	−0.10 ± 0.04 [e]	0.08	<0.05
In situ	$\text{Log } a^*_{ph}(676) = Y_{int} + \text{Slope} \times \text{Log } SI_{abs}$	77	−1.46 ± 0.06 [b]	−0.11 ± 0.05 [e]	0.06	<0.05
Culture	$\text{Log } \underline{b}^*_{ph}(676) = Y_{int} + \text{Slope} \times \text{Log } d$	26	−0.46 ± 0.18 [c]	−0.42 ± 0.20 [f]	0.16	<0.05
In situ	$\text{Log } \underline{b}^*_{ph}(676) = Y_{int} + \text{Slope} \times \text{Log } SI_{scat}$	58	−0.20 ± 0.23 [d]	−0.39 ± 0.19 [f]	0.07	<0.05

Table 4-2. Regression analysis between $\underline{b}^*_{ph}(676)$, C:Chl *a*, and POC:Chl *a* in cultural experiment (Chapter II) and *in situ* experiment (Chapter III). n, S.E., r^2, and *p* indicate the number of sample, standard error, determination coefficient, and probability, respectively. Alphabets indicate significant difference at $p<0.01$.

Population	Equation	n	Y_{int} ± S.E.	Slope ± S.E.	r^2	*p*
Culture	$\text{Log } \underline{b}^*_{ph}(676) = Y_{int} + \text{Slope} \times \text{Log C:Chl } a$	26	-2.16 ± 0.03^{c}	0.74 ± 0.15^{d}	0.52	<0.001
In situ	$\text{Log } \underline{b}^*_{ph}(676) = Y_{int} + \text{Slope} \times \text{Log POC:Chl } a$	62	-2.85 ± 0.31^{c}	0.94 ± 0.13^{d}	0.47	<0.001

REFERENCES

Aas, E. (1996) Refractive index of phytoplankton derived from its metabolite composition. Journal of Plankton Research, 18, 2223–2249.

Agustí, S. (1991a) Allometric scaling of light absorption and scattering by phytoplankton cells. Canadian Journal of Fisheries and Aquatic Sciences, 48, 763–767.

Agustí, S. (1991b) Light environment within dense populations: cell size influence on self-shading. Journal of Plankton Research, 13, 863–871.

Ahn, Y-H., Bricaud, A. and Morel, A. (1992) Light backscattering efficiency and related properties of some phytoplankters. Deep-Sea Research, 39, 1835–1855.

Alderkamp, A-C., Mills M. M., van Dijken. G, L, and Arrigo, K. R. (2013) Photoacclimation and non-photochemical quenching under in situ irradiance in natural phytoplankton assemblages from the Amundsen Sea, Antarctica. Marine Ecology Progress Series, 475, 15–34.

Ara, K., Fukuyama, S., Tashiro, M. and Hiromi, J. (2011) Seasonal and year-on-year variability in chlorophyll *a* and microphytoplankton assemblages for 9 years (2001 – 2009) in the neritic area of Sagami Bay, Japan. Plankton and Benthos Research, 6, 158–174.

Armstrong, R. A., Lee, C., Hedges, J. I., Honjo, S. and Wakeham, S. G. (2002) A new, mechanistic model for organic carbon fluxes in the ocean based on the quantitative association of POC with ballast minerals, Deep-Sea Research II, 49, 219–236.

Babin, M., Morel, A., Fournier-Sicre, V., Fell, F. and Stramski, D. (2003) Light scattering properties of marine particles in coastal and open ocean waters as related to the particle mass concentration. Limnology and Oceanography, 48, 843–859.

Babin, M. and Stramski, D. (2002) Light absorption by aquatic particles in the near-infrared spectral

region. Limnology and Oceanography, 47, 911-915.

Baek, S. H., Shimode, S., Han, M-S. and Kikuchi, T. (2008) Growth of dinoflagellates, *Ceratium furca* and *Ceratium fusus* in Sagami Bay, Japan: the role of nutrients. Harmful Algae, 7, 729-739.

Balch, W. M., Kilpatrick, K. A., Holligan, P., Harbour, D. and Fernandez, E. (1996) The 1991 coccolithophore bloom in the central North Atlantic. 2. Relating optics to coccolith concentration. Limnology and Oceanography, 41, 1684–1696.

Banse, K. (1976) Rate of growth, respiration and photosynthesis of unicellular algae as related to cell size–a review. Journal of Phycology, 12, 135–140.

Behrenfeld, M. J. and Boss, E. (2003) The beam attenuation to chlorophyll ratio: an optical index of phytoplankton physiology in the surface ocean? Deep-Sea Research I, 50, 1537–1549.

Behrenfeld, M. J. and Boss, E. (2006) Beam attenuation and chlorophyll concentration as alternative optical indices of phytoplankton biomass. Journal of Marine Research, 64, 431–451.

Behrenfeld, M. J., Boss, E., Siegel, D. A. and Shea, D. M. (2005) Carbon-based ocean productivity and phytoplankton physiology from space. Global Biogeochemical Cycles, 19, 1–14.

Behrenfeld, M. J. and Falkowski, P. G. (1997) Photosynthetic rates derived from satellite-based chlorophyll concentration. Limnology and Oceanography, 42, 1–20.

Berner, T., Dubinsky, Z., Wyman, K. and Falkowski, P. G. (1989) Photoadaptation and the “package” effect in *Dunaliella tertiolecta* (Chlorophyceae). Journal of Phycology, 25, 70–78.

Bidigare, R. R., Smith, R. C., Baker, K. S. and Marra, J. (1987) Oceanic primary production estimates from measurements of spectral irradiance and pigment concentrations. Global Biogeochemical Cycle, 1, 171–186.

Boyd, P. W., Doney, S. C., Strzepek, R., Dusenberry, J., Lindsay, K. and Fung, I. (2008) Climate-mediated changes to mixed-layer properties in the Southern Ocean : assessing the

phytoplankton response. Biogeosciences, 5, 847–864.

Brewin, R. J. W., Hardman-Mountford, N. J., Lavender, S. J., Raitsos, D. E., Hirata, T., Uitz, J., Devred, E., Bricaud, A., Ciotti, A. and Gentili, B. (2011) An intercomparison of bio-optical techniques for detecting dominant phytoplankton size class from satellite remote sensing. Remote Sensing of Environment, 115, 325–339.

Bricaud, A., Babin, M., Morel, A. and Claustre, H. (1995) Variability in the chlorophyll-specific absorption coefficients of natural phytoplankton: analysis and parameterization. Journal of Geophysical Research, 100, 13321–13332.

Bricaud, A., Bédhomme, A. and Morel, A. (1988) Optical properties of diverse phytoplanktonic species – experimental results and theoretical interpretation. Journal of Plankton Research, 10, 851–873.

Bricaud, A., Claustre, H., Ras, J., and Oubelkheir, K. (2004) Natural variability of phytoplanktonic absorption in oceanic waters : influence of the size structure of algal populations. Journal of Geophysical Research, 109, C11010.

Bricaud, A., Morel, A. and Prieur L. (1983) Optical efficiency factors of some phytoplankters. Limnology and Oceanography, 28, 816–832.

Brunet, C., Brylinski, J. M. and Lemoine, Y. (1993) In situ variations of the xanthophylls diatoxanthin and diadinoxanthin: photoadaptation and relationships with a hydrodynamical system in the eastern English Channel. Marine Ecology Progress Series, 102, 69–77.

Brunet, C., Johnsen, G., Lavaud, J., and Roy, S. (2011) Pigments and photoacclimation processes. In: Roy, S., Llewellyn, C. A., Egeland, S., Johnsen, G. (eds) Phytoplankton pigments: characterization, chemotaxonomy and applications in oceanography. Cambridge University Press, Cambridge, pp 445–471.

Campbell, J. W. and Aarup, T. (1992) New production in the North Atlantic derived from seasonal

patterns of surface chlorophyll. Deep-Sea Research, 39, 1669–1694.

Carder, K., Cannizzaro, J., Chen, R. and Lee, Z. (2006) MODIS semi-analytic algorithm for IOP. In: Stuart, V. (ed) Reports of the international ocean-colour coordinating group remote sensing of inherent optical properties : fundamentals, tests of algorithms, and applications. Report Number 5. Dartmaouth, Nova Scotia, Canada.

Carder, K. L., Chen, F. R., Lee, Z. P., Hawes, S. K. and Kamykowski, D. (1999) Semianalytic Moderate-Resolution Imaging spectrometer algorithms for chlorophyll *a* and absorption with bio-optical domains based on nitrate-depletion temperatures. Journal of Geophysical Research, 104, 5403–5421.

Cermeño, P., Marañón, E., Rodríguez, J. and Fernández, E. (2005) Large-sized phytoplankton sustain higher carbon-specific photosynthesis than smaller cells in a coastal eutrophic ecosystem. Marine Ecology Progress Series, 297, 51–60.

Chan, A. (1980) Comparative physiological study of marine diatoms and dinoflagellates in relation to irradiance and cell size. II. Relationship between photosynthesis, growth, and carbon chlorophyll *a* ratio. Journal of Phycology, 16, 428–432.

Chiba, S., Hirawake, T., Ushio, S., Horimoto, N., Satoh, R., Nakajima, Y., Ishimaru, T. and Yamaguchi, Y. (2000) An overview of the biological/oceanographic survey by the RTV Umitaka-Maru III off Adelie Land, Antarctica in January–February 1996. Deep-Sea Research II, 47, 2589–2613.

Chisholm, S. W. (1992) Phytoplankton size. In: Falkowski, P. G., Woodhead, A. D. (eds) Primary productivity and biochemical cycles in the sea. Plenum Press, New York. pp. 213-237.

Chisholm, S. W. (2000) Stirring times in the Southern Ocean. Nature, 407, 685–687.

Ciotti, A. M. and Bricaud, A. (2006) Retrievals of a size parameter for phytoplankton and spectral light absorption by colored detrital matter from water-leaving radiances at SeaWiFS channels in a continental shelf region off Brazil. Limnology and Oceanography:

Methods, 4, 237–253.

Ciotti, M., Lewis, M. R. and Cullen, J. J. (2002) Assessment of the relationships between dominant cell size in natural phytoplankton communities and the spectral shape of the absorption. Limnology and Oceanography, 47, 404–417.

Claustre, H., Kerhervé, P., Marty, J-C. and Prieur, L. (1994) Phytoplankton photoadaptation related to some frontal physical processes. Journal of Marine Systems, 5, 251–265.

Cleveland, J. and Weidemann, A. (1993) Quantifying absorption by aquatic particles – a multiple-scattering correction for glass-fiber filters. Limnology and Oceanography, 38, 1321–1327.

Cullen, J. J. (2008) Observation and prediction of harmful algal blooms. In: Babin, M., Roesler, C. S. and Cullen, J. J. (eds) Real-time coastal observing systems for marine ecosystem dynamics and harmful algal blooms. UNESCO Publishing, Paris, pp 1–41.

D'Sa, E. J., Miller, R. L. and Del Castillo, C. (2006) Bio-optical properties and ocean color algorithms for coastal waters influenced by the Mississippi River during a cold front. Applied Optics, 45, 7410–7428.

DuRand, M. D., Green, R. E., Sosik, H. M., and Olson, R. J. (2002) Diel Variation in optical properties of *Micromonas pusilla* (Prasinophyceae). Journal of Phycology, 38, 1132–1142.

DuRand, M. D. and Olson, R. J. (1996) Contributions of phytoplankton light scattering and cell concentration changes to diel variation in beam attenuation in the equatorial Pacific from flow cytometric measurements of pico-, ultra, and nanoplankton. Deep-Sea Research II, 43, 891–906.

Duysens, L. N. M. (1956) The flattening of the absorption spectrum of suspension, as compared to that of solutions. Biochimica et Biophysica Acta, 19, 1–12.

Eisner, L. B., Twardowski, M. S., Cowles, T. J. and Perry, M. J. (2003) Resolving phytoplankton photoprotective : photosynthetic carotenoid ratios on fine scales using in situ spectral absorption measurements. Limnology and Oceanography, 48, 632–646.

Eppley, R. W., Holmes, R. W. and Strickland, J. D. H. (1967) Sinking rates of marine phytoplankton measured with a fluorometer. Journal of Experimental Marine Biology and Ecology, 1, 191–208.

Eppley, R. W. and Sloan, P. R. (1966) Growth rates of marine phytoplankton: correlation with light absorption by cell chlorophyll *a*. Physiologia Plantarum, 19, 47–59.

Falkowski, P. G. and Raven, J. A. (2007) Aquatic Photosynthesis. Princeton University Press, Princeton. 500 pp.

Finkel, Z. V. (2001) Light absorption and size scaling of light-limited metabolism in marine diatoms. Limnology and Oceanography, 46, 86–94.

Finkel, Z. V., Beardall, J., Flynn, K. J., Quigg, A., Rees, T. A. V. and Raven, J. A. (2010) Phytoplankton in a changing world : cell size and elemental stoichiometry. Journal of Plankton Research, 32, 119–137.

Finkel, Z. V. and Irwin, A. J. (2000) Modeling size-dependent photosynthesis: light absorption and the allometric rule. Journal of Theoretical Biology, 204, 361–369.

Finkel, Z. V., Irwin, A. J. and Schofield, O. (2004) Resource limitation alters the 3/4 size scaling of metabolic rates in phytoplankton. Marine Ecology Progress Series, 273, 269–279.

Fofonoff, N. P. and Millard Jr, R. C. (1983) Algorithms for computation of fundamental properties of seawater. Unesco technical papers in marine science 44.

Fujiki, T. and Taguchi, S. (2002) Variability in chlorophyll *a* specific absorption coefficient in marine phytoplankton as a function of cell size and irradiance. Journal of Plankton Research, 24, 859–874.

Fujiki, T., Toda, T., Kikuchi, T. and Taguchi, S. (2003) Photoprotective response of xanthophyll pigments during phytoplankton blooms in Sagami Bay, Japan. Journal of Plankton Research, 25, 317–322.

Geider, R. J. (1987) Light and temperature dependence of carbon to chlorophyll *a* ratio in microalgae and cyanobacteria: implications for physiology and growth of phytoplankton. New Phytologist, 106, 1–34.

Geider, R. J., MacIntyre, H. L. and Kana, T. M. (1997) Dynamic model of phytoplankton growth and acclimation : responses of the balanced growth rate and the chlorophyll *a* : carbon ratio to light , nutrient-limitation and temperature. Marine Ecology Progress Series, 148, 187–200.

Geider, R. J. and Osborne, B. A. (1987) Light absorption by a marine diatom: experimental observations and theoretical calculations of the package effect in a small *Thalassiosira* species. Marine Biology, 96, 299–308.

Glibert, P. M., Burkholder, J. M. and Kana, T. M. (2012) Recent insights about relationships between nutrient availability, forms, and stoichiometry, and the distribution, ecophysiology, and food web effects of pelagic and benthic *Prorocentrum* species. Harmful Algae, 14, 231–259.

Gordon, H. R., Brown, O. B. and Jacobs, M. M. (1975) Computed relationships between the inherent and apparent optical properties of a flat homogeneous ocean. Applied Optics, 14, 417–427.

Gordon, H. R. and Morel, A. (1983) Remote assessment of ocean colour for interpretation of satellite visible imagery. A reviews. Lecture notes on coastal and estuarine studies, Volume 4. Springer-Verlag. New York. 114 pp.

Griffith, G. P., Vennell, R. and Williams, M. J. M. (2010) An algal photoprotection index and vertical mixing in the Southern Ocean. Journal of Plankton Research, 32, 515–527.

Guillard, R. R. L. and Ryther, J. H. (1962) Studies of marine plankton diatoms. 1. *Cyclotella nana* Hustedt and *Detonula confervacea* (Cleave.) Gran. Canadian Journal of Microbiology, 8, 229–239.

Hashihama, F., Horimoto, N., Kanda, J., Furuya, K., Ishimaru, T. and Saino, T. (2008) Temporal variation in phytoplankton composition related to water mass properties in the central part of Sagami Bay. Journal of Oceanography, 64, 23–37.

Heil, C. A., Glibert, P. M. and Fan, C. (2005) *Prorocentrum minimum* (Pavillard) Schiller: A review of a harmful algal bloom species of growing worldwide importance. Harmful Algae, 4, 449–470.

Hillebrand, H., Durselen, C., Kirschtel, D., Pollingher, U. and Zohary, T. (1999) Biovolume calculation for pelagic and benthic microalgae. Journal of Phycology, 35, 403–424.

Hirata, T., Aiken, J., Hardman-Mountford, N., Smyth, T. J. and Barlow, R. G. (2008) An absorption model to determine phytoplankton size classes from satellite ocean colour. Remote Sensing of Environment, 112, 3153–3159.

Hitchcock, G. L. (1982) A comparative study of the size-dependent organic composition of marine diatoms and dinoflagellates. Journal of Plankton Research, 4, 363–377.

Hoepffner, N. and Sathyendranath, S. (1991) Effect of pigment composition on absorption properties of phytoplankton. Marine Ecology Progress Series, 73, 11–23.

Hovis, W. A. and Leung, K. C. (1977) Remote sensing of ocean color. Optical Engineering, 16, 158–166.

Johnsen, G., Nelson, N. B., Jovine, R. V. M. and Prezelin, B. B. (1994) Chromoprotein- and pigment-dependent modeling of spectral light absorption in two dinoflagellates, *Prorocentrum minimum* and *Heterocapsa pygmaea*. Marine Ecology Progress Series, 114, 245–258.

Johnsen, G. and Sakshaug, E. (1993) Bio-optical characteristics and photoadaptative responses in the toxic and bloom-forming dinoflagellates *Gyrodinium aureolum*, *Gymnodinium galatheanum*, and two strains of *Prorocentrum minimum*. Journal of Phycology, 29, 627–642.

Jonasz, M. and Fournier, G. R. (2007) Light scattering by particles in water. Academic Press, San Diego. CA. 704 pp.

Kiefer, D. A. and Mitchell, B. G. (1983) A simple, steady state description of phytoplankton growth based on absorption cross section and quantum efficiency. Limnology and Oceanography, 28, 770–776.

Kirk, J. T. O. (1975) A theoretical analysis of the contribution of algal cells to the attenuation of light within natural waters. New Phytologist, 75, 21–36.

Kirk, J. T. O. (1981) Monte Carlo study of the nature of the underwater light field in, and the relationships between optical properties of, turbid yellow waters. Australian Journal of Marine and Freshwater Research, 32, 517–532.

Kirk, J. T. O. (2011) Light and Photosynthesis in Aquatic Ecosystems. 3rd Edition. Cambridge University Press, Cambridge.

Kishino, M., Takahashi, M., Okami, N. and Ichimura, S. (1985) Estimation of the spectral absorption-coefficients of phytoplankton in the sea. Bulletin of Marine Science, 37, 634–642.

Kopczyńska, E. E., Savoye, N., Dehairs, F., Cardinal, D. and Elskens, M. (2007) Spring phytoplankton assemblages in the Southern Ocean between Australia and Antarctica. Polar Biology, 31, 77–88.

Lalli, M. L. and T. R. Parsons (1997) Biological Oceanography: An Introduction. 2nd Edition. Butterworth Heinemann, Oxford, 314 pp.

Laws, E. A., Falkowski, P. G., Smith Jr., W. O., Ducklow, H. and McCarthy J. J. (2000)

Temperature effects on export production in the open ocean. Global Biogeochemical Cycles, 14, 1231–1246.

Leong, S. C. Y. and Taguchi, S. (2006) Detecting the bloom-forming dinoflagellate *Alexandrium tamarense* using the absorption signature. Hydrobiologia, 568, 299–308.

Loisel, H., Mériaux, X., Berthon, J.-F. and Poteau, A. (2007) Investigation of the optical backscattering to scattering ratio of marine particles in relation to their biogeochemical composition in the eastern English Channel and southern North Sea. Limnology and Oceanography, 52, 739–752.

Loisel, H. and Morel, A. (1998) Light scattering and chlorophyll concentration in case 1 waters: a reexamination. Limnology and Oceanography, 43, 847–858.

Loisel, H. and Stramski, D. (2000) Estimation of the inherent optical properties of natural waters from the irradiance attenuation coefficient and reflectance in the presence of Raman scattering. Applied Optics, 39, 3001–3011.

MacIntyre, H., Kana, T., Anning, T. and Geider, R. (2002) Photoacclimation of photosynthesis irradiance response curves and photosynthetic pigments in microalgae and cyanobacteria. Journal of Phycology, 38, 17–38.

MacIntyre, H. L., Kana, T. M. and Geider, R. J. (2000) The effect of water motion on short-term rates of photosynthesis by marine phytoplankton. Trends Plant Science, 5, 12–17.

Malone, T. C. (1980) Algal size. In: Morris, I. (ed) Studies in ecology, Vol. 7, The physiological ecology of phytoplankton. University of California Press, Berkley, CA, pp.433–463.

Menden-Deuer, S. and Lessard, E. J. (2000) Carbon to volume relationships for dinoflagellates, diatoms, and other protist plankton. Limnology and Oceanography, 45, 569–579.

Michaels, A. F. and Silver, M. W. (1988) Primary production, sinking fluxes and the microbial food web. Deep-Sea Research, 35, 473–490.

Millie, D., Schofield, O., Kirkpatrick, G., Johnsen, G., Tester, P. and Vinyard, B. (1997) Detection of harmful algal blooms using photopigments and absorption signatures: A case study of the Florida red tide dinoflagellate, *Gymnodinium breve*. Limnology and Oceanography, 42, 1240–1251.

Mitchell, B. G. and Kiefer, A. (1988) Chlorophyll *a* specific absorption and fluorescence excitation spectra for light-limited phytoplankton. Deep-Sea Research, 35, 639–663.

Moline, M. A. (1998) Photoadaptive response during the development of a coastal Antarctic diatom bloom and relationship to water column stability. Limnology Oceanography, 43, 146–153.

Morel, A. (1987) Chlorophyll-specific scattering coefficient of phytoplankton. A simplified theoretical approach. Deep-Sea Research, 34, 1093–1105.

Morel, A. (1988) Optical modeling of the upper ocean in relation to its biogenous matter content (case I waters). Journal of Geophysical Research, 93, 10749–10768.

Morel, A. and Ahn, Y-H. (1991) Optics of heterotrophic nanoflagellates and ciliates: a tentative assessment of their scattering role in oceanic waters compared to those of bacterial and algal cells. Journal of Marine Research, 49, 177–202.

Morel, A. and Bricaud, A. (1981) Theoretical results concerning light-absorption a discrete medium, and application of phytoplankton. Deep-Sea Research, 28, 1375–1393.

Morel, A. and Bricaud, A. (1986) Inherent optical properties of algal cells including picoplankton: theoretical and experimental results. Canadian Bulletin Fisheries and Aquatic Science, 214, 521–559.

Morel, A., Gentili B., Chami, M. and Ras, J. (2006) Bio-optical properties high chlorophyll case 1 waters and of yellow-substance-dominated case 2 waters. Deep-Sea Research I, 53, 1439–1459.

Morel, A. and Prieur, L. (1977) Analysis of variations in ocean color. Limnology and Oceanography,

22, 709–722.

Motokawa, S., Hattori, H., Sasaki, H. and Taguchi, S. (2014) Photoprotective acclimation of micro- and nano-size phytoplankton assemblages in the Indian sector of the Southern Ocean. Polar Biology, 37, 1373–1381.

Motokawa, S. and Taguchi, S. (2015) Scattering properties of the dinoflagellates *Prorocentrum micans* and *P. minimum*. Plankton and Benthos Research, in press.

Nagao, N., Toda, T., Takahashi, K., Hamasaki, K., Kikuchi, T. and Taguchi, S. (2001) High ash content in net-plankton samples from shallow coastal water: possible source of error in dry weight measurement of zooplankton biomass. Journal of Oceanography, 57, 105–107.

Odate, T. and Fukuchi, M. (1995) Physical and chemical properties of surface water in the Southern ocean in summer 1991/92. Proceedings of NIPR Symposium Polar Biology, 8, 77–85.

O'Reilly, J. E., Maritorena, S., Mitchell, B. G., Siegel, D. A., Carder, K. L. Garver, S. A., Kahru, M., and McClain, C. (1998) Ocean color chlorophyll algorithms for SeaWiFS. Journal of Geophysical Research, 103, 24937–24953.

Orsi, A. H., Whitworth, T. and Nowlin Jr, W. D. (1995) On the meridional extent and fronts of the Antarctic Circumpolar Current. Deep-Sea Research I, 42, 641–673.

Osborne, B. A. and Geider, R. J. (1989) Problems in the assessment of the package effect in five small phytoplankters. Marine Biology, 100, 151–159.

Pak, H., Beardsley, G. F., Heath, G. R. and Curl, H. (1970) Light-scattering vectors of some marine particles. Limnology and Oceanography, 15, 683–687.

Parsons, T. R., Maita, Y. and Lalli, C. M. (1984) A manual of chemical and biological methods for seawater analysis. Pergamon Press, Oxford. 173 pp.

Pegau, W., Gray, D. and Zaneveld, J. (1997) Absorption and attenuation of visible and near-infrared light in water: dependence on temperature and salinity. Applied Optics, 36, 6035–6046.

Preisendorfer, R. W. (1976) Hydrologic Optics. Volume 5. Properties. U.S. Department of Commerce, National Oceanic and Atmospheric Administration, Environmental Research laboratories.

Prieur, L. and Sathyendranath, S. (1981) An optical classification of coastal and oceanic waters based on the specific spectral absorption curves of phytoplankton pigments, dissolved organic matter, and other particulate materials. Limnology and Oceanography, 26, 671–689.

Reynolds, R. A., Stramski, D. and Kiefer, D. A. (1997) The effect of nitrogen limitation on the absorption and scattering properties of the marine diatom *Thalassiosira pseudonana*. Limnology and Oceanography, 42, 881–892.

Reynolds, R. A., Stramski, D., Wright, V. M. and Wozniak, S. B. (2008) particle size distributions of coastal waters measured with an *in situ* laser diffractometer. Proceedings of the Ocean Optics XIX Conference, Pascoli, Italy.

Roy, S., Sathyendranath, S. and Platt, T. (2011) Retrieval of phytoplankton size from bio-optical measurements: theory and applications. Journal of the Royal Society Interface, 8, 650–660.

Saggiomo, V., Carrada, G. C., Mangoni, O., Ribera d'Alcalà, M. and Russo, A. (1998) Spatial and temporal variability of size-fractionated biomass and primary production in the Ross Sea (Antarctica) during austral spring and summer. Journal of Marine Systems, 17, 115–127.

Sancetta, C., Villareal, T. and Falkowski, P. G. (1991) Massive flux of rhizosolenid diatoms: a common occurrence? Limnology and Oceanography, 36, 1452–1457.

Sarmiento, J., Slater, R. D., Barber, R., Bopp, L., Doney, S. C., Hirst, A. C., Kleypas, J., Matear, R., Mikolajewicz, U., Monfray, P., Soldatov, V., Spall, S. A. and Stouffer, R. (2004) Response of ocean ecosystems to climate warming. Global Biochemical Cycles, 18,

1–23.

Satoh, F., Hamasaki, K., Toda, T. and Taguchi, S. (2000) Summer phytoplankton bloom in Manazuru Harbor, Sagami Bay, central Japan. Plankton and Benthos Research, 47, 73–79.

Sieburth, J. M., Smetacek, V. and Lenz, J. (1978) Pelagic ecosystem structure: heterotrophic compartments of the plankton and their relationship to plankton size fractions. Limnology and Oceanography, 23, 1256–1263.

Smith, R. C. and Baker, K. S. (1978) The bio-optical state of ocean waters and remote sensing. Limnology and Oceanography, 24, 247–259.

Spinrad, R. W. (1986) A calibration diagram of specific beam attenuation. Journal of Geophysical Research, 91, 7761–7764.

Stramski, D. (1999) Refractive index of planktonic cells as a measure of cellular carbon and chlorophyll *a* content. Deep-Sea Research I, 46, 335–351.

Stramski, D., Bricaud, A. and Morel, A. (2001) Modeling the inherent optical properties of the ocean based on the detailed composition of the planktonic community. Applied Optics, 40, 2929–2945.

Stramski, D. and Kiefer, D. A. (1991) Light scattering by microorganisms in the open ocean. Progress in Oceanography, 28, 343–383.

Stramski, D., Rosenberg, G. and Legendre, L. (1993) Photosynthetic and optical properties of the marine chlorophyte *Dunaliella tertiolecta* grown under fluctuating light caused by surface-wave focusing. Marine Biology, 115, 363–372.

Stramski, D., Sciandra, A., and Claustre, H. (2002). Effects of temperature, nitrogen, and light limitation on the optical properties of the marine diatom *Thalassiosira pseudonana*. Limnology and Oceanography, 47, 392–403.

Strathmann, R. (1967) Estimating the organic carbon content of phytoplankton from cell volume or plasma volume. Limnology and Oceanography, 12, 411–418.

Sullivan, C. W., McClain, C. R., Comiso, J. C. and Smith, W. O. Jr. (1988) Phytoplankton standing crops within an Antarctic ice dege assessed by satellite remote sensing. Journal of Geophysical Research, 93, 12487–12498.

Suzuki, R. and Ishimaru, T. (1990) An improved method for the determination of phytoplankton chlorophyll using *N,N*-dimethylformamide. Journal of Oceanography, 46, 190-194.

Taguchi, S. (1976) Relationship between photosynthesis and cell size of marine diatoms. Journal of Phycology, 12, 185–189.

Takao, S., Hirawake, T., Wright, S. W. and Suzuki, K. (2012) Variations of net primary productivity and phytoplankton community composition in the Indian sector of the Southern Ocean as estimated from ocean color remote sensing data. Biogeosciences, 9, 3875–3890.

Tang, E. P. Y. (1996) Why do dinoflagellates have lower growth rates? Journal of Phycology, 32, 80–84.

Uitz, J., Claustre, H., Morel, A. and Hooker, S. B. (2006) Vertical distribution of phytoplankton communities in open ocean: an assessment based on surface chlorophyll. Journal of Geophysical Research, 111, C08005.

Ulloa, O., Sathyendranath, S. and Platt, T. (1994) Effects of the particle-size distribution on the backscattering ratio in seawater. Applied optics, 33, 7070–7077.

Vaillancourt, R. D., Brown C. W., Guillard, R. R. L. and Balch, W. M. (2004). Light backscattering properties of marine phytoplankton: relationships to cell size, chemical composition and taxonomy. Journal of Plankton Research, 26, 191–212.

van de Hulst, H. C. (1957) Light scattering by small particles. John Wiley and Sons, New York. 470 pp.

Vidussi, F., Claustre, H., Manca, B. B., Luchetta, A. and Marty, J. (2001) Phytoplankton pigment

distribution in relation to upper thermocline circulation in the eastern Mediterranean Sea during winter. Journal of Geophysical Research, 106, 19939-19956.

WET Labs, Inc. (2008) Absorption and attenuation meter (ac-9) user's guide, p. 6.

Woźniak, B. and Dera, J. (2007) Light absorption by phytoplankton in the sea. In: Woźniak, B., Dera, J. (eds) Light absorption in sea water. Springer, New York, pp. 295–394.

Wright, S. W., Jeffrey, S. W. and Mantoura, R. F. C. (1997) Evaluation of methods and solvents for pigment extraction. In: Jeffrey, S. W., Mantoura, R. F. C., Wright, S. W. (eds) Phytoplankton pigments in oceanography: guidelines to modern methods. UNESCO Publishing, Paris, pp 261–282.

Wright, S. W., Thomas, D. P., Marchant, H. J., Higgins, H. W., Mackey, M. D. and Mackey, D. J. (1996) Analysis of phytoplankton of the Australian sector of the Southern Ocean: comparisons of microscopy and size frequency data with interpretations of pigment HPLC data using the 'CHEMTAX' matrix factorisation program. Marine Ecology Progress Series, 144, 285–298.

Zaneveld, J. R. V., Kitchen, L. C. and Moore, C. C. (1994) Scattering error correction of reflecting tube absorption meter. Proceedings of the Society for Photo-Optical Instrumentation in England (SPIE), 2258, 44–55.

APPENDICES

Appendix 1. Variations in bulk, < 20 μm, and < 2 μm fractions of chlorophyll *a* conceantrations at the optical depths of 0.39, 2.3, and 4.6 in the Indian sector of the Southern Ocean. Sampling depth with a hyphen indicates no data available. N.D. indicates not detect.

Station	Samling date	Chlorophyll *a* concentration (mg m^{-3})								
		Bulk fraction			<20 μm fraction			<2 μm fraction		
	Local time	ζ = 0.39	ζ = 2.3	ζ = 4.6	ζ = 0.39	ζ = 2.3	ζ = 4.6	ζ = 0.39	ζ = 2.3	ζ = 4.6
C01-10	Dec. 26 2010	0.24	0.29	0.43	0.22	0.25	0.37	0.08	0.10	0.17
C02-10	Dec. 27 2010	0.16	0.20	0.45	—	—	0.42	—	—	0.17
C03-10	Dec. 28 2010	0.17	0.16	0.19	0.15	0.15	0.16	0.05	0.05	0.06
C04-10	Dec. 29 2010	0.30	0.41	0.34	0.22	0.23	0.33	0.07	0.09	0.04
C05-10	Dec. 30 2010	0.38	0.35	0.45	0.19	0.18	0.28	0.04	0.03	0.05
C06-11	Dec. 31 2010	0.48	0.56	0.43	0.21	0.26	0.22	0.05	0.03	0.04
C10-11	Jan. 2 2011	0.57	0.48	0.73	0.38	0.41	0.54	0.03	0.03	0.05
D15-11	Jan. 18 2011	0.23	0.33	0.21	0.13	0.18	0.14	0.03	0.05	0.05
D14-11	Jan. 17 2011	0.17	0.21	0.18	0.10	0.10	0.09	0.03	0.03	0.02
D12-11	Jan. 15 2011	0.22	0.20	0.19	0.18	0.17	0.19	0.02	0.02	0.02
D10-11	Jan. 14 2011	0.72	0.93	0.67	0.26	0.23	0.24	0.02	0.03	0.02
D07-11	Jan. 11 2011	0.21	0.28	0.42	0.16	0.12	0.25	0.02	0.03	0.13
C02-11	Dec. 30 2011	—	0.24	0.31	—	0.17	0.29	—	0.09	0.18
C07-12	Jan. 3 2012	—	0.48	0.34	—	0.31	0.30	—	0.07	N.D.
D13-12	Jan. 27 2012	0.36	0.22	0.28	0.30	0.21	0.23	0.11	0.09	0.10
D07-12	Jan. 21 2012	0.19	0.19	0.15	0.11	0.15	0.14	N.D.	0.06	0.08

Appendix 2. Variations in bulk, < 20 μm, and < 2 μm fractions of chlorophyll *a* conceantrations at the optical depths of 0.0, 2.3, and 4.6 at station M in Sagami Bay. Sampling depth with a hyphen indicates no data available. N.D. indicates not detect.

Station	Samling date	Chlorophyll *a* concentration (mg m^{-3})								
		Bulk fraction			<20 μm fraction			<2 μm fraction		
	Local time	ζ = 0.0	ζ = 2.3	ζ = 4.6	ζ = 0.0	ζ = 2.3	ζ = 4.6	ζ = 0.0	ζ = 2.3	ζ = 4.6
M	Jul. 16 2009	1.50	1.25	0.24	—	—	—	—	—	—
M	Aug. 20 2009	1.47	0.39	0.58	0.36	—	—	0.24	—	—
M	Sep. 10 2009	0.49	0.54	0.28	0.42	0.41	0.24	0.29	0.27	0.15
M	Oct. 23 2009	2.24	1.24	1.58	1.81	0.96	1.53	0.84	0.33	0.23
M	Dec. 1 2009	0.51	0.47	0.46	0.44	0.45	0.43	0.29	0.23	0.20
M	Dec. 18 2009	0.32	0.39	N.D.	0.23	0.38	N.D.	0.14	0.22	N.D.
M	Jan. 22 2010	0.33	0.28	0.16	0.30	0.25	0.12	0.13	0.11	0.07
M	Feb. 26 2010	0.95	0.46	0.25	0.73	0.46	0.22	0.49	0.25	0.10
M	Mar. 15 2010	2.42	3.62	2.94	0.86	1.21	0.95	0.33	0.72	0.22
M	Apr. 14 2010	0.23	0.44	0.32	0.18	0.29	0.22	0.11	0.14	0.11
M	May. 12 2010	1.11	1.49	1.18	1.06	0.94	0.40	0.36	0.35	0.11
M	Jun. 19 2010	1.13	0.71	0.26	0.70	0.42	0.21	0.24	0.21	0.11
M	Jul. 21 2010	3.40	1.12	0.33	1.06	0.59	0.22	0.30	0.13	0.09
M	Aug. 18 2010	1.71	0.36	0.64	0.84	0.29	0.51	0.46	0.17	0.28
M	Sep. 13 2010	3.80	1.48	1.44	0.59	0.44	0.48	0.23	0.15	0.16
M	Oct. 16 2010	2.66	0.46	0.22	0.53	0.22	0.09	0.14	0.05	0.02
M	Nov. 13 2010	2.51	3.62	2.57	1.74	1.35	1.47	0.65	0.21	0.41
M	Dec. 14 2010	0.60	0.42	0.38	0.43	0.36	0.23	0.25	0.16	0.14